

**CORRELATION BETWEEN ROADSIDE SAFETY HARDWARE
AND VEHICLE SAFETY STANDARDS EVALUATION CRITERIA**

A Thesis

by

HARIKA REDDY PRODDUTURU

Submitted to the Office of Graduate and Professional Studies of
Texas A&M University
in partial fulfillment of the requirements for the degree of

MASTER OF SCIENCE

Chair of Committee,	Stefan Hurlebaus
Co-Chair of Committee,	Harry Jones
Committee Member,	Sevan Goenezen
Head of Department,	Robin Autenrieth

May 2016

Major Subject: Civil Engineering

Copyright 2016 Harika Reddy Prodduturu

ABSTRACT

Roadside safety devices are designed to protect vehicle occupants from injuries. As the purpose of roadside safety hardware is to be functional while minimizing the risk of occupant injury, the occupant risk criteria are vital to the assessment of these devices. The “Manual for Assessing Safety Hardware (MASH)”, specifies guidelines for crash tests and gives evaluation criteria for safety devices. As per MASH, the risk of injury to the occupant is assessed based on the concept of “Flail Space Model (FSM). The Occupant Impact Velocity (OIV) and Occupant Ridedown Acceleration (ORA) are used for assessing the injury criteria of an occupant.

It is assumed that the model is an “unrestrained” point mass which can move as a free missile. There is a growing usage of restraints such as seatbelts and airbags. Hence, attempts are made in this study to assess real-world occupant injury risk associated with current MASH criteria using crash tests performed with instrumented ATD’s and comparing them with injury criteria provided by US-NCAP regulations.

A crash test was conducted with a passenger car impacting a rigid wall at 90-degree angle, and with 34.7 mph (56 km/h) impact speed. The vehicle was instrumented according to MASH requirements, and an instrumented ATD was included as required by US-NCAP standards. The full-scale crash test was designed to replicate testing criteria from MASH and US-NCAP testing standards to the maximum possible extent. As per the results from vehicle dynamics, the crash test was found to be a fail according to MASH evaluation criteria but a pass according to US-NCAP standards from ATD dynamics. Therefore a correlation was established between the roadside safety evaluation criteria and occupant injury risk. Additionally, finite element models for a passenger car, passive restraint systems (seatbelt and airbags), and anthropomorphic test ATD were calibrated against this full-scale frontal crash test which can be used for parametric simulations in future with a few modifications.

TABLE OF CONTENTS

	Page
ABSTRACT	ii
TABLE OF CONTENTS	iii
LIST OF TABLES	vi
LIST OF FIGURES.....	viii
1. INTRODUCTION.....	1
2. METHODOLOGY	5
2.1 Overview of Roadside Safety Features	5
2.2 Finite Element Simulations	5
2.3 Full-Scale Crash Test and Test Data Analysis.....	6
2.4 Finite Element Model Calibration.....	6
2.5 Correlation of Evaluation Criteria of MASH and FMVSS.....	6
2.6 Final Report.....	6
3. LITERATURE REVIEW	7
3.1 Overview of Roadside Safety Devices Standards	7
3.1.1 Manual for Assessing Safety Hardware (MASH)	8
3.1.2 MASH – Crash Test Matrices	8
3.1.3 Evaluation Criteria for Crash Testing.....	10
3.1.4 History and Overview of Flail Space Model	15
3.2 Overview of Vehicle Testing	21
3.2.1 FMVSS Standard 208 and US-NCAP Testing	21
3.2.2 Test Procedures.....	22
3.3 History and Overview of the Crash Test ATD's.....	23
3.4 Injury Criteria.....	25
3.4.1 Head and Neck Injury Criteria.....	26
3.4.2 Thoracic Injury Criteria	27
3.4.3 Leg Injury Criteria	28
3.5 Restraint Systems	30
3.6 Previous Research Efforts	31
4. FINITE ELEMENT MODELS OF COMPONENTS FOR COMPUTER SIMULATIONS.....	39
4.1 Finite Element Model of Toyota Yaris	39
4.2 Finite Element Model of Hybrid III Anthropomorphic Test ATD	40
4.3 Finite Element Model of Seatbelt.....	41

4.3.1	Retractor	42
4.3.2	Pretensioner	43
4.3.3	D-Ring	44
4.4	Finite Element Airbag Model Development	44
5.	FINITE ELEMENT PREDICTIVE SIMULATIONS	48
5.1	Initial Simulations at Different Speeds	49
5.2	Occupant Risk Assessment	58
5.3	Conclusions	59
6.	CRASH TESTING	60
6.1	Design and Construction of Rigid Impact Wall	60
6.2	Material Specifications	63
6.3	Test Facility	63
6.4	Data Acquisition Systems	64
6.4.1	Vehicle Instrumentation and Data Processing	64
6.4.2	Seat Adjustments and Steering Wheel Data	66
6.4.3	Anthropomorphic ATD Instrumentation and Positioning	68
6.4.4	Photographic Instrumentation and Data Processing	73
6.5	Crash Test 602761-13	73
6.5.1	Test Vehicle	73
6.5.2	Test Description	74
6.5.3	Test Article and Component Damage	75
6.5.4	Test Vehicle Damage	75
6.6	Crash Test Results	76
6.6.1	Occupant Risk Values as per Vehicle Dynamics	79
6.6.2	Occupant Injury Criteria as per ATD Dynamics	79
6.6.3	Assessment of Test Results as per Vehicle Dynamics	97
6.6.3.1	Structural Adequacy	97
6.6.3.2	Occupant Risk	97
6.6.4	Assessment of Test Results as per ATD Dynamics	98
7.	FINITE ELEMENT MODEL CALIBRATION	100
7.1	Seat Adjustment and Steering Wheel Data	100
7.2	Anthropomorphic Test Device Position	101
7.3	Airbag Adjustment	101
7.4	Simulation of FE Model Frontal Crash	108
7.5	Finite Element Simulation Results	117
7.5.1	Occupant Risk Values as per Vehicle Dynamics	117
7.5.2	Occupant Injury Criteria as per ATD Dynamics	118
7.5.3	Seatbelt Forces	133
7.6	Conclusions	135
8.	CORRELATION OF EVALUATION CRITERIA OF MASH AND FMVSS	136

9. SUMMARY AND CONCLUSIONS.....	138
10. FUTURE WORK	140
REFERENCES.....	141
APPENDIX A	144

LIST OF TABLES

	Page
Table 3-1. Test Levels for Safety Features (MASH, 2009)	9
Table 3-2. Test Matrices for Longitudinal Barriers (MASH, 2009)	11
Table 3-3. Allowable Deformations of Occupant Compartment (MASH, 2009)	13
Table 3-4. Safety Evaluation Criteria Pertinent to Present Study (MASH, 2009)	13
Table 3-5. Injury Scale Specified by AAAM, 2001 (Michie, 1981)	19
Table 3-6. Occupant Impact Velocity and Occupant Ride Down Acceleration Values for Safety Features (Michie, 1981)	20
Table 3-7. Recommended Values of OIV and RDA as per MASH, 2009	20
Table 3-8. Injury Criteria for Head and Neck	26
Table 3-9. Injury Criteria for Thorax	28
Table 3-11. Injury Assessment Reference Values	30
Table 3-12. Summary of Selected Full Scale Crash Test (Gabauer and Gabler, 2006)	32
Table 3-13. Equations used for Computing Injury Risk from Head and Chest Injury Criteria	34
Table 3-14. Crash Test Results as per (Gabauer and Gabler 2008a).	35
Table 4-1. External Dimensions of the ATD	41
Table 4-2. Process For Seatbelt Modeling of Retractor And Pretensioner	44
Table 5-1. Occupant Risks Values at Different Speeds	58
Table 5-2. Comparison of OIV from Pre-Simulations and Literature Review	59
Table 6-1. Positioning of Seat and Steering Wheel	66
Table 6-2. ATD Positioning According to US-NCAP Guidelines	69
Table 6-3. Results of Accelerations, Forces and Moments in ATD and Loads in Shoulder and Lap Belts.	79
Table 6-4. Comparison of Occupant Injury Risk Parameters to IARV	99
Table 7-1. Sequential Images of Airbag Deflation in Different Cases	104
Table 7-2. Comparison Of Occupant Risk Assessment Values from Crash Test and Computer Simulation	118

Table 7-3. Comparison of Head, Chest, Neck and Femur Injury Criteria from the Crash Test and FE Simulation.....	119
Table 8-1: Recorded MASH Occupant Risk Parameters from Full-Scale Crash Test	136
Table 8-2: Recorded FMVSS Occupant Injury Risk Parameters from Full-Scale Crash Test.....	137

LIST OF FIGURES

	Page
Figure 3-1. Occupant Position at Instant of Vehicle/Barrier Impact (Michie, 1981).....	16
Figure 3-2. Occupant Position during Subsequent Vehicle Ridedown (Michie, 1981).....	16
Figure 3-3. Schematic Representation of Flail – Space Model (Michie, 1981).....	18
Figure 3-4. OIV AIS 3+ Injury Risk Curve, Belted (Gabauer and Gabler, 2008a) ...	21
Figure 3-5. Schematic Representation of Full Frontal Barrier Test	23
Figure 3-6. Front and Side View of Transparent ATD with Accelerometer.....	25
Figure 3-7. Probability of Head and Chest Injury to Occupants Restrained with Airbag Only (Gabauer and Gabler, 2008a).....	36
Figure 3-8. Probability of Head and Chest Injury to Occupants Restrained with 3- Point Seatbelt Only (Gabauer and Gabler, 2008a).....	36
Figure 3-9. Probability of Head and Chest Injury to Occupants Restrained with 3- Point Seatbelt and Airbag (Gabauer and Gabler, 2008a).....	37
Figure 4-1. FE Model of Toyota Yaris 2010.....	39
Figure 4-2. FE Model of H3 50 th Percentile ATD.....	40
Figure 4-3. FE Model of Seatbelt.....	41
Figure 4-4. Belt Material Force versus Strain Loading and Unloading Curves.....	42
Figure 4-5. Seatbelt Retractor Curves Representing Force versus Payout	43
Figure 4-6. ATD Placed in Position and Restrained with Seatbelt	45
Figure 4-7. Finite Element Computer Model of the Airbag.....	45
Figure 4-8. Comparison of NCAC Toyota Yaris FE Steering wheel (Left) and FE Steering Wheel (Right)	46
Figure 4-9. Original Steering Wheel (Left) Replaced with Steering Wheel with Airbag (Right) and Connected to Steering Main Rod in a Similar Manner	46
Figure 5-1. ATD Placed in Position and Restrained with Seatbelt and Airbag	48
Figure 5-2. Sequential Images of Toyota Yaris with Positioned ATD and Restrained with Seatbelt and Airbag @ 25 mph (Side View)	49

Figure 5-3. Sequential Images of Toyota Yaris with Positioned ATD and Restrained with Seatbelt and Airbag @ 25 mph (Perspective View).....	50
Figure 5-4. Sequential Images of Toyota Yaris with Positioned ATD and Restrained with Seatbelt and Airbag @ 25 mph (Top View).....	51
Figure 5-5. Sequential Images of Toyota Yaris with Positioned ATD and Restrained with Seatbelt and Airbag @ 30 mph (Side View)	52
Figure 5-6. Sequential Images of Toyota Yaris with Positioned ATD and Restrained with Seatbelt and Airbag @ 30 mph (Perspective View).....	53
Figure 5-7. Sequential Images of Toyota Yaris with Positioned ATD and Restrained with Seatbelt and Airbag @ 30 mph (Top View).....	54
Figure 5-8. Sequential Images of Toyota Yaris with Positioned ATD and Restrained with Seatbelt and Airbag @ 35 mph (Side view)	55
Figure 5-9. Sequential Images of Toyota Yaris with Positioned ATD and Restrained with Seatbelt and Airbag @ 35 mph (Perspective View).....	56
Figure 5-10. Sequential Images of Toyota Yaris with Positioned ATD and Restrained with Seatbelt and Airbag @ 35 mph (Top View)	57
Figure 6-1. Details of the Rigid Impact Wall.....	62
Figure 6-2. Rigid Wall Prior to Testing	63
Figure 6-3. Seat/ Steering Wheel Positioning	67
Figure 6-4. Front and Side View of Transparent ATD with Accelerometer.....	69
Figure 6-5. ATD Positioning According to US-NCAP Guidelines	71
Figure 6-6. ATD Position during Crash Test	71
Figure 6-7. Vehicle/Installation Geometrics for Test No. 602761-13	74
Figure 6-8. Vehicle before Test No. 602761-13	74
Figure 6-9. Vehicle/Rigid Wall Positions after Test No. 602761-13.....	75
Figure 6-10. Vehicle after Test No. 602761-13	76
Figure 6-11. Interior of Vehicle for Test No. 602761-13.....	76
Figure 6-12. Summary of Results for Test No. 602671-13 on the Rigid Wall.	78
Figure 6-13. Head X-Accelerations	82
Figure 6-14. Head Y-Accelerations	83
Figure 6-15. Head Z-Accelerations	83
Figure 6-16. Resultant Head Accelerations.....	84

Figure 6-17. Chest Deflections.....	84
Figure 6-18. Chest X-Accelerations	85
Figure 6-19. Chest Y- Accelerations.....	85
Figure 6-20. Chest Z-Accelerations	86
Figure 6-21. Chest Resultant Accelerations	86
Figure 6-22. Pelvis X-Accelerations	87
Figure 6-23. Pelvis Y-Accelerations	87
Figure 6-24. Pelvis Z-Accelerations.....	88
Figure 6-25. Pelvis Resultant Accelerations	88
Figure 6-26. Upper Neck X-Forces	89
Figure 6-27. Upper Neck Y-forces.....	89
Figure 6-28. Upper Neck Z-Forces	90
Figure 6-29. Upper Neck Resultant Forces	90
Figure 6-30. Upper Neck X-Moments	91
Figure 6-31. Upper Neck Y-Moments	91
Figure 6-32. Upper Neck Z-Moments	92
Figure 6-33. Upper Neck Resultant Moments	92
Figure 6-34. Left Femur X-Forces	93
Figure 6-35. Left Femur Y-Forces	93
Figure 6-36. Left Femur Z-Forces.....	94
Figure 6-37. Right Femur X-Forces	94
Figure 6-38. Right Y-Forces	95
Figure 6-39. Right Z-Forces.....	95
Figure 6-40. Shoulder Belt Loads	96
Figure 6-41. Lap Belt Loads	96
Figure 7-1. Position of Drivers' Seat and Steering Wheel Adjusted as per US-NCAP Regulations	100
Figure 7-2. Original Mass Flow Rate vs. Time Curve for Airbag Inflation	102
Figure 7-3. Airbag Curve Tailored Slope with Different Deflation Peaks (Mass Flow Rate vs. Time).....	103

Figure 7-4. Sequential Images of Simulations of Crash Test at 34.7 mph (Side View)	109
Figure 7-5. Sequential Images of Simulations of Crash Test at 34.7 mph (Top View)	113
Figure 7-6. Head X-Accelerations vs. Time.....	119
Figure 7-7. Head Y-Accelerations vs. Time.....	120
Figure 7-8. Head Z-Accelerations vs. Time	120
Figure 7-9. Resultant Head Accelerations vs. Time.....	121
Figure 7-10. Chest Deflections vs. Time.....	121
Figure 7-11. Chest X-Accelerations vs. Time	122
Figure 7-12. Chest Y-Accelerations vs. Time.....	122
Figure 7-13. Chest Z-Acceleration vs. Time.....	123
Figure 7-14. Chest Resultant Accelerations vs. Time	123
Figure 7-15. Pelvis X-Acceleration vs. Time.....	124
Figure 7-16. Pelvis Y-Acceleration vs. Time.....	124
Figure 7-17. Pelvis Z-Acceleration vs. Time	125
Figure 7-18. Resultant Pelvis Acceleration vs. Time.....	125
Figure 7-19. Upper Neck X-Force vs. Time	126
Figure 7-20. Upper Neck Y-Forces vs. Time.....	126
Figure 7-21. Upper Neck Z-Forces vs. Time	127
Figure 7-22. Resultant Neck Force vs. Time.....	127
Figure 7-23. Upper Neck X-Moments vs. Time	128
Figure 7-24. Upper Neck Y-Moments vs. Time	128
Figure 7-25. Upper Neck Z-Moment vs. Time	129
Figure 7-26. Upper Neck Resultant Moment vs. Time	129
Figure 7-27. Left Femur X-Force vs. Time.....	130
Figure 7-28. Left Femur Y-Force vs. Time.....	130
Figure 7-29. Left Femur Z-Forces vs. Time.....	131
Figure 7-30. Right Femur X-Force vs. Time	131
Figure 7-31. Right Femur Y-Force vs. Time	132

Figure 7-32. Right Femur Z-Force vs. Time	132
Figure 7-33. Shoulder Belt Loads vs. Time	134
Figure 7-34. Lap Belt Loads vs. Time	134

1. INTRODUCTION

The University of Michigan Transportation Research Institute (UMTRI) and the Texas A&M Transportation Institute (TTI) conducted a joint project to investigate the correlation between occupant risk evaluated according to roadside safety hardware standards and vehicle safety standards.

Roadside safety devices are designed to protect vehicle occupants from injuries. As the purpose of roadside safety hardware is to be functional while minimizing the risk of occupant injury, the occupant risk criteria are vital to the assessment of these devices. The criteria for success of these devices are structural adequacy, vehicle trajectory after collision and occupant risk. Full-scale crash testing is the traditional method used to assess the crashworthiness of these devices. The Manual for Assessing Safety Hardware (MASH) specifies guidelines for crash tests and gives evaluation criteria for safety devices (MASH, 2009).

Within MASH criteria, the risk of injury to the occupant is assessed based on the concept of the Flail Space Model (FSM) (Michie, 1981). This model estimates the average deceleration that an unrestrained occupant would experience when contacting the vehicle interior during the impact event for evaluation of Occupant Impact Velocity (OIV) and Occupant Ridedown Acceleration (ORA), which are used for assessing the injury criteria of an occupant. In order to simplify the application of FSM to a full-scale crash testing, the occupant is modeled as an “unrestrained” point mass which can move as a free missile. The impact velocity of the occupant with the vehicle interior at the point when the free body traverses 2 ft (0.6 m) longitudinally and 1 ft (0.3 m) laterally is used to assess the injury criteria of the occupant.

Better prediction of occupant injury is possible with the use of Anthropomorphic Test ATD's (ATDs), which have a humanlike response to impact and contain instrumentation that can be used to assess the potential for injury to different body regions. The first instrumented ATD was developed by Samuel W. Alderson in 1949. The most commonly used of these ATD's are the Hybrid III family, which were developed by General

Motors. Tests for assessing vehicle performance and pass/fail criteria based on ATD injury metrics are specified in Part 571 of standard No. 208 for passenger vehicles. This same standard also specifies about the type of active and passive occupant restraints required for different vehicles such as passenger cars, trucks and buses.

There is a growing use of passive restraint systems such as seatbelts and airbags. At the time at which the flail space model was proposed, seat belt use was ~14% and 3-point belts were not available at every seating position, and airbags had effectively zero penetration into the vehicle fleet. Currently, nearly all vehicle occupants involved in vehicles are equipped with these technologies and the national average seat belt use rate is 87%. The development of consumer advocacy crash tests over the past 30-40 years have resulted in dramatic improvements in the crash performance of vehicle structures and occupant compartment integrity. Taken together, these factors have resulted in currently death rates in crashes that are less than 1/3 of what they were in the early 1980's.

As indicated above, the MASH criteria for occupant protection are unbelted occupants who are not restrained by an airbag. However, this rarely represents current scenarios where vehicle impact roadside objects and as a result, the evaluation criteria set by MASH for designing roadside safety devices are likely conservative in nature. Therefore, there is potential for increasing the maximum limits dictated by MASH for occupant risk evaluation.

Hence, attempts were made in this study to assess real-world occupant injury risk associated with current MASH criteria using crash tests performed with instrumented ATD's and comparing them with injury criteria used in the US New Car Assessment Program (US-NCAP). Finite element models for a passenger car, restraint systems (seatbelt and airbags), and a Hybrid III midsize male anthropomorphic test ATD were calibrated against a full-scale frontal crash test. The crash test was conducted with a passenger car impacting a rigid wall at 90-degree angle, and at a nominal speed of 35 mph (56 km/h). The vehicle was instrumented according to MASH requirements, and an instrumented ATD was included in the driver seating position as required by US-NCAP

standards. The full-scale crash test was defined as to replicate to the maximum extent possible testing criteria found in MASH and US-NCAP testing standards. The goal of this study was to investigate the relationships between occupant risk determined according to MASH criteria and ATD injury metrics defined by US-NCAP/FMVSS standards.

As an initial step towards this study, the researchers conducted a literature review about MASH and FMVSS No. 208 standards for occupant risk criteria during evaluation of roadside safety barrier and vehicle safety during full-scale crash testing, respectively. Past research effort of investigating these standards were also reviewed. Pertinent domestic and international studies were considered within this process to get an elevated idea about the study being conducted.

Finite element (FE) computer analyses were performed to determine the appropriate impact testing conditions for the full-scale crash test. These analyses were conducted with use of a finite element model of a Toyota Yaris small passenger car, available from the National Crash Analysis Center (NCAC) website.

(<http://www.ncac.gwu.edu/vml/models.html>). An FE model of the instrumented H3 50th percentile male ATD was properly positioned as a driver in the vehicle, and restrained with use of an FE seatbelt model. The FE computer analyses were performed with use of the LS-DYNA non-linear finite element software and were post-processed with the use of LS-PREPOST.

A full-scale crash test was then performed at the Texas A&M University Riverside Campus, with use of a 2010 Toyota Yaris passenger car. This vehicle is chosen as it is one of those acceptable for use in full scale crash tests according to MASH. A fully instrumented H3 50th percentile male ATD provided by UMTRI was included in the vehicle, at the driver position, for recording occupant acceleration and displacement. The vehicle was ballasted and instrumented according to MASH testing standard requirements. The H3 ATD acceleration and displacement data were recorded throughout the impact event for evaluation according to FMVSS occupant injury criteria. Test results were used to explore the correlation between the FMVSS and the MASH occupant risk results, which would serve as a basis for

suggestions of MASH occupant risk upper limits to assist with the design of roadside safety hardware for applications at critical roadside locations.

The full-scale crash test was also used for calibration of the FE model previously developed. The FE model could be employed in future research studies to develop parametric simulations by varying vehicle nominal impact speed and angle conditions. These analyses are recommended to support the researcher's recommendations on needed MASH occupant risk upper limits adjustment to compensate for the modified severity of the impact, dictated by the combination of speed and angle impact conditions.

2. METHODOLOGY

2.1 Overview of Roadside Safety Features

As an initial step, the researchers conducted a literature review to address all pertinent domestic and international studies. The researchers investigated requirements, test matrices and procedures defined by MASH, FMVSS and US-NCAP standards. Past research effort of investigating and correlating these standards were studied and evaluated. The researchers reviewed the history and instrumentation of the ATDs as well as the restraint systems. Section 3 describes testing standards, and includes a basis overview of these procedures, history of instrumented ATDs and restraint systems. Section 3 also includes a summary on past research efforts looking at combining injury criteria and occupant safety through full scale crash testing and statistical analysis.

2.2 Finite Element Simulations

During this task, the researchers worked on assembling the FE models of the car, ATD and passive restraint systems. The FE computer model of the Toyota Yaris passenger car vehicle is publicly available upon request to the Federal Highway Administration (FHWA). Although, this model is validated against full scale crash tests, the interiors of the vehicle (e.g. seat, dashboard) were not validated from material perspective, representing only a realistic geometry. The model of a Hybrid III 50th percentile male instrumented ATD was included and positioned in the driver's seat. It was restrained with a seatbelt model available from the LSTC website. Some modifications were applied to the available seatbelt model. Also, the researchers included the FE model of the airbag provided by LSTC. The compiled FE model of Toyota Yaris with the fully restrained occupant was run using LS DYNA to check for compatibility and robustness of the assembly. Section 4 describes details of FE model of the Toyota Yaris, the instrumented ATD and the restraint systems used for this purpose. Section 5 gives the details of simulation and results of occupant injury risk assessment. Conclusions on occupant risk were made by comparing the results with available literature.

2.3 Full-Scale Crash Test and Test Data Analysis

A full-scale crash test was conducted according to MASH and US-NCAP testing standards and was evaluated according to both standards' criteria. A 2010 Toyota Yaris vehicle model was used for testing to allow a direct comparison to the FE computer analyses results. The researchers ballasted and instrumented the vehicle according to MASH standard requirements. The ATD was instrumented and positioned according to US-NCAP standard criteria. Details of the test and the performed test data analysis are reported in Section 6.

2.4 Finite Element Model Calibration

During this task, efforts were made to calibrate the FE model against full scale crash test. The ATD was positioned according to US-NCAP regulations. The seat, seatbelt, and airbag models used in the research had to be modified so that the simulated injury measures can match the crash test results. Section 7 gives the details of FE model calibration and the results of occupant injury risk as per vehicle and ATD dynamics were compared with that of the crash test.

2.5 Correlation of Evaluation Criteria of MASH and FMVSS

Results of full-scale crash test were reviewed in terms of MASH occupant risk and ATD recorded internal forces and displacements to establish a correlation between the MASH occupant risk evaluation criteria and the US-NCAP occupant injury criteria.

Recommendation for adjusted MASH occupant risk upper limits was also made. Details of this effort are reported in Section 8.

2.6 Final Report

A final report was prepared to document the research effort, computer simulations and full-scale test results. Conclusions of the study investigation and suggestions for future research work are also included.

3. LITERATURE REVIEW

3.1 Overview of Roadside Safety Devices Standards

Roadside safety devices are designed to contain and redirect an errant vehicle during an impact event, while they need to maintain their structural adequacy, they need to protect the occupants by minimizing his risk of injury. Full-scale crash tests have historically been the most common method of evaluating the performance of roadside safety devices.

Guidelines and procedures for conducting and evaluating full-scale crash tests of roadside safety devices were first published in the Highway Research Correlation Services Circular 482, in 1962 by the Transportation Research Board (TRB). This document was amended to address additional questions that were not covered and to include a few changes. A new standard document was published under the name of National Cooperative Highway Research Program (NCHRP) Report 153. Recommended Procedures for Vehicle Crash Testing of Highway Appurtenances in 1974.

Due to the evolution of roadside safety concepts, practices and technology, the NCHRP Report 153 was updated to Report 230. Recommended Procedures for Safety Performance Evaluation of Highway Safety Appurtenances. With significant changes in vehicle fleet, advances in computer simulations and evaluation methods, emergence of new barrier design etc., NCHRP Report 350: Recommended Procedures for Safety Performance Evaluation of Highway Safety Features was published in 1993 and superseded Report 230. The American Association of State Highway and Transport Officials (AASHTO, 2009) published the latest standard “Manual for Assessing Safety Hardware” in 2009 which is an update to and supersede NCHRP Report 350. This publication addresses officially adopted crash-testing procedures by AASHTO (2009). The major revisions incorporated include (but are not limited to) changes to the test vehicles, number and impact conditions of the test matrices, changes to the evaluation criteria and addition of new features to the test guidelines.

3.1.1 Manual for Assessing Safety Hardware (MASH)

MASH contains uniform guidelines for crash testing both temporary and permanent hardware devices and evaluation criteria to assess test results. MASH guidelines provide a basis for comparison and formulation of impact performance specifications of safety features and guidance for developing new safety features. The following sections describe MASH test matrices and evaluation criteria.

3.1.2 MASH – Crash Test Matrices

MASH provides guidelines for crash test of highway safety features which include (but are not limited to).

- Longitudinal Barriers – Flexible, semi-rigid and rigid barriers
- Terminals – Guardrails and Median Barriers
- Crash Cushions – Redirective and Non-redirective
- Support Structures – Utility poles, Breakaway Luminaries and signs, Traffic Gates
- Work zone attenuation and Channelizers – Truck mounted attenuators (TMAs)

MASH developed its guidelines based on the philosophy of “worst practical condition”, which assumes that the roadside safety features work well for all the impact conditions between two extremes if they satisfactorily perform well at the two extremes. Also, the devices developed according to these guidelines are cost-effective and provide optimal level of safety without an unrealistic financial burden on the user.

Each of the roadside safety devices is tested to a different test levels which are defined by different impact conditions such as speed and angle of approach and the type of test vehicle ranging from small size passenger cars to fully loaded tractor-trailer truck. Six test levels are defined by MASH and longitudinal barriers are the only safety features which are tested for all the six levels. All the other safety features are tested only up to three levels depending on its location and usage. Table 3-1 shows the test levels with different impact conditions for safety features.

Table 3-1. Test Levels for Safety Features (MASH, 2009)

Test Level	Test Vehicle Designation and Type	Test Conditions	
		Speed mph (km/h)	Angle (Degrees)
1	1100C (Passenger Car)	31(50)	25
	2270P (Pickup Truck)	31(50)	25
2	1100C (Passenger Car)	44(70)	25
	2270P (Pickup Truck)	44(70)	25
3	1100C (Passenger Car)	62 (100)	25
	2270P (Pickup Truck)	62 (100)	25
4	1100C (Passenger Car)	62 (100)	25
	2270P (Pickup Truck)	62 (100)	25
	10000S (Single - Unit Truck)	56 (90)	15
5	1100C (Passenger Car)	62 (100)	25
	2270P (Pickup Truck)	62 (100)	25
	36000V (Tractor - Van Trailer)	50 (80)	15
6	1100C (Passenger Car)	62 (100)	25
	2270P (Pickup Truck)	62 (100)	25
	36000T (Tractor – Tank Trailer)	50 (80)	15

The impact performance of temporary and permanent highway safety features is evaluated in terms of occupant risk injury, structural adequacy of the hardware device and the vehicle trajectory. As shown in Table 3-1, the test levels differ with respect nominal impact conditions and vehicle type. These parameters are selected to represent the “worst practical condition” of a crash. The 85th percentile level has been traditionally set to be the worst practical condition for an impact angle and speed of the vehicle. According to the available information of vehicle crashes on high speed roadways, MASH concluded that an impact speed of 62 mph (100 km/h) and 44 mph (71 km/h) at

an impact angle of 25⁰ and 15⁰ approximate the 85th percentile of respective real world impact conditions for high speed, high-volume roadways and low speed, low-volume roadways respectively. With varied vehicle weights, sizes and models, MASH selected the smallest car test vehicle weighing approximately 2,420 lbs. (1,100 kg) to be representative of 2nd percentile lightest passenger vehicle. The light truck test vehicle weighing approximately 5,000 lbs. (2,270kg) was selected to be the 90th percentile heaviest passenger vehicle. Similarly, impact locations for crash tests are selected to represent the critical condition that would most likely lead to test failure.

Test matrices describing procedures for crash tests have been defined for each type of roadside safety features. These are established by a two-digit naming system. The test level is identified by the first digit and the specific test for each type of safety feature is identified by the second digit. Table 3-2 shows test matrices for longitudinal barriers, as specified by MASH. For instance, Test 10 is designed to check on occupant risk and on barrier's strength to redirect small passenger vehicles impacting within the length-of-need. In particular, concerns for small cars include under-ride, wheel snag, rollover and head-slap.

3.1.3 Evaluation Criteria for Crash Testing

The two main evaluation criteria used to evaluate the results of a roadside safety crash testing are structural adequacy and occupant risk. Roadside safety devices should perform successfully according to these requirements. Structural adequacy is the first factor against which a safety feature should perform successfully. The device must satisfy this criterion depending on its intended function by redirecting the vehicle, by stopping the vehicle in a controlled manner or by permitting the vehicle to break through the device. Structural adequacy is related only to the structural requirements associated with the impact and it should be noted that it does not include any other structural aspects of the device. The other important evaluation criterion for performance of roadside safety features is occupant risk. The risk of occupant injury depends to a large extent on the crashworthiness of the impacting vehicle which in turn depends on the

design of the occupant compartment, structural integrity, padding, restraint conditions, etc. According to MASH, the occupant injury risk is evaluated using the vehicle dynamics and accelerations during and after impact by use of “flail-space model”. Also, penetrations of any detached elements, fragments or other debris from the test article are permitted to a certain degree. For instance, a sign that have a tendency to scatter the detached elements from test article over a wide range of area may not be appropriate design for the use in the median of a highway barrier as the detached elements could potentially encroach into the opposite lanes of traffic.

Table 3-2. Test Matrices for Longitudinal Barriers (MASH, 2009)

Test level	Barrier Section	Test No.	Vehicle type	Impact Speed mph (km/h)	Impact angle
1	Length –of- need	1-10	1100C	31 (50)	25
		1-11	2270P	31 (50)	25
	Transition	1-20	1100C	31 (50)	25
		1-21	2270P	31 (50)	25
2	Length –of- need	2-10	1100C	44 (70)	25
		2-11	2270P	44 (70)	25
	Transition	2-20	1100C	44 (70)	25
		2-21	2270P	44 (70)	25
3	Length –of- need	3-10	1100C	62 (100)	25
		3-11	2270P	62 (100)	25
	Transition	3-20	1100C	62 (100)	25
		3-21	2270P	62 (100)	25

Table 3-2 Continued

Test level	Barrier Section	Test No.	Vehicle type	Impact Speed mph (km/h)	Impact angle
4	Length - of-need	4-10	1100C	62 (100)	25
		4-11	2270P	62 (100)	25
		4-12	10000S	56 (90)	15
	Transition	4-20	1100C	62 (100)	25
		4-21	2270P	62 (100)	25
		4-22	10000S	56 (90)	15
5	Length - of-need	5-10	1100C	62 (100)	25
		5-11	2270P	62 (100)	25
		5-12	36000V	50 (80)	15
	Transition	5-20	1100C	62 (100)	25
		5-21	2270P	62 (100)	25
		5-22	36000V	50 (80)	15
6	Length - of-need	6-10	1100C	62 (100)	25
		6-11	2270P	62 (100)	25
		6-12	36000T	50 (80)	15
	Transition	6-20	1100C	62 (100)	25
		6-21	2270P	62 (100)	25
		6-12	36000T	50 (80)	15

However no penetration into the occupant compartment is allowed. There may also be an intrusion or deformation of the occupant compartment during the impact which is permissible to a degree depending on the area of the vehicle damaged. These limitations are given in Table 3-3.

Table 3-3. Allowable Deformations of Occupant Compartment (MASH, 2009)

Compartment elements	Allowable deformations
Roof	≤ 4 in. (102mm)
Windshield	≤ 3 in. (76mm) with no tear of plastic liner
Window	No shattering of a side window resulting from direct contact with a structural member of the test article. In case where the windows are laminated, windshield guidelines are applied.
Wheel/foot well and toe pan areas	≤ 9 in. (229 mm)
Side front panel	≤ 12 in. (305 mm)
Front side door area (above seat)	≤ 9 in. (229 mm)
Front side door area (below seat)	≤ 12 in. (305 mm)
Floor pan and transmission tunnel areas	≤ 12 in. (305 mm)

The safety evaluation guidelines are shown in Table 3-4. The applicable tests are also listed in Table 5-1 of MASH.

Table 3-4. Safety Evaluation Criteria Pertinent to Present Study (MASH, 2009)

Evaluation Factors	Evaluation Criteria
Structural Adequacy	A. Test article should contain and redirect the vehicle or bring it to a controlled stop; the vehicle should not penetrate, underride or override the installation although controlled lateral deflection of the test article is acceptable
	B. The test article should readily activate in a predictable manner by breaking away, fracturing, or yielding

Table 3-4 Continued

Evaluation Factors	Evaluation Criteria		
Structural Adequacy	C. Acceptable test article performance may be by redirection, controlled penetration, or controlled stopping of the vehicle		
Occupant risk	D. Detached elements, fragments or other debris from the test article should not penetrate or show potential for penetrating the occupant compartment or present undue hazard to other traffic, pedestrians, or personnel in a work zone.		
	E. Detached elements, fragments, or other debris from the test article, or vehicular damage should not block the drivers' vision or otherwise cause the driver to lose control of the vehicle		
	F. The vehicle should remain upright during the collision. The maximum roll, pitch angles are not to exceed 75 degrees.		
	G. It is preferable, although not essential, that the vehicle remain upright during and after collision.		
	H. Occupant impact velocities (OIV) should satisfy the following limits.		
	Component	Preferred	Maximum
	Longitudinal and Lateral	30 ft/s (9.1 m/s)	40 ft/s (12.2 m/s)
	I. The occupant ride down accelerations should satisfy the limits.		
	Component	Preferred	Maximum
	Longitudinal and Lateral	15 G	20.49 G

3.1.4 History and Overview of Flail Space Model

There have been past attempts to evaluate the results of vehicle crash tests of highway safety devices in terms of occupant injury risk. The first attempt was made by Shoemaker (1961) who presented threshold vehicle lateral, longitudinal and total accelerations along with three restrained conditions – no belt, lap belt only and three point belt conditions. Edwards (Edwards et al., 1969) conducted a second attempt to measure the collision severity based on the change in velocity. His work was based on the fact that head and chest injuries occur when the impact velocity is approximately equal to the change in velocity of the vehicle during the collision event (Mertz et al., 1967; Blamey, 1964). Another vehicle-dynamic criterion was developed by Tamanini (1970) which concluded that vehicles with weight range between 2000 and 4500 lbs. (907 and 2041 kg), hitting a crash cushion at an average speed of 60 mph (96 km/h), should be stopped at an average acceleration less than 12 G. These past vehicle dynamics determine the risk of injury in two stages. The first stage of the collision is indicated by the momentum change criterion and the second stage of collision is indicated by the stopping distance. These criteria, however, appeared to have been overly conservative. The flail space model was introduced to overcome some limitations of previous models. This model is based on the hypothesis that the collision occurs in two stages. The first one assumes the occupant striking the interior of the compartment or the windshield with a certain velocity, while the second one considers the rate of change in velocity as the occupant rides down (ride down acceleration).

Figure 3-1 and Figure 3-2 represents the two stages of collision.

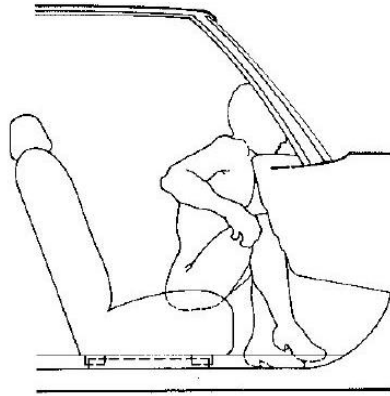


Figure 3-1. Occupant Position at Instant of Vehicle/Barrier Impact (Michie, 1981)

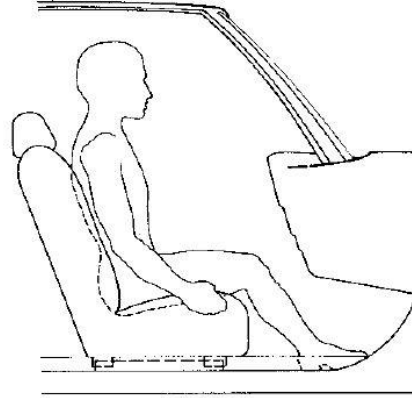


Figure 3-2. Occupant Position during Subsequent Vehicle Ridedown (Michie, 1981)

There are three injury mechanisms for the flail space model that were described by Michie (1981). The first mechanism is based on injury potential with the dynamic forces being of short duration (less than the natural period of the body elements). These dynamic factors are identified by the duration and intensity of the pulse (Chi, 1976). The sustained dynamic force results in deformation of the body elements. This injury potential is given by Equation (3-1).

$$\int_0^t a dt = \Delta V \leq (\Delta V)_{limit} \quad (3-1)$$

where a is the acceleration of the body element (ft/s²)

t is the time duration of the impulse

ΔV is the change in velocity of the body element (ft/s²)

The other injury mechanism described considers the dynamic forces having sufficient duration for body response to be fully developed. According to this theory, the injury potential depends on the amount of force that acts on the body rather than the momentum and is given by Equation 3-2 (Kornhauser et al., 1961).

$$a \leq (a)_{limit} \quad (3-2)$$

where a is the acceleration of the body element (ft/s^2). The third injury mechanism is based on a hydraulic phenomenon in which the dynamic forces act for an extremely long duration, where body fluids may drain out and cause hemorrhage. However, all the collisions do not last for more than 1 second and hence the hydraulic phenomenon does not occur. In order to simplify the application of FSM to the full scale crash testing, few assumptions are made by Michie (1981). They include the following:

- It is considered that the occupant moves as a free missile (no ATD is required) during impact and the vehicle acceleration and compartment geometry are used to calculate the impact time and velocity of the occupant at initial contact with the compartment surface.
- It is assumed that the occupant also rebounds and hence the occupant impact velocity is also the occupant relative velocity change. Also, it is assumed that the occupant remains in contact with the compartment after collision occurs and is subjected to vehicle accelerations.
- At the time of invention of FSM, there was only 15% usage of manual restraints such as seatbelts and airbag. Hence it is assumed that the occupant is unrestrained by shoulder belt, lap belt or airbag.
- The occupant is assumed to be a 50th percentile male and it is considered to be in an upright position. This also accounts to the distance the occupant can travel before any impact with the compartment of the vehicle.
- It is assumed that the compartment remains intact during the event of collision without any inward penetration and partial collapse. This way the occupant trajectory is also not affected.
- Only lateral and longitudinal accelerations are considered and measured at the center of mass. The vertical accelerations of the vehicle are minute and can be ignored
- It is assumed that pitching and rolling of the vehicle are not explicitly considered as these motions do not significantly affect the motion of the vehicle.

The occupant impact velocity is determined after the initial vehicle impact, at the instant where the occupant has travelled 2 ft (0.6 m) in longitudinal direction and 1 ft (0.3 m) in lateral direction. Figure 3-3 shows schematic representation of FSM.

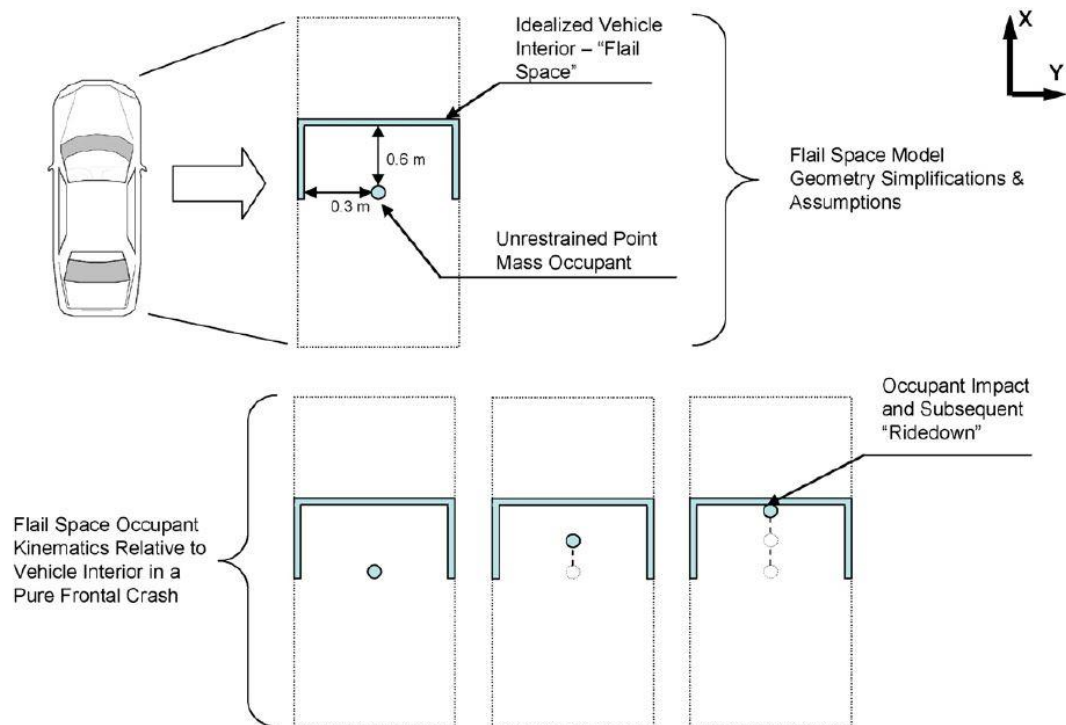


Figure 3-3. Schematic Representation of Flail – Space Model (Michie, 1981)

Based on the above assumptions, Michie set limits on occupant impact velocity and occupant ride down acceleration considering the degree of occupant injury. They are calculated based on the injury scale set by the American Association for Automotive medicine (AAAM, 2001) which is given in Table 3-5.

Table 3-5. Injury Scale Specified by AAAM, 2001 (Michie, 1981)

Code	Category
0	No injury
1	Minor
2	Moderate
3	Serious (No life-threatening)
4	Severe (life-threatening)
5	Critical (Survival uncertain)

The upper limit for occupant protection falls under the code 3 and 4 as per FMVSS Standard 208 which means the injury can be serious but not life threatening. The threshold limit for occupant impact velocity was set at 40 ft/s (12 m/s) based on the head impact of the occupant with the windshield that ranges from 44 to 51 ft/s (13 to 16 m/s) and head injury criteria of 1000 as per the FMVSS Standard 208. However, it was noted that in a crash cushion test designed as per TRC 191, that the occupant could subject to a 39 ft/s (11.88 m/s) impact velocity. Hence a roadside safety developer strives to achieve a lower occupant impact velocity and thus further reduce the risk of occupants. In order to achieve a lower value of the impact velocity and thus reducing the risk of occupant injury, a design velocity for each type of roadside safety hardware device is given by dividing the limit value with an appropriate factor of safety (F).

During the second stage of impact (where the occupant is already in contact with the interior of occupant compartment), it is assumed that the occupant undergoes the same acceleration of the compartment. Therefore, further occupant injury depends on the magnitude of this acceleration. As per previous studies, a threshold value of 20 G is applicable in both longitudinal and lateral directions (Ross et al., 1993). The design occupant impact velocity values for a few safety features are shown in Table 3-6.

Table 3-6. Occupant Impact Velocity and Occupant Ride Down Acceleration Values for Safety Features (Michie, 1981)

Type of safety feature	Occupant Impact Velocity (mph)		Occupant Ride Down Acceleration (G's)	
	Factor of safety (F)	Flail space recommendatio n	Factor of safety (F)	Flail space recommendation
Longitudinal Direction				
Breakaway/Yielding Support				
Sign and luminaire	2.67	15	1.33	15
Timber utility pole	1.33	20	1.33	15
Vehicle Deceleration Devices				
Crash Cushions and	1.33	20	1.33	15
Barrier terminals	1.33	20	1.33	15

The evaluation criteria have been reviewed through the years and the latest thresholds dictated by MASH are reported in Table 3-7.

Table 3-7. Recommended Values of OIV and RDA as per MASH, 2009

OIV	Preferred	Maximum
Longitudinal and Lateral	30 ft/s (9.1 m/s)	40 ft/s (12.2 m/s)
ORA	Preferred	Maximum
Longitudinal and Lateral	15 G	20.49 G

Gabauer and Gabler (2008a) made an attempt to compare and contrast the injury predicting capability of the FSM. Injury risk curves were developed using logistic regression and are represented as the probability of injury risk at AIS 3+ level with respect to longitudinal OIV. Figure 3-4 shows the probability of AIS 3+ occupant injury with respect to the OIV. The shaded area represents the 95% confidence bounds.

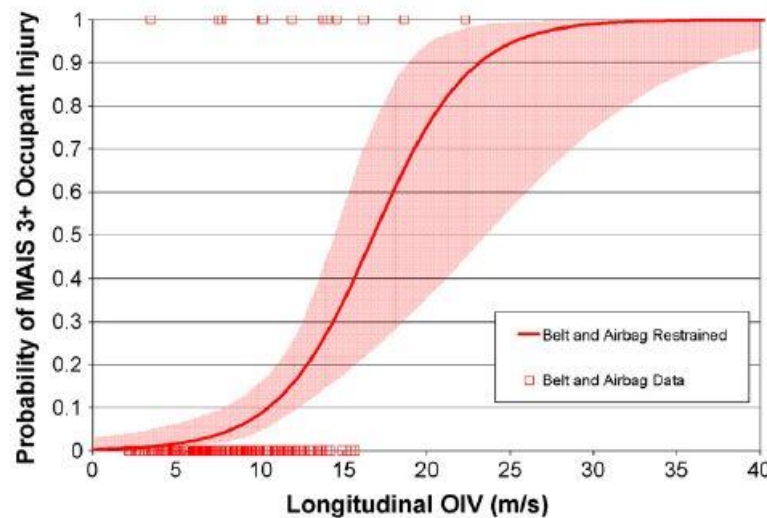


Figure 3-4. OIV AIS 3+ Injury Risk Curve, Belted (Gabauer and Gabler, 2008a)

3.2 Overview of Vehicle Testing

Vehicle crash test procedures are specified in both Federal Motor Vehicle Safety Standards (FMVSS) and New Car Assessment Program (US-NCAP) under the National Highway Transportation and Safety Administration. Testing procedures and specifications are discussed in this section.

3.2.1 FMVSS Standard 208 and US-NCAP Testing

The FMVSS are laws promulgated by the US National Highway Traffic Safety Administration to set minimum safety performance requirements for motor vehicles to

be sold in the United States. One part of FMVSS 208 defines crash test used to assess occupant protection where the front plane of a vehicle impacts a flat, rigid barrier at 30 mph (48 km/h). Crash test ATD's in the front-outboard seating positions of this vehicle are used to measure the potential for injury to different body regions that an occupant exposed to a similar crash would have sustained. These crash test ATD measurements are compared to injury assessment reference values (IARVs), which are pass/fail criteria.

The US New Car Assessment Program (US NCAP) is a test program aimed at providing consumers with information of vehicle safety and encouraging competition among manufactures on vehicle safety. US-NCAP does not require a particular level of crashworthiness performance as it is a response to the marketplace rather than in response to a legal requirement.

3.2.2 Test Procedures

Frontal crash protection is evaluated according to FMVSS and US-NCAP through the development of a full frontal test against a rigid barrier is intended to represent most real world crashes with significant engagement in a perpendicular impact direction. The FMVSS Standard No. 208 specifies an impact velocity 30 mph (48 km/h), while US-NCAP specifies a velocity of up to 35 mph (56 km/h), and barrier rebound velocity ranging up to 10% of the impact velocity. These test procedures can be applied to both belted and unbelted passengers. A schematic representation of Full Frontal Barrier test is shown in Figure 3-5.

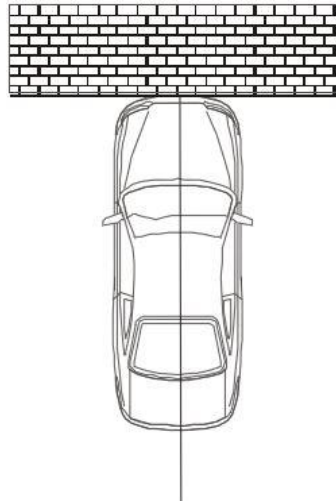


Figure 3-5. Schematic Representation of Full Frontal Barrier Test

3.3 History and Overview of the Crash Test ATD's

Crash test ATD's in today's industrial society have had great significance in providing crucial information about the effects of vehicle impacts on the human body. Previous methods used to record data of simulated vehicle impacts have not been as effective. Data collected from cadaver and animal testing was used by Alderson Research Labs (ARL) and Sierra Engineering Company to create the first engineering ATD, "Sierra Sam" for aviation testing in 1949. This was a "95th percentile ATD", meaning it modeled the 95th percentile of human males in height, width, and proportion. A subsequent '5th percentile' female ATD was also produced. When General Motors and Ford requested for an ATD, ARL and Sierra Engineering built two different competing models. GM, dissatisfied with both, combined the best characteristics of each to create a new ATD called Hybrid I in 1971. This was a 50th percentile male ATD, meaning it represented the average male. An ATD with improvements in the shoulders, spine, and knees called Hybrid II was developed in 1972. The following year, Hybrid II 50th percentile ATD was introduced. The National Highway Transportation Safety Administration contracted with GM to improve a number of its features. A major setback to Hybrid I and II was that

they could only be used to test the effectiveness of seat belt designs. GM researchers developed the current line of crash test ATD's, Hybrid III, primarily to explore other areas of injury reduction.

The 50th percentile Hybrid III ATD was introduced in 1976. He is 69 in. (1.75 m) tall and has a mass of 170 lbs. (77 kg). He is used to in frontal crash testing in the driver's seat. The testing procedure for the Hybrid III ATD's involving calibration, including calibrating the head, neck, and knees separately before a crash test. Calibration marks on the ATD are used to aid researchers that review footage after a test. Since Hybrid III's main purpose is to access effects of frontal impacts, other ATD's, including the Side Impact ATD (measures rib, spine, and internal organ effects in side collisions), BioRID (observes rear impact effects), CRABI (measures effectiveness of child restraint devices), and THOR (advanced 50th percentile male ATD) were other ATD's designed to study the effects of other types of impact.

In addition to real life ATD's, the use of computer finite element models of humans and crash test ATD's for high acceleration and impact biomechanics studies have been proven valuable in studying the impacts of human injury. Livermore Software Technology Corporation develops free or low cost finite element models and crash test ATD's that come with sensors that measure forces, moments, displacements, and accelerations. They have many Hybrid III models. The Hybrid III 50th percentile male is a joint development with the National Crash Analysis Center at George Washington University.

Crash test ATD's and computer models have greatly helped efforts to minimize injury. With the rise of automated vehicles in the use of transportation, there has been a greater push to develop protective systems. Crash test devices, or anthropomorphic test devices, are now the most commonly used subjects to test protective systems. They have been proven to be close substitutes for humans, are more readily available than humans and animals, and therefore, have the potential to make a greater impact in a faster and more reliable way. In this study, a Hybrid III 50th percentile ATD was used as the most

representative ATD for occupants. To determine acceleration results of the ATD, several accelerometers were placed throughout the ATD in different body regions. The accelerometers were placed in the head, chest, left and right femur and left and right tibia. Figure 3-6 illustrates the different locations of the ATD accelerometers.

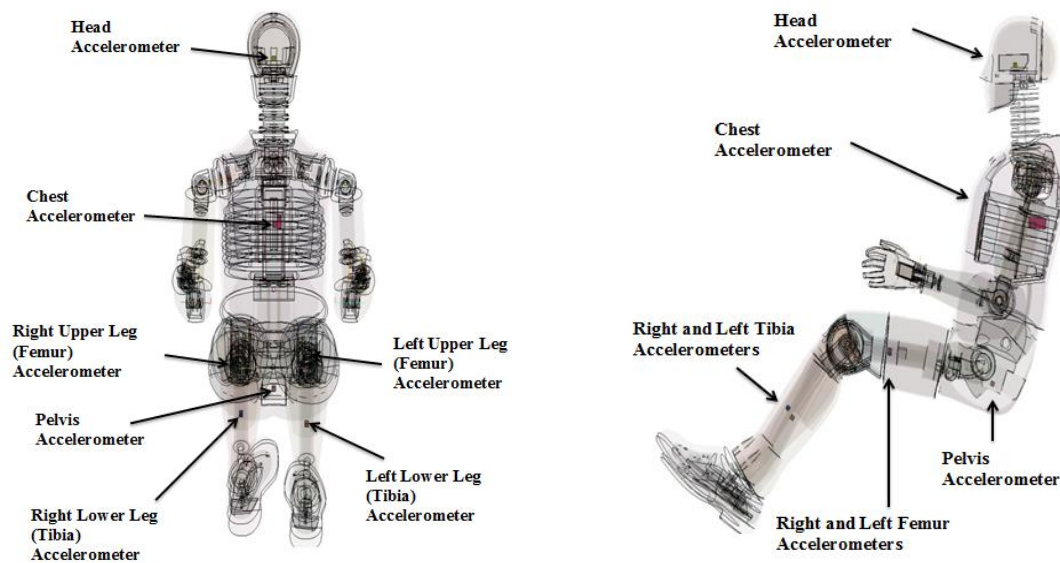


Figure 3-6. Front and Side View of Transparent ATD with Accelerometer

3.4 Injury Criteria

Another critical aspect of this study is the calibration of ATD injury predictions. Criteria for predicting injury have been developed that use responses of ATD's, as measured by internal instrumentation, to estimate risk of injury for a similarly exposed living human. The probability of injury is generally classified within the Abbreviated Injury Score (AIS) scale. This scale was created by the Association for the Advancement of Automotive Medicine (AAAM, 2001) and is used to classify and describe the severity of

individual injuries. It is a system to classify the trauma injuries into six different categories from 0 to 5 based on the severity. Table 3-5 summarizes the injury scaling according to AIS.

Below is a summary of injury criteria from previous tests for the different body regions of the ATD. A Hybrid III 50th percentile ATD was used in all the previous tests. A study conducted by Eppinger et al. (1999) on developing improved injury criteria summarized equations for each injury criteria which are further discussed in this section.

3.4.1 Head and Neck Injury Criteria

NHTSA performed injury analysis for frontal crashes to update frontal crash protection safety standards to improve protection of occupants. NHTSA regulations specify a Head Injury Criterion (HIC) that is determined based on the acceleration of the head during the crash (Versace, 1971). These values were determined from tests where acceleration pulses were applied to the ATD. Further head injury risk analysis was performed to determine the probability of skull fracture for injury severity greater than or equal to AIS 3. Along with head injury criteria NHTSA developed injury criteria for the neck. Injury criteria for the neck were developed based on tolerance limits for axial loads and bending moments. A standard 6-axis upper neck load cell records the values for axial loads and moments in all three directions. An injury risk curve was developed to determine the probability of injury based of the neck injury criteria. Table 3-8 further summarizes these injury criteria, equations, and parameters.

Table 3-8. Injury Criteria for Head and Neck

Injury Criteria	Equation	Parameters
Head Injury Criterion (HIC)	$HIC = \max \left[\left[\frac{\int_{t_2}^{t_1} a(t) dt}{t_2 - t_1} \right]^{2.5} (t_2 - t_1) \right]$	a(t) is resultant linear acceleration time of center of gravity of the head.

Table 3-8 Continued

Injury Criteria	Equation	Parameters
Probability of Skull Fracture (AIS \geq 3)	$p(fracture)$ $= N\left(\frac{\ln(HIC) - \mu}{\sigma}\right)$	μ and σ are statistical parameters of an HIC injury risk curve. $\mu = 6.96352$, $\sigma = 0.84664$
Neck Injury Criteria	$N_{ij} = \frac{F_z}{F_{int}} + \frac{M_y}{M_{int}}$	<ul style="list-style-type: none"> - F_z is the axial load - F_{int} - corresponding intercept value of load used for normalization - M_y is flexion/extension bending moment - M_{int} is corresponding intercept value used for normalization
Probability of Neck Injury	$p(AIS \geq 3)$ $= \frac{1}{1 + e^{2.054 - 1.195N_{ij}}}$	N_{ij} is corresponding resultant Neck Injury Criteria

3.4.2 Thoracic Injury Criteria

Seventy-one frontal impact sled tests were examined and analyzed to determine thoracic injury criteria for the ATD. Injury risk curves were developed to analyze the risk of injury based off the maximum chest deflection, spinal acceleration, and combined

thoracic injury criteria. According to US-NCAP, the thorax injury criteria is predicted using chest deflections which is limited to 2.48 in. (63 mm) and chest accelerations which is limited to 60 G. Table 3-9 summarizes the injury criteria and probability of injury for the thorax.

Table 3-9. Injury Criteria for Thorax

Injury Criteria	Equation	Parameters
Probability of thoracic injury	$p(AIS \geq 2) = \frac{1}{1 + e^{(1.8706 - 0.04439D_{max})}}$ $p(AIS \geq 3) = \frac{1}{1 + e^{(1.2324 - 0.0576Ac)}}$ $p(AIS \geq 4) = \frac{1}{1 + e^{(4.847 - 6.036CTI)}}$	<ul style="list-style-type: none"> - D_{max} is maximum chest deflection - Ac is spinal acceleration - CTI is the resultant combined thoracic injury
Combined Thoracic Injury Criteria (CTI)	$CTI = \frac{A_{max}}{A_{int}} + \frac{D_{max}}{D_{int}}$	<ul style="list-style-type: none"> - A is value of spinal acceleration - D is value of ATD deflection.

3.4.3 Leg Injury Criteria

Analysis of the National Automotive Sampling System/ Crashworthiness Data System was conducted during the years 1993 to 1999 to determine the risk of injury to different regions of the body in frontal crashes. Specifically lower extremity injuries were analyzed due to being the most frequent AIS 2+ injured body region for occupants in airbag equipped vehicles. Lower extremity injury criteria was determined for different

regions of the lower body including, knee-thigh-hip complex fractures, knee ligament tears, tibial plateau/condyle fractures, tibia/ fibula shaft fractures, calcaneus, ankle and midfoot fractures, malleolar ligament and ankle injuries. A summary for probability of injury to the different regions of the lower body can be seen in Table 3-10.

Table 3-10. Injury Criteria for Leg

Injury Criteria	Equation	Parameters
Probability of KTH injury	$p(AIS\ 2+) = \frac{1}{1 + e^{(5.7949 - 0.5196F)}}$ $p(AIS\ 3+) = \frac{1}{1 + e^{4.9795 - 0.326F}}$	F is femur axial force
Injury Criteria for Tibia and Fibula Shaft Fractures	$TI = \frac{F}{F_c} + \frac{M}{M_c} < 1$	<ul style="list-style-type: none"> - F is measured compressive axial force - M is measured bending moment in the leg - M_c and F_c are critical values of bending moment and axial compressive force in tibia.
Probability of leg fracture versus Revised Tibia Index (RTI)	$p(AIS\ 2+) = 1 - \exp\left(-e^{\frac{\ln(RTI) - 0.2728}{0.2468}}\right)$ $\text{where, } RTI = \frac{M}{240} + \frac{F}{12}$	<ul style="list-style-type: none"> - F is measured compressive axial force - M is measured bending moment in the leg

Table 3-10 Continued

Probability of Foot Injury	$p(AIS\ 2+) = \frac{1}{1 + e^{4.572 - 0.670F}}$	F is lower tibia axial force
----------------------------	---	--------------------------------

Injury risk curves were established with the help of the above equations for computing the probability of injury risks of head, chest, neck and legs and certain reference values were set up for each occupant injury risk. These are tabulated in Table 3-11.

Table 3-11. Injury Assessment Reference Values

Injury Criteria	IARVs
HIC -15	700
Neck Tension Force	937 lbs. (4.17 kN)
Neck Compression Force	900 lbs. (4 kN)
Chest Accelerations	60 G
Chest Deflections	2.48 in. (63 mm)
Femur Axial Force	2248 lbs. (10 kN)
Tibia Axial Force	1798 lbs. (8 kN)

3.5 Restraint Systems

The development of restraint systems in recent history have been an important advocate in reducing the potential for serious injuries from automobile crash incidents. The following will include an overview of common seat-belt restraint systems including two to six-point systems, belt-in-seats, and the process used to develop our restraint system.

Two-point belts that attach at two endpoints include lap belts and sashes. The lap belt was introduced in 1957 by Stapp. The primary purpose of the lap belt was to prevent occupants from crashing into the car interior since they moved with the car during a crash incident. Serious injury caused by crashing into the car's interior was an imminent problem for unrestrained occupants. The lap belt was a band that wrapped tightly around the occupant's pelvis and ran down to the floor where it was bolted down by screws. Lap belts were only successful in restraining occupants from crashing into the car's interior in large vehicles, as the distance to the interior was larger than in smaller vehicles. Lap belts are now only primarily used in older cars. Sashes go over the shoulder and are buckled by the lap. Sashes are used in conjunction with lap belts. Otherwise, the occupant would slip out of the belt, resulting in a frontal collision.

3.6 Previous Research Efforts

There are a number of past researches developed on the evaluation criteria of roadside safety devices and the risk of occupant injuries. Full scale crash tests have been employed previously to compare the roadside crash test injury criteria to vehicle crashworthiness. Also researchers have put efforts to understand the risk of occupant injury with the help such as event data recorders (EDRs) (Gabauer and Gabler, 2005).

Thomson and Gabauer (2005) made an attempt to correlate between vehicle dynamics to crash test injury criteria using the flail space model with various restrained conditions of airbag and seatbelt. Twenty-four crash tests were conducted and 44 occupant responses were noted to relate Head Injury Criteria (HIC), chest deflections and accelerations and maximum femur forces against the flail space parameters, i.e., occupant impact velocity (OIV), occupant ride down accelerations (ORA) and acceleration severity index (ASI). Fifty percent of these tests were performed on passenger cars with most of the tests having ATD's in the drivers' position and the front seat passenger. The remaining of the tests was performed on vehicles which include pickup trucks, sport utility vehicles, full size minivans, etc. The tests conducted with various restraint conditions, vehicle speeds and occupant responses are given in Table 3-12.

The OIV and ORA were evaluated as per the NCHRP Report 350 criteria whereas ASI was calculated in a slightly modified manner. Since the tests were fully frontal, information regarding accelerations only pertaining to longitudinal direction was available. It was then assumed that the lateral and vertical motion of the vehicle were negligible, which simplified the ASI calculation to a maximum 50 ms average acceleration over the pulse, divided by the respective acceleration limit in longitudinal direction (12 G).

Table 3-12. Summary of Selected Full Scale Crash Test (Gabauer and Gabler, 2006)

Test Speed/type	Number of tests	Occupant Responses	Restraint Status
25/frontal	4	8	Airbag only
30/frontal	4	8	Airbag only
35/frontal	12	24	Airbag and Belt
40/frontal offset (40%)	3	3	Airbag and Belt
40/frontal	1	1	Airbag and Belt

Each of the roadside evaluation criteria was correlated to the occupant injury criteria and was plotted individually as function of HIC, chest deflections and accelerations and leg injury. Researchers concluded that HIC and chest deflections severely depend on vehicle restrained conditions; ORA appeared to have stronger correlation with HIC, whereas ASI appeared to have stronger correlation with chest accelerations.

An attempt was also made by Gabauer and Gabler (Gabauer and Gabler 2008b) to adjust the maximum change in vehicle velocity over the duration of a crash event to improve the prediction of chest acceleration. The assumption was that the occupant response is a linear function of primarily the vehicle crash severity, performance of the vehicle and occupant restraint performance. Vehicle crash severity is measured in terms of change in

vehicle velocity after collision event and the average acceleration. The performance of the vehicle is measured by the ridedown efficiency, moving average accelerations and relative centroid location of the vehicle. The occupant restraint performance is measured by restraint quotient which is typically computed for the thorax and the relative kinetic energy factor. Full scale crash tests were performed on a vehicle impacting a flat rigid barrier with a 50th percentile male ATD seated in drivers position and restrained with either a seatbelt or an airbag or both. These metrics are calculated by the methods and relations provided in the article. They were then correlated using linear regression analysis and was found that the augmentation of maximum change in velocity improves the prediction of 3ms chest clip of the occupant. However, this work had limitations in view of vehicle speed. There is a possibility that both vehicle structure and occupant restraint performance may vary with impact speed, degree of impact and object collided due to which approximately 98% of the case studies have a delta-V value ranging from 30 to 45 mph (48 to 72 km/h). This study was also limited to only frontal barrier crash tests and the correlation may vary in a frontal offset test.

With recent updates in technology Gabauer and Gabler (2004) used Event Data Recorders Technology to attain more précised vehicle kinematics data to match with the occupant injury risk. These devices allow for an opportunity to obtain information on seatbelts, airbag deployment and vehicle speed prior to the impact. Based on the EDR data, OIV and ASI were evaluated along with Delta – V. To predict the probability of occupant injury risk in frontal collisions, this study has generated injury risk curves, however, it was found that the more computationally intensive OIV and ASI offered no significant advantage over the simple Delta – V predictions.

These authors also worked on comparing the comparing the roadside and vehicle crash test injury criteria in frontal crash tests. The flail space model that is used for evaluation criteria of the roadside safety features assumes that the occupant is unrestrained. But in recent years, there has been a drastic increase of seatbelts and airbags which urges a need to revisit these criteria. The occupant injury risk is related to the impact velocity of

the occupant with the interior of the vehicle and is measured using the vehicle kinematics. Although there were previous attempts made to link flail space model to the occupant injury (Ray et al., 1986; Council and Stewart, 1993) there were limitations of these methods due to unrestrained occupants. Gabauer and Gabler (2008b) made attempts to compare the risk of head and chest injury of a restrained occupant to the roadside evaluation criteria.

Similarly, the chest injury criterion used in this research work is taken based on the limitations on maximum acceleration of 60 G and maximum chest deflection of 2.5 in. (63 mm) set by NHSTA. The injury risk is computed based on the values of head and chest injury criteria using the following equations tabulated in Table 3-13.

Table 3-13. Equations used for Computing Injury Risk from Head and Chest Injury Criteria

Body region	Injury criteria	Probability of AIS 3+
Head	15 ms (HIC)	$p(AIS \geq 3)$ $= \frac{1}{1 + e^{((3.39 + \frac{200}{HIC}) - 0.00372HIC)}}$
Chest	3 ms (G)	$p(AIS \geq 3) = \frac{1}{1 + e^{3.1493 - 0.0630A_c}}$

The ATD based occupant risk and roadside occupant risk were first compared graphically and a combined probability of AIS 3+ was calculated as shown in Equation (3-3).

$$p(Head/Chest) = p(head) + p(Chest) - p(head) * p(chest) \quad (3-3)$$

Different types of crash tests such as frontal crash cushion test, frontal offset barrier crash test were performed and the probability of serious injury of the occupants with various restrained conditions were plotted against the different types of vehicle used.

Table 3-14 shows the crash test results performed with different vehicles at different speeds and restrained conditions along with the range of probability of injury risk.

Table 3-14. Crash Test Results as per (Gabauer and Gabler 2008a)

S. No	Figures	ATD/ Restrained System	Speed, mph (km/h)	Range of Combined head and chest injury probability (%)	Occupant Impact Velocity, ft/s (m/s)
1.	Figure 3-7	Hybrid III 50th% males with only an airbag restraint	25 (40)	16 - 58	40 +/- 2.64 (12.2 +/- 0.8)
2.	Figure 3-8	Hybrid II 50th% males with only a three-point belt restraint	30 (48)	18 - 94	46 +/- 5 (14 +/- 1.5)
3.	Figure 3-9	Hybrid III 50th% males with airbag and three- point belt restraints	35 (56)	30 - 68	53 +/- 3.28 (16 +/- 1)

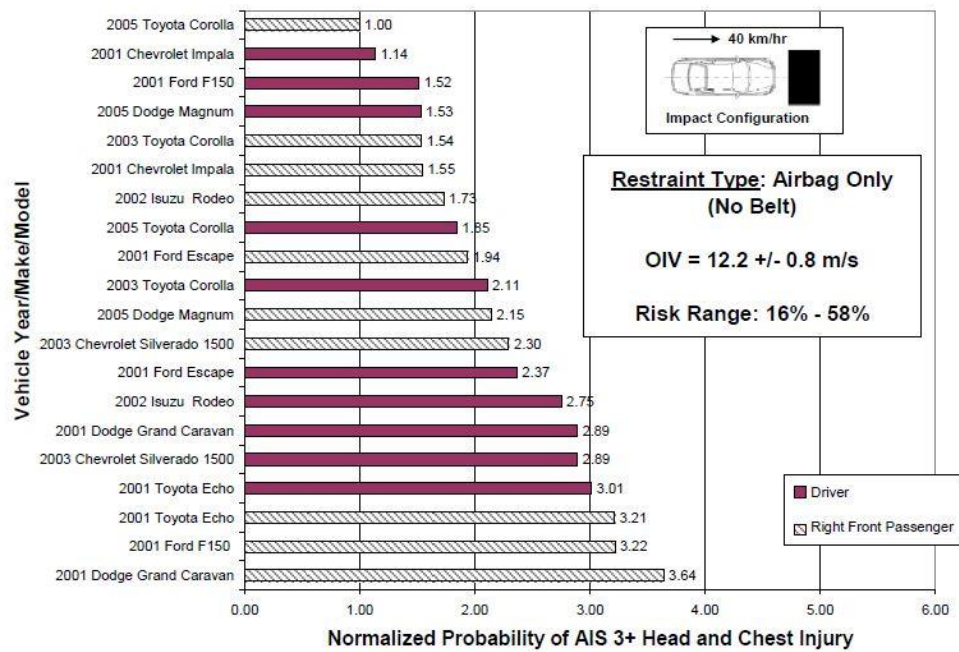


Figure 3-7. Probability of Head and Chest Injury to Occupants Restrained with Airbag Only (Gabauer and Gabler, 2008a)

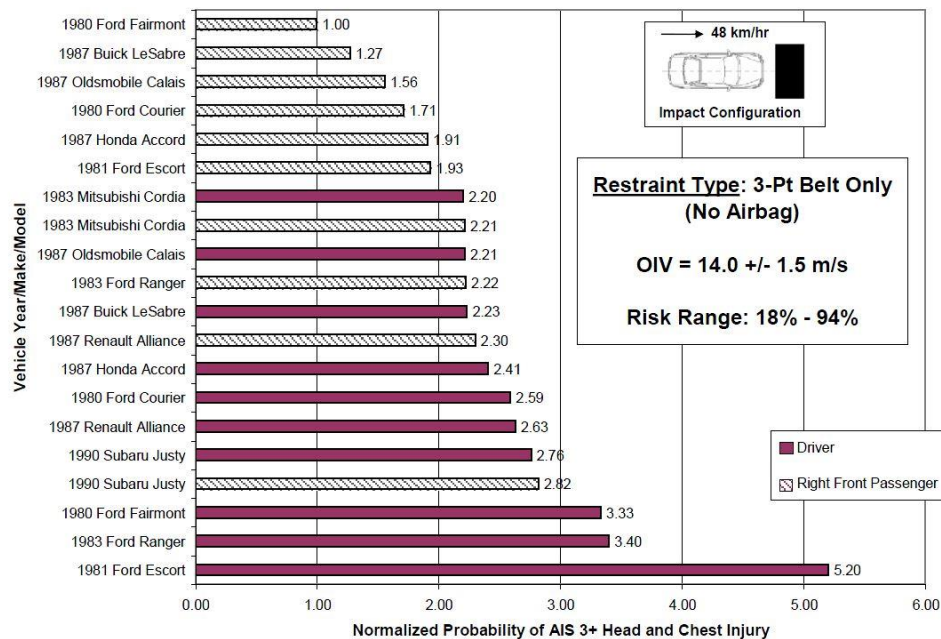


Figure 3-8. Probability of Head and Chest Injury to Occupants Restrained with 3-Point Seatbelt Only (Gabauer and Gabler, 2008a)

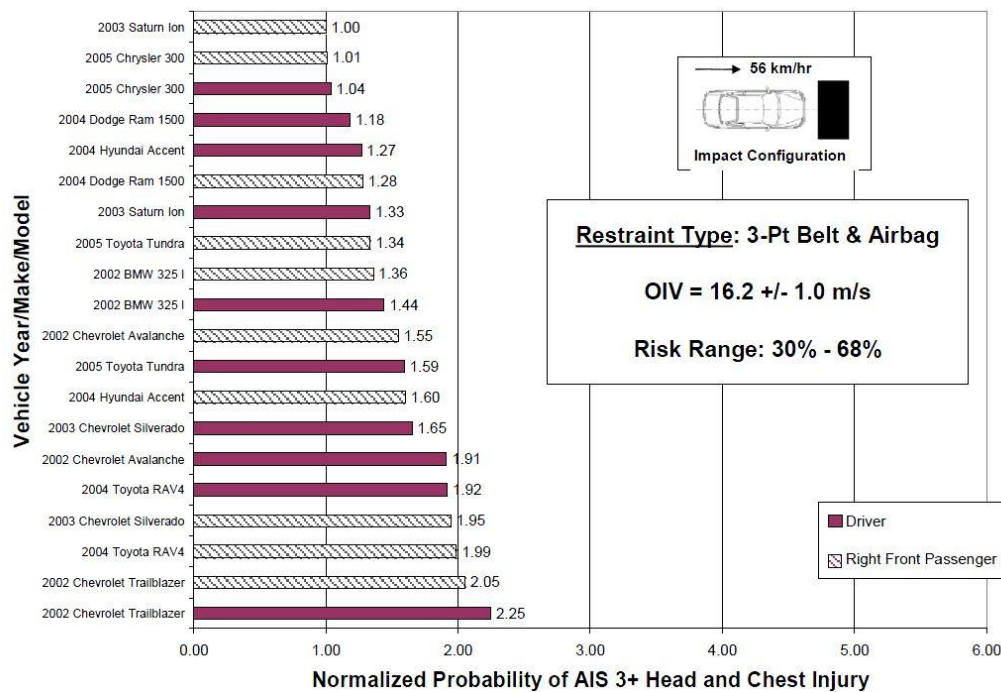


Figure 3-9. Probability of Head and Chest Injury to Occupants Restrained with 3-Point Seatbelt and Airbag (Gabauer and Gabler, 2008a)

Linear regression analysis was performed in the research to correlate between the ATD based injury criteria and the roadside safety feature evaluation criteria and it was concluded that the flail space algorithm no longer a correct prediction of variation in occupant risk for unbelted, belted, airbag only or belt and airbag restrained occupants.

Past research suggests that the flail space algorithm does not predict the difference in occupant injury risk in different restrained conditions. The roadside metrics are solely based on the response of the vehicle and not on the occupant injury risk. In addition, large improvements to occupant protection, whose contribution is not being considered within MASH occupant risk criteria, can significantly reduce the risk of injury to an occupant in a collision. Therefore, there is potential for increasing the maximum limits dictated in MASH for occupant risk evaluation. This becomes extremely important for designing and evaluating barrier systems that must fit within geometrical site constraints,

which do not provide adequate length to redirect test vehicles according to MASH conservative evaluation criteria.

4. FINITE ELEMENT MODELS OF COMPONENTS FOR COMPUTER SIMULATIONS

The following section mentions the details about each component of the FE model used for computer simulations namely the Toyota Yaris, Hybrid III instrumented 50th percentile male ATD, seatbelt model and the airbag model.

4.1 Finite Element Model of Toyota Yaris

For the present research, the FE model of a Toyota Yaris of model 2010 is used. The complete detailed model that is publicly available on the NCAC website (<http://www.ncac.gwu.edu/vml/models.html>) is validated against frontal crash testing. However, a notable limitation regarding this model is that the interior parts of the car were not validated. Though the detailed model with 1,480,426 nodes and 1,514,068 elements is available, a reduced model with 393,120 nodes and 378,352 elements is used in this research to save computational time. Figure 4-1 shows the FE model of 2010 Toyota Yaris.

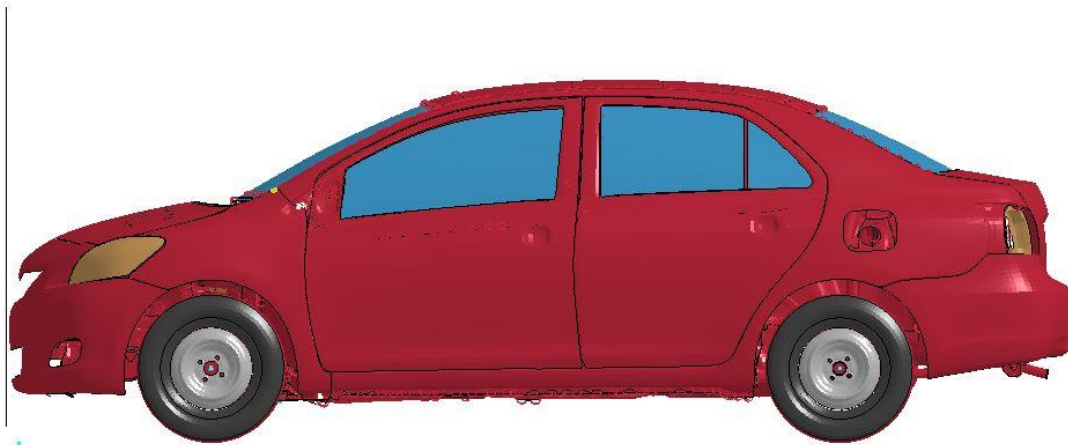


Figure 4-1. FE Model of Toyota Yaris 2010

4.2 Finite Element Model of Hybrid III Anthropomorphic Test ATD

The Hybrid III 50th Percentile Male Crash Test ATD is the most widely used crash test ATD in the world for the evaluation of automotive safety restraint systems in frontal crash testing. Figure 4-2 shows the FE model of H3 ATD.

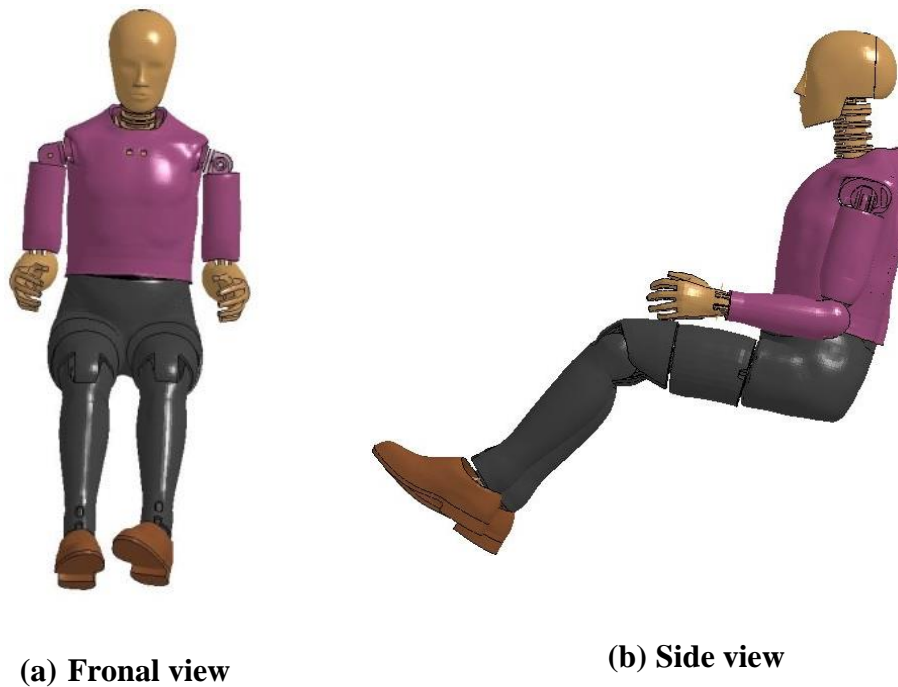


Figure 4-2. FE Model of H3 50th Percentile ATD

The total weight of the ATD is 171 \pm 2.6 lbs (77 \pm 1 kg). with external dimensions design criteria as listed in Table 4-1.

Table 4-1. External Dimensions of the ATD

Description	Dimensions (in)	Dimensions (mm)
Total Sitting Height	34.8+/-0.2	883 +/- 5
Shoulder Pivot Height	20.2+/-0.3	513 +/- 7.63
Shoulder to Elbow	13.3+/-0.3	338 +/- 7.63
Buttock to Knee	23.3+/-0.5	592 +/- 12.7
Knee Pivot to Floor	19.4+/-0.3	237 +/- 7.63
Chest Depth	8.7+/-0.3	221 +/- 7.63
Foot Length	10.2+/-0.3	260 +/- 7.63
Foot Width	3.9+/-0.3	96.5 +/- 7.63
Shoulder Width	16.9+/-0.3	430 +/- 7.63
Chest Circumference	38.8+/-0.6	985.5 +/- 15.24
Waist Circumference	33.5+/-0.6	851 +/- 15.24

4.3 Finite Element Model of Seatbelt

A generic model of seatbelt available on LSTC website is being used for the present research. The seatbelt model consists of 833 nodes and a total of 1259 elements.

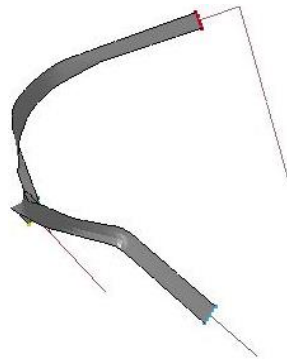


Figure 4-3. FE Model of Seatbelt

The FE model presently used consists of general 1D seatbelt elements and 2D shell elements. Also, several specialized elements were used to model specific parts of the seatbelt such as the pretensioner, retractor, and D-ring. The general seatbelt element is represented with a material that contains loading and unloading curves based on force vs. engineering strain.

Figure 4-4 represents the material curves used in this study. The beam-like elements exert force only in tension and generate zero force whenever the strain is negative.

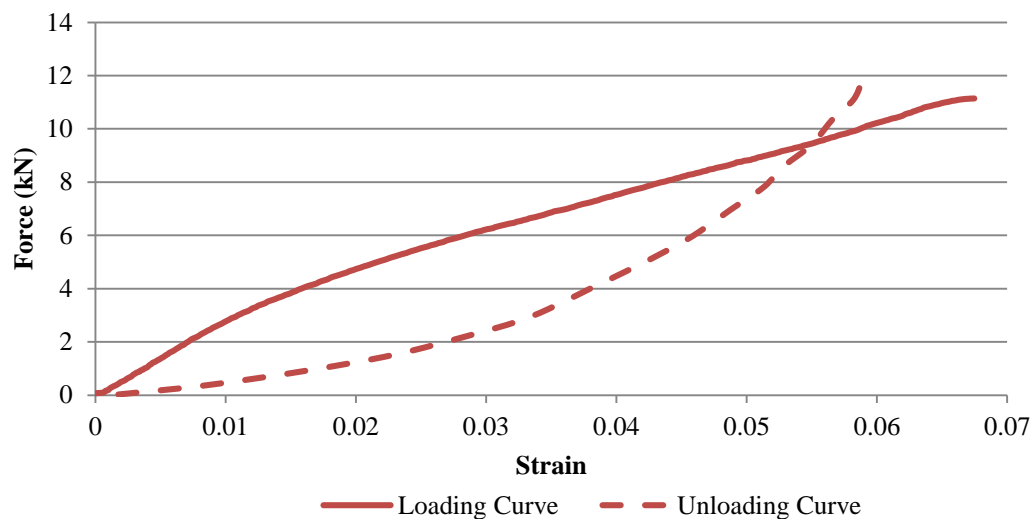


Figure 4-4. Belt Material Force versus Strain Loading and Unloading Curves

UMTRI researchers provided a working FE model of a seatbelt and the material, retractor, and pretensioner curves were implemented in the seatbelt model used in this study.

4.3.1 Retractor

Retractors operate in two different ways and allow belt material to be paid out or reeled in. The first way a retractor operates is in the unlocked role, where the belt material is

paid out, or reeled in under constant tension. The second way a retractor operates is the locked role, where a user-defined force-pullout curve applies. A seatbelt sensor element fires and acts on the retractor causing it to enter into a locked state and allowing the force-pullout relationship to take over. The sensor fires at 1 ms after the simulation has begun. When the belt is in tension the retractor will give out belt material by lengthening the last element attached to the retractor. The last element will lengthen based on the force-pullout relationship of the retractor that is shown in Figure 4-5.

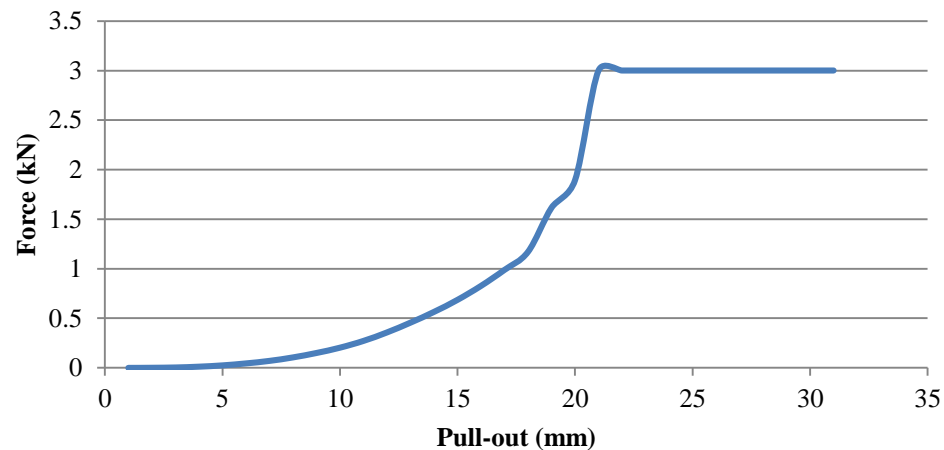


Figure 4-5. Seatbelt Retractor Curves Representing Force versus Payout

The load limit on the retractor curve has been set to 3 kN to match the maximum shoulder belt force measured in the crash test.

4.3.2 Pretensioner

A pretensioner was used in conjunction with the retractor to remove initial slack. Similar to the retractor, the pretensioner fires based on a timed seatbelt sensor. Once the sensor is triggered at 10 ms, the pretensioner fires and pulls in belt material to create 1.8 kN of tension in the belt. Once the tension in the belt reaches 1.8 kN the pretensioner disengages and the retractor takes over again.

Table 4-2 shows a step-by-step process of the retractor and pretensioner working together.

Table 4-2. Process for Seatbelt Modeling of Retractor and Pretensioner

Event	Action
1 ms	Retractor sensor fires – enters locked mode
10 ms	Pretensioner sensor fires – enters locked
1.8 kN tension reached	Pretensioner disengages – retractor active
3 kN tension reached	Load limiter engages

4.3.3 D-Ring

There are two D-ring elements used in the three-point belt system. One is used for the lap belt and the other is used for the shoulder belt. D-rings allow the seatbelt to be redirected with the option of adding some friction to the moving seatbelt. A friction coefficient of 0.3 is used in the present study. The location of the D-ring and anchor positions is very important when modeling a seatbelt. Exact positions were provided by UMTRI as part of the cloud point scans for the D-ring and anchors. After the D-ring and anchor points were set for the FE seatbelt model an LS-PrePost seatbelt fitting tool was used to fit the seatbelt around the ATD chest and pelvis. Figure 4-6 shows ATD placed in the seat and restrained with seatbelt.

4.4 Finite Element Airbag Model Development

The primary purpose of airbags is to protect passengers in head-on collisions. It is a folded nylon bag which becomes inflated with nitrogen gas after impact. An airbag responds within milliseconds of a crash.

The National Crash Analysis Center (NCAC) developed a working FE model of a steering wheel and airbag that is publicly available for download on their website. This

airbag model was used in our frontal simulation to analyze the effects of an airbag restraint system on occupant injury criteria. The airbag model consists of 4742 nodes and 4588 elements. Figure 4-7 shows (a) the folded FE airbag before inflation and (b) the fully inflated airbag.

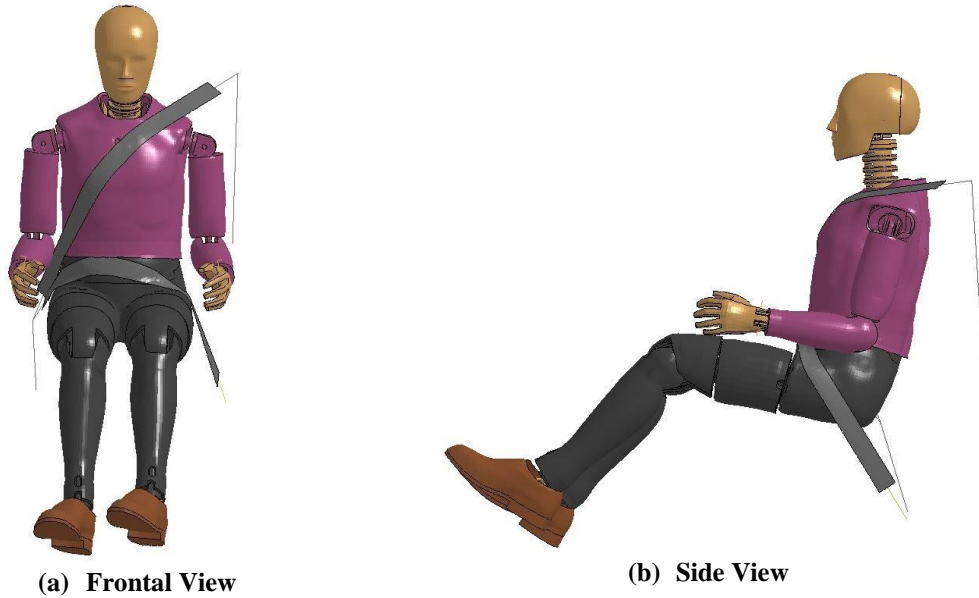


Figure 4-6. ATD Placed in Position and Restrained with Seatbelt

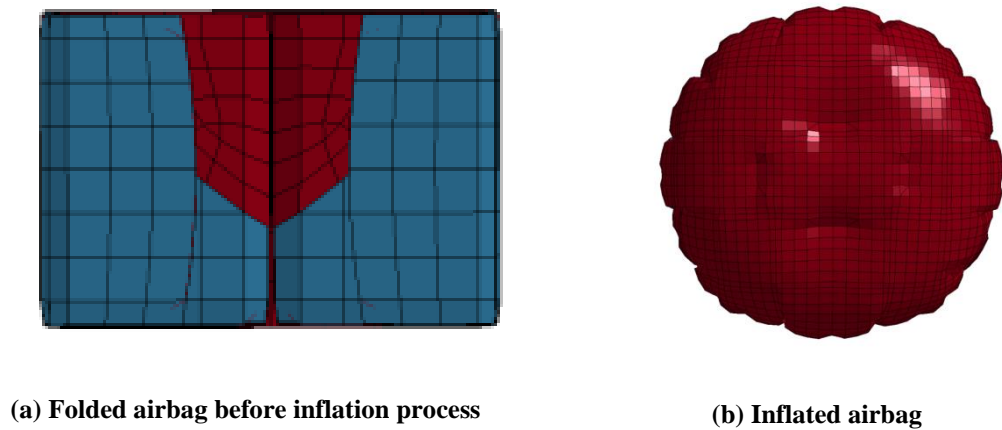


Figure 4-7. Finite Element Computer Model of the Airbag

The steering wheel used in Toyota Yaris has different geometrical dimensions relative to the FE steering wheel containing the airbag. Therefore the airbag was placed within our car by replacing the steering wheel with the airbag and connected it to the steering rod of the car as the original steering wheel was connected. Figure 4-8 compares the NCAC steering wheel to the truck cabin steering wheel. Figure 4-9 shows how the Original steering wheel (left) replaced with the steering wheel with airbag (right) and connected to the steering main rod in a similar manner.

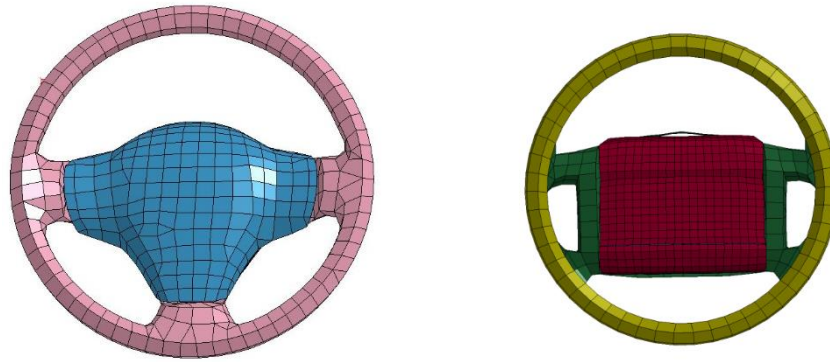


Figure 4-8. Comparison of NCAC Toyota Yaris FE Steering wheel (Left) and FE Steering Wheel (Right)

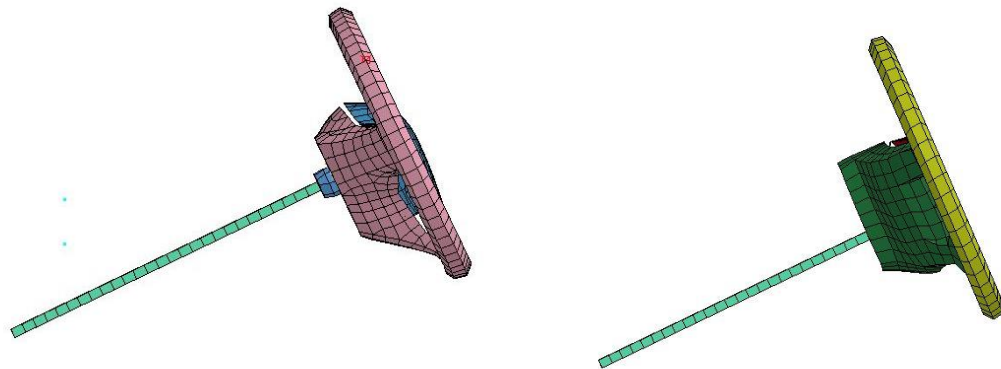
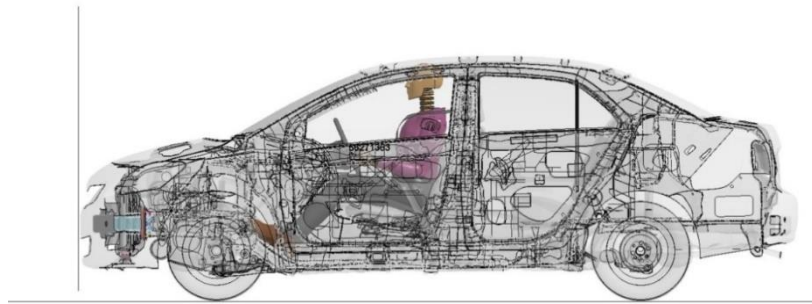


Figure 4-9. Original Steering Wheel (Left) Replaced with Steering Wheel with Airbag (Right) and Connected to Steering Main Rod in a Similar Manner

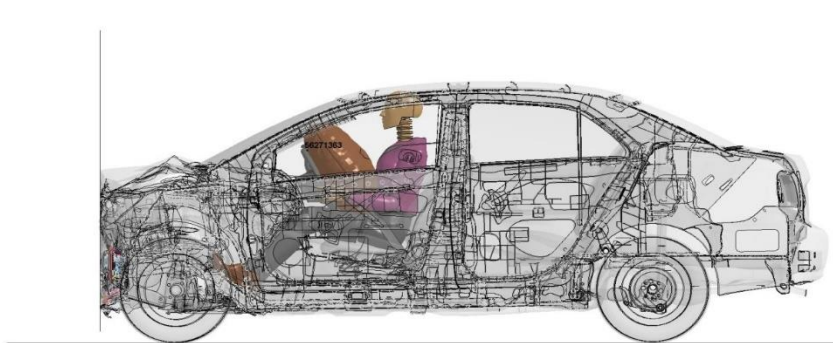
The input curve used to inflate the airbag was developed as mass flow rate into the airbag versus time. 25 ms after impact the airbag begins to inflate, and it takes approximately 25 ms more to achieve full inflation during the test. The airbag inflation input curve from the NCAC model was modified according to these two parameters. In general the deflation of the airbag is controlled by the venting size. To replicate this scenario, a negative mass flow rate curve is used. This was adjusted to match the test data. The stiffness of the airbag plays an important role on the rebound of the ATD after collision. The deflation of the airbag curve has been modelled with a negative mass flow rate to replicate the test scenario. The airbag was only implemented and analyzed for the frontal crash scenario.

5. FINITE ELEMENT PREDICTIVE SIMULATIONS

This section describes the finite element computer simulations performed to check for compatibility and robustness of the model assembly. Figure 5-1 shows the ATD properly positioned in the vehicle and restrained with seatbelt and airbag. The ATD model was positioned in the driver seat and was restrained with seatbelts. Computer simulations of a full frontal barrier impact where the direction of travel of the vehicle is perpendicular to the plane of the barrier were performed at impact speeds of 25 mph (40 km/h), 30 mph (48 km/h), 35 mph (56 km/h)



(a) ATD Placed in with Seatbelt (Just Before Crash)



(b) ATD Placed in with Seatbelt (Just After Crash)

Figure 5-1. ATD Placed in Position and Restrained with Seatbelt and Airbag

5.1 Initial Simulations at Different Speeds

Figure 5-2 through Figure 5-10 shows frames of the simulated crash event, performed at different speeds.





Time (s)	FE Model of Car, ATD and Restraints (25 mph, 40 km/h)
0.000	
0.02	
0.06	
0.085	

Figure 5-2. Sequential Images of Toyota Yaris with Positioned ATD and Restrained with Seatbelt and Airbag @ 25 mph (Side View)





Time (s)	FE Model of Car, ATD and Restraints (25 mph, 40 km/h)
0.000	
0.02	
0.06	
0.085	

Figure 5-3. Sequential Images of Toyota Yaris with Positioned ATD and Restrained with Seatbelt and Airbag @ 25 mph (Perspective View)



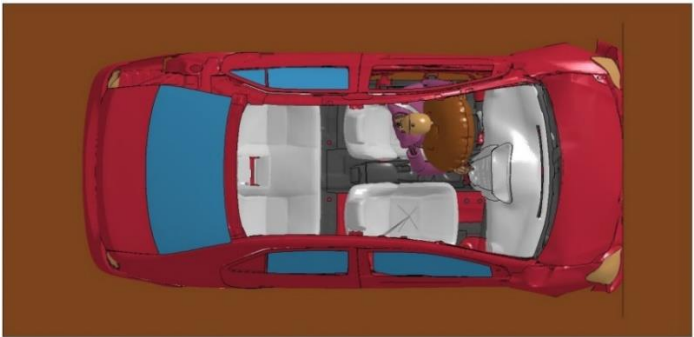
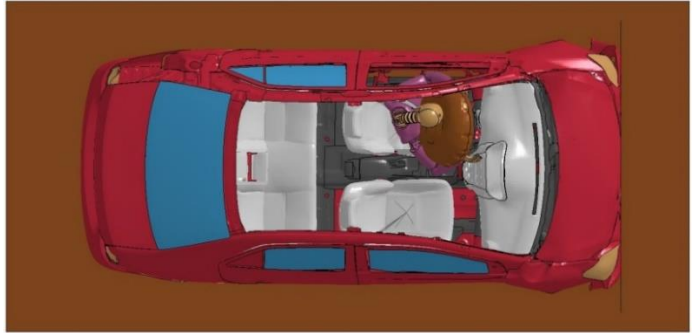
Time (s)	FE Model of Car, ATD and Restraints (25 mph, 40 km/h)	
0.000		 A top-down view of a red Toyota Yaris. The interior is shown with white seats and a blue dashboard. A purple ATD (Anthropomorphic Test Dummy) is seated in the driver's seat, facing forward. The car is on a brown surface.
0.02		 A top-down view of the same red Toyota Yaris. The purple ATD is now slightly tilted back, and a yellow airbag is visible deployed from the dashboard area. The car is on a brown surface.
0.06		 A top-down view of the same red Toyota Yaris. The purple ATD is now fully reclined, and the yellow airbag is fully deployed, covering the ATD's head and upper torso. The car is on a brown surface.
0.085		 A top-down view of the same red Toyota Yaris. The purple ATD is now fully reclined, and the yellow airbag is fully deployed, covering the ATD's head and upper torso. The car is on a brown surface.

Figure 5-4. Sequential Images of Toyota Yaris with Positioned ATD and Restrained with Seatbelt and Airbag @ 25 mph (Top View)




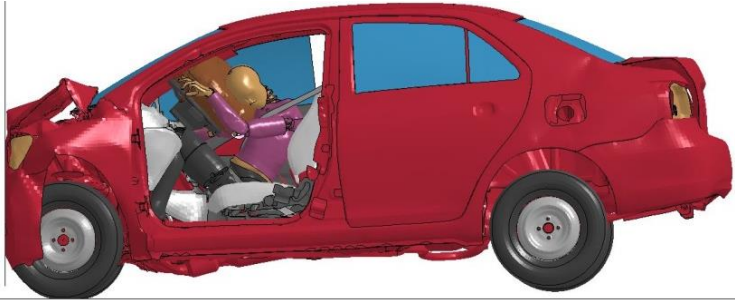
Time (s)	FE Model of Car, ATD and Restraints (30 mph, 48 km/h)
0.000	
0.02	
0.06	
0.085	

Figure 5-5. Sequential Images of Toyota Yaris with Positioned ATD and Restrained with Seatbelt and Airbag @ 30 mph (Side View)





Time (s)	FE Model of Car, ATD and Restraints (30 mph, 48 km/h)
0.000	 A red Toyota Yaris sedan is shown from a side-rear perspective. The driver-side door is open. A pink and white ATD (Anthropomorphic Test Dummy) is seated in the driver's seat, facing forward. A vertical brown barrier is positioned to the left of the car, representing a wall or obstacle.
0.02	 The car and ATD are shown at 0.02 seconds. The ATD is beginning to move forward, and the front of the car is slightly deformed by the impact with the barrier.
0.06	 At 0.06 seconds, the ATD is further forward, and the front of the car shows more significant deformation. The barrier is still visible to the left.
0.085	 At 0.085 seconds, the ATD is in a more pronounced forward position, and the front of the car is heavily deformed. The barrier is still visible to the left.

Figure 5-6. Sequential Images of Toyota Yaris with Positioned ATD and Restrained with Seatbelt and Airbag @ 30 mph (Perspective View)

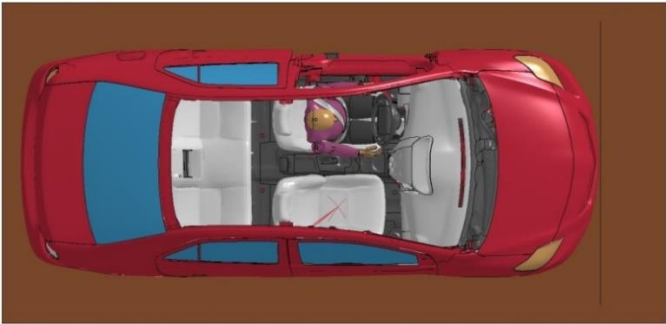

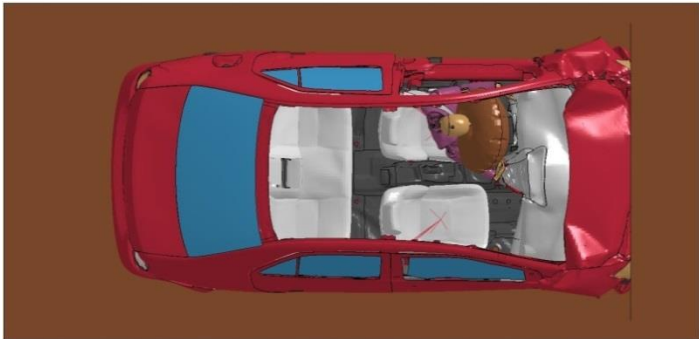
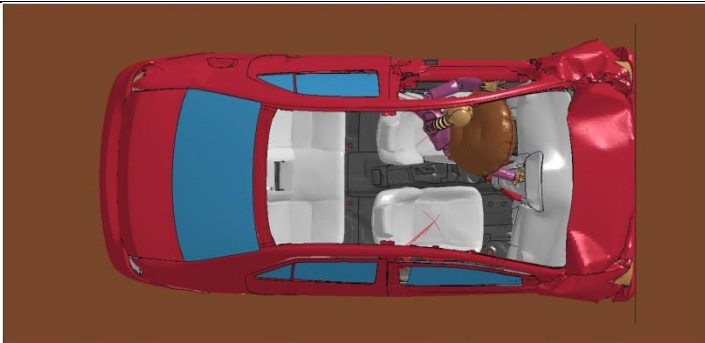
Time (s)	FE Model of Car, ATD and Restraints (30 mph, 48 km/h)
0.000	 A top-down view of a red Toyota Yaris. The interior is white. A purple ATD is seated in the driver's seat. The car is on a brown surface.
0.02	 A top-down view of the same car. The purple ATD is now shifted slightly to the right. A yellow airbag is visible in the center console area.
0.06	 A top-down view of the car. The purple ATD is shifted further to the right. The yellow airbag is now fully deployed from the center console.
0.085	 A top-down view of the car. The purple ATD is shifted even further to the right. The yellow airbag is fully deployed and appears to be in contact with the ATD.

Figure 5-7. Sequential Images of Toyota Yaris with Positioned ATD and Restrained with Seatbelt and Airbag @ 30 mph (Top View)

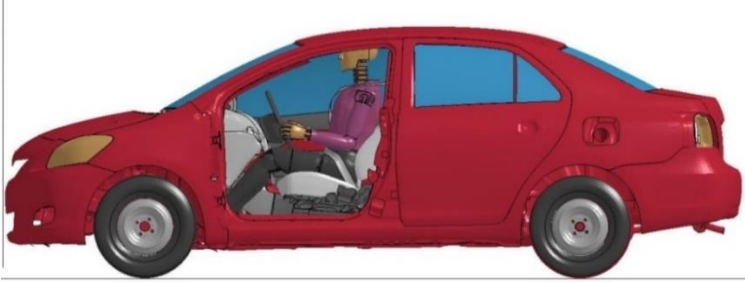



Time (s)	FE Model of Car, ATD and Restraints (35 mph, 56 km/h)
0.000	
0.02	
0.06	
0.085	

Figure 5-8. Sequential Images of Toyota Yaris with Positioned ATD and Restrained with Seatbelt and Airbag @ 35 mph (Side view)





Time (s)	FE Model of Car, ATD and Restraints (35 mph, 56 km/h)
0.000	 A red Toyota Yaris sedan is shown in a perspective view, facing left. The car is positioned on a brown ground plane. A vertical brown barrier is located to the left of the car. The car's interior is visible, showing a pink ATD (Anthropomorphic Test Dummy) seated in the driver's seat. The car is in its initial state, before the impact.
0.02	 The car and ATD are shown at 0.02 seconds. The car's front end is slightly deformed, and the ATD is beginning to move forward, indicating the start of the impact.
0.06	 The car and ATD are shown at 0.06 seconds. The car's front end is significantly deformed, and the ATD is moving forward, indicating the peak of the impact.
0.085	 The car and ATD are shown at 0.085 seconds. The car's front end is severely deformed, and the ATD is moving forward, indicating the end of the impact.

Figure 5-9. Sequential Images of Toyota Yaris with Positioned ATD and Restrained with Seatbelt and Airbag @ 35 mph (Perspective View)

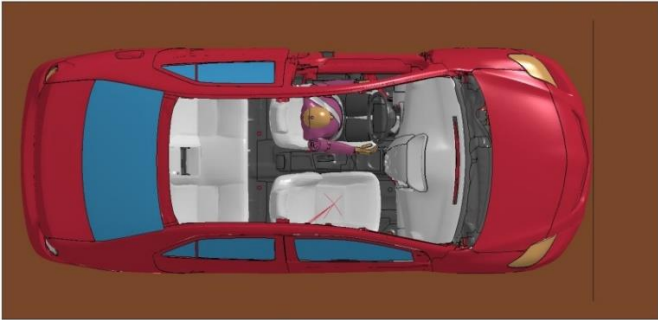

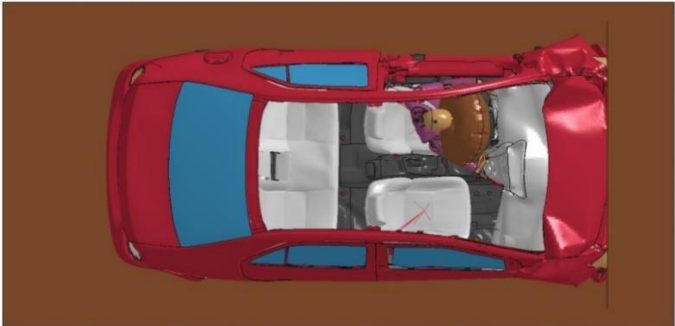
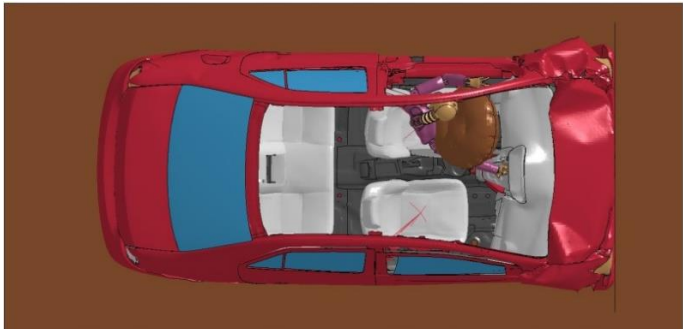
Time (s)	FE Model of Car, ATD and Restraints (35 mph, 56 km/h)	
0.000		 A top-down view of a red Toyota Yaris. The interior is white. A purple ATD is seated in the driver's seat, wearing a seatbelt. The car is on a brown surface.
0.02		 A top-down view of the same car at 0.02s. The ATD is now wearing a yellow airbag. The airbag is inflated and positioned in front of the ATD. The car is on a brown surface.
0.06		 A top-down view of the same car at 0.06s. The ATD is now wearing a yellow airbag. The airbag is inflated and positioned in front of the ATD. The car is on a brown surface.
0.085		 A top-down view of the same car at 0.085s. The ATD is now wearing a yellow airbag. The airbag is inflated and positioned in front of the ATD. The car is on a brown surface.

Figure 5-10. Sequential Images of Toyota Yaris with Positioned ATD and Restrained with Seatbelt and Airbag @ 35 mph (Top View)

5.2 Occupant Risk Assessment

The Test Risk Assessment Program (TRAP) program was used to evaluate occupant risk factors based on the applicable *MASH* safety evaluation criteria. The modeled Toyota Yaris remained upright during and after the modeled collision events. Table provides a summary of results for the frontal collision of Toyota Yaris with H3 50th percentile ATD in the drivers' position and restrained with seatbelt and airbag. The occupant impact velocities and ridedown accelerations calculated for each simulated speed impact, i.e., 25 mph (40 km/h), 30 mph (48 km/h), 35 mph (56 km/h) are reported in Table 5-1.

Table 5-1. Occupant Risks Values at Different Speeds

Speed mph (km/h)	Occupant Impact Velocity ft/s (m/s)		Occupant Ridedown Acceleration (G)	
	x-direction	y-direction	x-direction	y-direction
25 (40)	41.67 (12.7)	0.0 (0.0)	4.5	2.2
30 (48)	49.54 (15.1)	0.98 (0.3)	5.9	2.1
35 (56)	55.44 (16.9)	0.33 (0.1)	8.6	1.3

The occupant risk values obtained from simulations prove the validation of the finite element model of Toyota Yaris Model against the evaluation criteria of MASH. The OIVs obtained from the conducted simulations are in the range specified by work done by Gabauer and Gabler (2008a). The comparison is shown in Table 5-2. In the research done by Gabauer and Gabler, attempts were made to correlate the roadside safety hardware to the occupant injury risk using different ATDs with different restrained systems. However, since the OIV depends on the vehicle kinematics and not on the ATD and its behavior with different restrained systems, the OIV obtained from the computer simulations developed in this study can be directly compared to their values.

Table 5-2. Comparison of OIV from Pre-Simulations and Literature Review

Speed (mph)	Occupant Impact Velocity, ft/s (m/s)	
	From Simulation	From Literature
25	41.67 (12.7)	40 +/- 2.64 (12.2 +/- 0.8)
30	49.54 (15.1)	46 +/- 5 (14 +/- 1.5)
35	55.44 (16.9)	53 +/- 3.28 (16 +/- 1)

5.3 Conclusions

Predictive simulations were performed with an FE model of a 2010 Toyota Yaris impacting a rigid wall. Impacts were performed at a 90⁰ angle and at the speeds of 25 mph (40 km/h), 30 mph (48 km/h) and 35 mph (56 km/h). The obtained occupant impact velocity values all favorable compared to the values obtained by Gabauer and Gabler (2008a) in their study. Although the research done by Gabauer and Gabler employed different types of ATDs and restraint conditions, since the occupant risk values do not depend on ATD kinematics, a direct occupant risk comparison was possible between the values obtained from the computer simulations and the values reported by Gabauer and Gabler's study (2008a).

6. CRASH TESTING

This section presents a brief description about the frontal impact crash test done with a Toyota Yaris and H3 ATD restrained with seatbelt and airbag. The crash was against a rigid impact wall at an angle of 90^0 and at a speed of 35 mph (56 km/h).

The car was instrumented as per MASH standards and the ATD was placed as per the US-NCAP guidelines. A speed of 35 mph (56 km/h) was chosen as per the US-NCAP testing guidelines and a direction perpendicular to rigid wall was chosen as it causes the most severe impact. Details of the rigid impact wall, ATD instrumentation and positioning, instrumentation of Toyota Yaris are presented in different sections of this section.

6.1 Design and Construction of Rigid Impact Wall

The test target impact structure consisted of a solid concrete wall measuring 10 ft wide \times 5 ft tall \times 2 ft thick (3 m wide \times 1.5 m tall \times 0.6 m thick) with an approximate mass of 150,000 lbs. (68038 kg) constructed on a concrete extension of the Proving Ground's concrete apron. The wall was buttressed with a structural steel brace assembly comprised of two parallel structures spaced at 84 in. (2.1 m) center-to-center and symmetrical about the centerline of the concrete wall. The assembly consisted of two steel backing plates, each 28 in. wide \times 60 in. tall \times $\frac{1}{2}$ in. thick (0.7 m wide \times 1.5 m tall \times 0.01 m thick), two gusseted vertical W8 \times 20 column legs (59 in. i.e., 1.49 m tall), and four horizontal W8 \times 20 beams (top flanges at 15 $\frac{1}{4}$ in. and 36 $\frac{3}{4}$ in. i.e., 0.4 m \times 0.93 m, above grade), which connected to two knee-brace W8 \times 20 beams (at 28^0 from horizontal) that were secured to two shorter vertical W8 \times 20 legs (25 in. i.e., 0.635 m tall) to the foundation. Each of the four legs were welded to 15 in. (0.38 m) square \times $\frac{3}{4}$ in. (0.02 m) thick base plates, each secured with four 1 $\frac{1}{4}$ in. (0.03 m) UNC anchor bolts and nuts on 10 $\frac{3}{4}$ in. (0.27 m) centers to the foundation.

Additionally, two 10 ft (3 m) long W12 \times 40 beams, longitudinally stitch-welded (6 in. \times 18 in. i.e., 0.15 m \times 0.45 m) at the flange edges, sat atop the concrete wall flush with the

face, and were connected to the aforementioned steel brace assembly via two HSS $4 \times 4 \times \frac{1}{4}$ in. ($0.1 \times 0.1 \times 0.25$ m) knee braces to the top of the brace assembly. The top edge of the flange of the upper W12 \times 40 beam was 73 in. (1.85 m) above grade. All structural material was grade A-36. All welds were full fillet unless otherwise noted.

The bare concrete wall was faced with two adjoining sheets of 4 ft wide \times 6 ft tall \times $\frac{3}{4}$ in. thick (1.2 m wide \times 1.83 m tall \times 0.02 m thick) plywood that were centered horizontally on the 10 ft (3 m) wide face and secured with twelve $\frac{3}{8}$ in. (10 mm) diameter \times 4 in. (100 mm) long mechanical wedge anchor studs installed in drilled holes in the wall. The studs were located approximately $2\frac{1}{4}$ in. (0.057 m) from the vertical edge of each piece of plywood at heights above grade of 7 in. (0.17 m), 38 in. (0.96 m), and 54 in. (1.37 m). Excess stud projections were sawed off flush with the nut after tightening.

Figure 6-1 and Figure 6-2 presents further information on the rigid wall, and provides photographs of the installation.

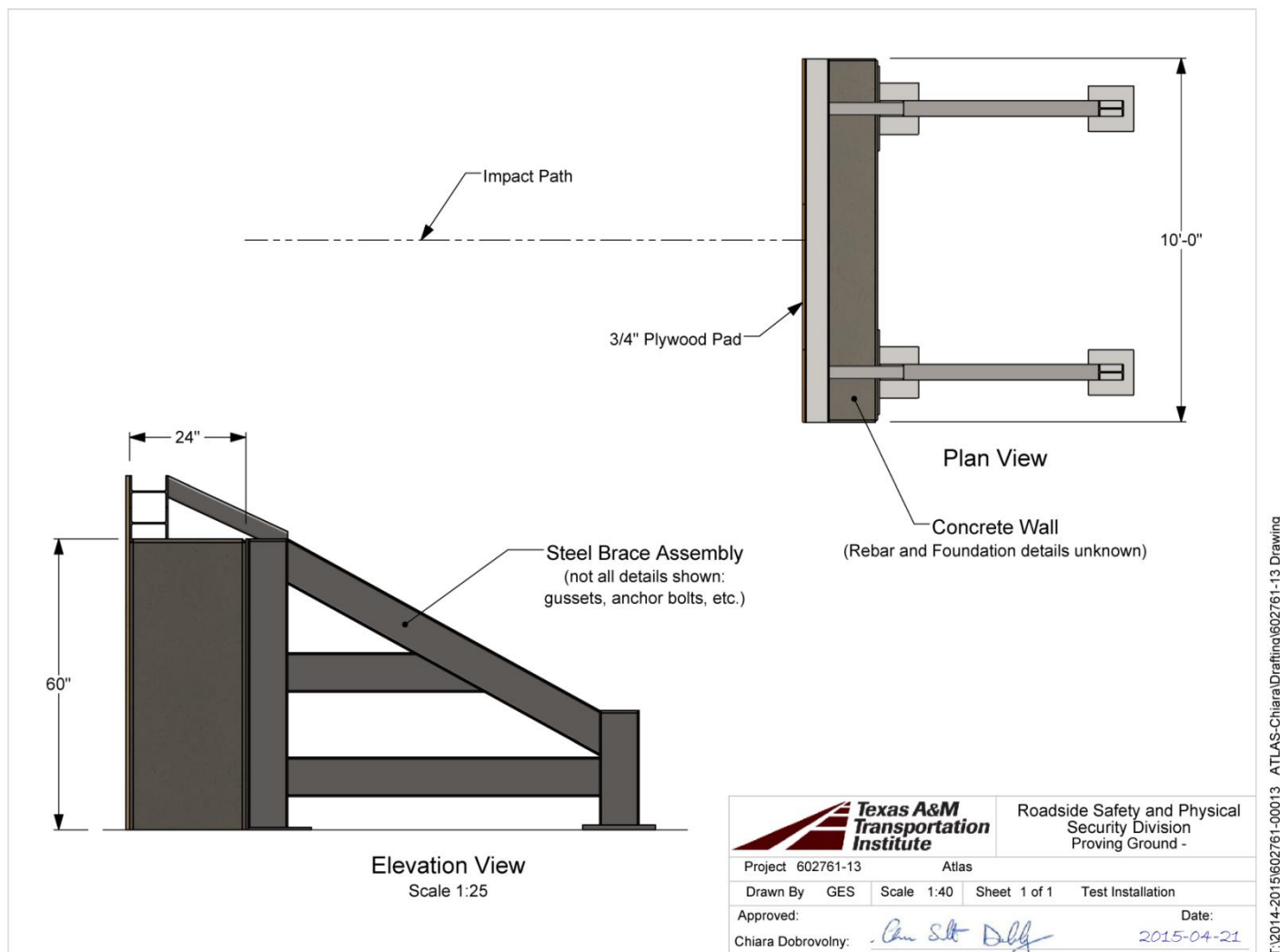


Figure 6-1. Details of the Rigid Impact Wall.

6.2 Material Specifications

The target impact wall was constructed many years ago at the Proving Ground site and details of the internal reinforcing steel and foundation are unknown. Numerous sleeves, mounting holes, and bolts from past tests were present in the concrete structure.



Figure 6-2. Rigid Wall Prior to Testing

6.3 Test Facility

The full-scale crash test reported herein was performed at TTI Proving Ground. TTI Proving Ground is an International Standards Organization (ISO) 17025 accredited laboratory with American Association for Laboratory Accreditation (A2LA) Mechanical Testing certificate 2821.01. The full-scale crash test was performed according to TTI

proving Ground quality procedures and according to the *MASH* guidelines and standards.

The test facilities at the TTI Proving Ground consist of a 2000 acre complex of research and training facilities situated 10 miles (16 km) northwest of the main campus of Texas A&M University. The site, formerly a United States Army Air Corps Base, has large expanses of concrete runways and parking aprons well suited for experimental research and testing in the areas of vehicle performance and handling, vehicle-roadway interaction, durability and efficacy of highway pavements, and evaluation of roadside safety hardware. The site selected for the installation of the Rigid Impact Wall was along a wide out-of-service apron. The apron consists of an unreinforced jointed-concrete pavement in 12.5 ft × 15 ft (3.8 m × 3.8 m) blocks nominally 6 in. (0.15 m) thick. The apron was built in 1942, and the joints have some displacement, but are otherwise flat and level.

6.4 Data Acquisition Systems

The following section gives the details of data acquisition systems used in the vehicle and ATD. The positioning of the ATD and certain vehicle adjustments have also been discussed in this section

6.4.1 Vehicle Instrumentation and Data Processing

The test vehicle was instrumented with a self-contained, on-board data acquisition system. The signal conditioning and acquisition system is a 16-channel, Tiny Data Acquisition System (TDAS) Pro that Diversified Technical Systems, Inc. produced. The accelerometers, which measure the x, y, and z axis of vehicle acceleration, are strain gauge type with linear millivolt output proportional to acceleration. Angular rate sensors, measuring vehicle roll, pitch, and yaw rates, are ultra-small, solid state units designed for crash test service. The TDAS Pro hardware and software conform to the latest SAE J211, Instrumentation for Impact Test. Each of the 16 channels is capable of providing precision amplification, scaling, and filtering based on transducer specifications and

calibrations. During the test, data are recorded from each channel at a rate of 10,000 values per second with a resolution of one part in 65,536. Once data are recorded, internal batteries back these up inside the unit should the primary battery cable be severed. Initial contact of the pressure switch on the vehicle bumper provides a time zero mark as well as initiates the recording process. After each test, the data are downloaded from the TDAS Pro unit into a laptop computer at the test site. The Test Risk Assessment Program (TRAP) software then processes the raw data to produce detailed reports of the test results.

Each of the TDAS Pro units is returned to the factory annually for complete recalibration. Accelerometers and rate transducers are also calibrated annually with traceability to the National Institute for Standards and Technology. All accelerometers are calibrated annually according to SAE J211 4.6.1 by means of an ENDEVCO® 2901, precision primary vibration standard. This device and its support instruments are returned to the factory annually for a National Institute of Standards Technology (NIST) traceable calibration. The subsystems of each data channel are also evaluated annually, using instruments with current NIST traceability, and the results are factored into the accuracy of the total data channel, per SAE J211. Calibrations and evaluations are also made any time data are suspect. Acceleration data is measured with an expanded uncertainty of $\pm 1.7\%$ at a confidence factor of 95% ($k=2$).

TRAP uses the data from the TDAS Pro to compute occupant/compartiment impact velocities, time of occupant/compartiment impact after vehicle impact, and the highest 10 ms average ridedown acceleration. TRAP calculates change in vehicle velocity at the end of a given impulse period. In addition, maximum average accelerations over 50 ms intervals in each of the three directions are computed. For reporting purposes, the data from the vehicle-mounted accelerometers are filtered with a 60-Hz digital filter, and acceleration versus time curves for the longitudinal, lateral, and vertical directions are plotted using TRAP. TRAP uses the data from the yaw, pitch, and roll rate transducers to compute angular displacement in degrees at 0.0001s intervals, then plots yaw, pitch, and

roll versus time. These displacements are in reference to the vehicle-fixed coordinate system with the initial position and orientation of the vehicle-fixed coordinate systems being initial impact. Rate of rotation data is measured with an expanded uncertainty of $\pm 0.7\%$ at a confidence factor of 95 % ($k=2$).

6.4.2 Seat Adjustments and Steering Wheel Data

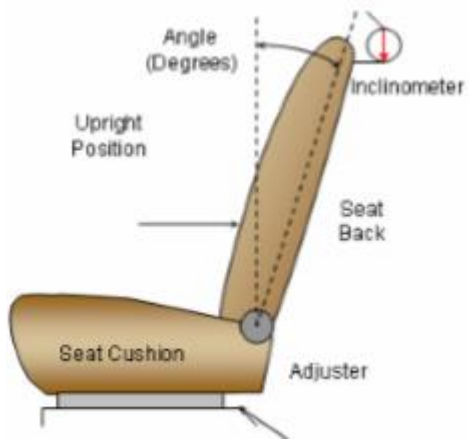
According to US-NCAP Standards, the procedure for driver's seat adjustment is as follows:

- i. The seat back angle is set to 0.5° .
- ii. The seat travel is measured from the forward most possible position to the rear most possible position. The driver's seat is set to the middle of the fore aft travel.
- iii. The steering wheel and the column adjustments are made so that the steering wheel hub is at the geometric center of the locus it describes when moved through its full range of motion a digital inclinometer is used to measure a plate which is placed across the rim of the steering wheel for angular measurements.

The details of the angles of the driver's seat angle, seat distance and the steering wheel angles are listed in Table 6-1. Figures show the procedure followed for measurements and adjustments of the seating.

Table 6-1. Positioning of Seat and Steering Wheel

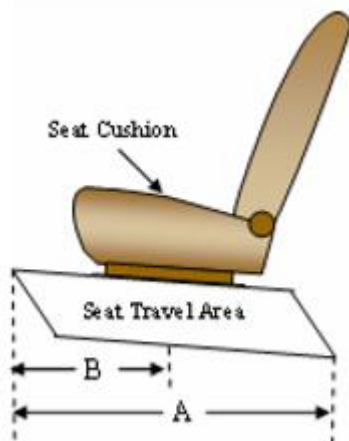
Steering Wheel position	US-NCAP Standards	Test
Lowermost	23.6°	23.8°
Uppermost	26.7°	26°
Steering Wheel Position	25.1°	24.9°
Drivers Back Seat Angle	0.5°	0.5°
Seat Fore/Aft Positioning	Total Fore-Aft Travel	Placed in Position
Driver Seat	237 mm 14 detents	116 mm



Seat Back Angle Adjustment
according to US-NCAP Standards



Seat Back Angle Adjustment during the test

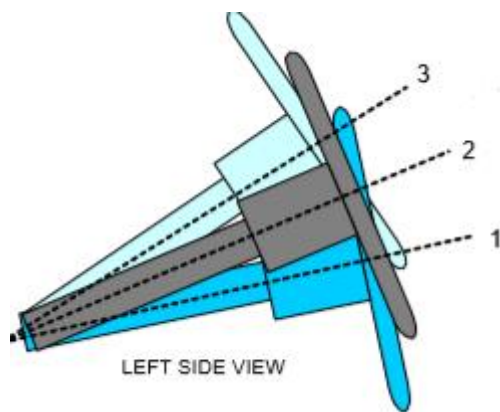


Seat Positioning according to US-
NCAP Standards



Seat Positioning during the test

Figure 6-3. Seat/ Steering Wheel Positioning



Steering wheel adjustment
according to US-NCAP Standards



Steering wheel adjustment during the test

Figure 6-3 Continued

6.4.3 Anthropomorphic ATD Instrumentation and Positioning

Before the H3 ATD can be used for US-NCAP Test Program, a test instrumentation calibration system must be implemented and maintained in accordance with established calibration practices. The calibration system shall include minimum standards of calibrating and storing the measuring and test equipment under appropriate environmental conditions. Accelerometers should be calibrated at a minimum of every six months or after a vehicle fails to meet any minimum performance requirements or after any indication from calibration checks or recent test data that there may be a problem with the accelerometer (whichever comes sooner). The accelerometers were placed in the head, chest, left and right femur and left and right tibia. Figure 6-4 illustrates the different locations of the ATD accelerometers. These accelerometers are connected to the data acquisition system as shown in Figure 6-4.

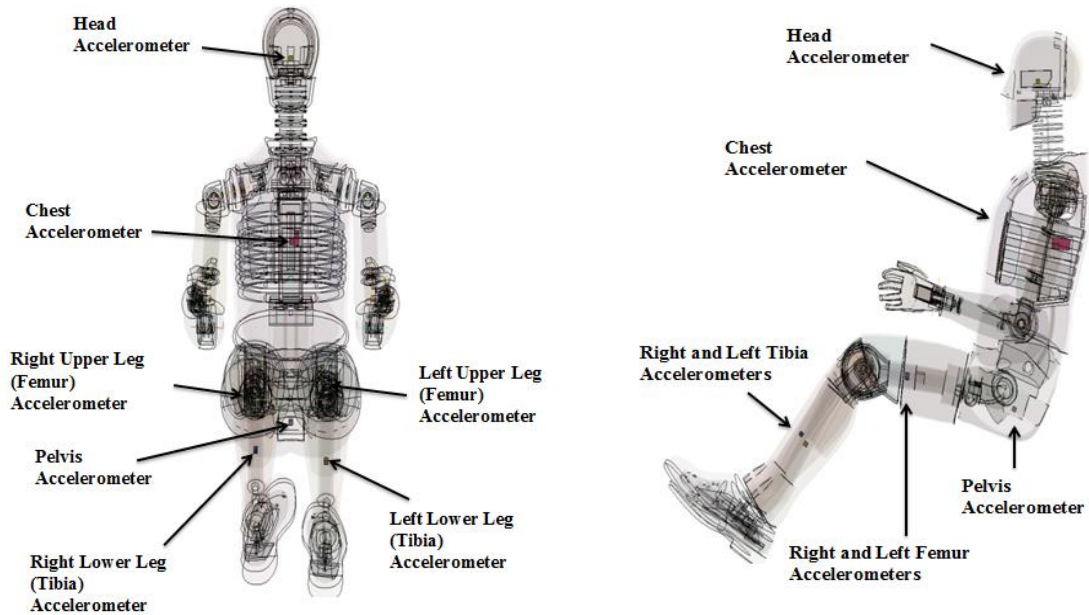


Figure 6-4. Front and Side View of Transparent ATD with Accelerometer

The ATD is positioned in the drivers' seat as compared to similar test performed on MY Yaris by UMTRI which was according to US-NCAP. The ATD positioning in the test is given in Table 6-2 and Figure 6-5. Figure 6-6 shows the ATD positioning during the crash test.

Table 6-2. ATD Positioning According to US-NCAP Guidelines

Code Measurement Description		Test		US-NCAP Test of 201X Yaris	
		Length (mm)	Angle (degrees)	Length (mm)	Angle (degrees)
WA	Windshield Angle	-	26.5	-	23.2
SWA	Steering Wheel Angle	-	-	-	64.9
SCA	Steering Column Angle	-	-	-	25.1

Table 6-2 Continued

Code Measurement Description		Test		US-NCAP Test of 201X Yaris	
		Length (mm)	Angle (degrees)	Length (mm)	Angle (degrees)
SA	Seat Back Angle (on Headrest Post)	-	-	-	0.5
HZ	Head to Roof	183	-	219	90
HH	Head to Header	320	25	380	25.5
HW	Head to Windshield	625	-	693	-
NR	Nose to Rim	362	16.5	404	15.2
CD	Chest to Dash	590	2.5	522	8.2
CS	Chest to Steering Hub	320	0	294	0
RA	Rim to Ab	200	-	203	-
KDL	Left Knee to Dash	150	36	147	32.8
KDR	Right Knee to Dash	130	26	145	28.8
PA	Pelvic Angle	-	24	-	21.9
TA	Tibia Angle	-	51.6	-	57
SK	Striker to Knee	590	6	577	5.7
ST	Striker to Head	500	70	457	79.5
SH	Striker to H-Point	270	41	294	48.6
AD	Arm to Door	100	-	126	-
HD	H-Point to Door	135	-	140	-
HR	Head to Side Header	220	-	243	-
HS	Head to Side Window	330	-	320	-
KK	Knee to Knee	265	-	330	-
SHY	Striker To H-Point	340	-	238	-

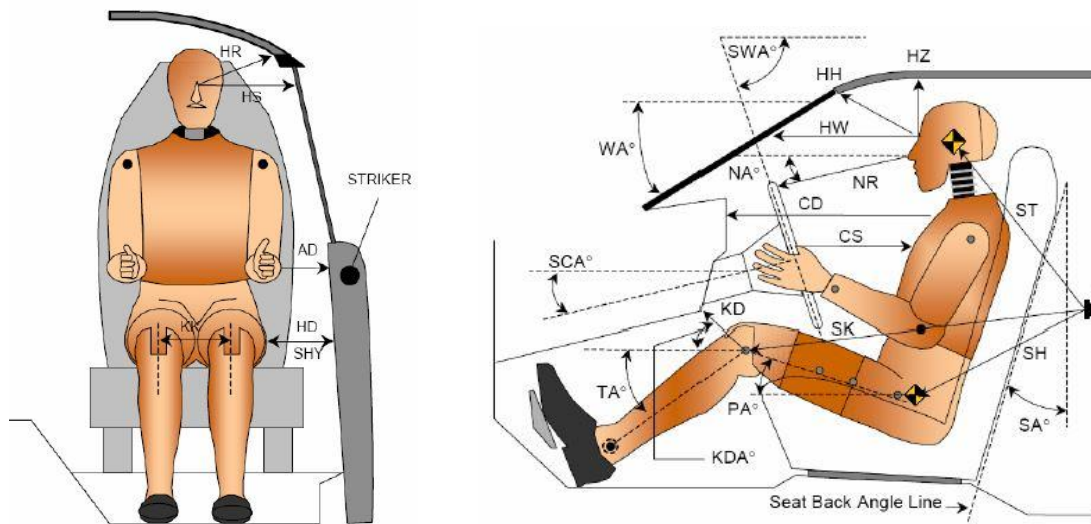


Figure 6-5. ATD Positioning According to US-NCAP Guidelines



Figure 6-6. ATD Position during Crash Test

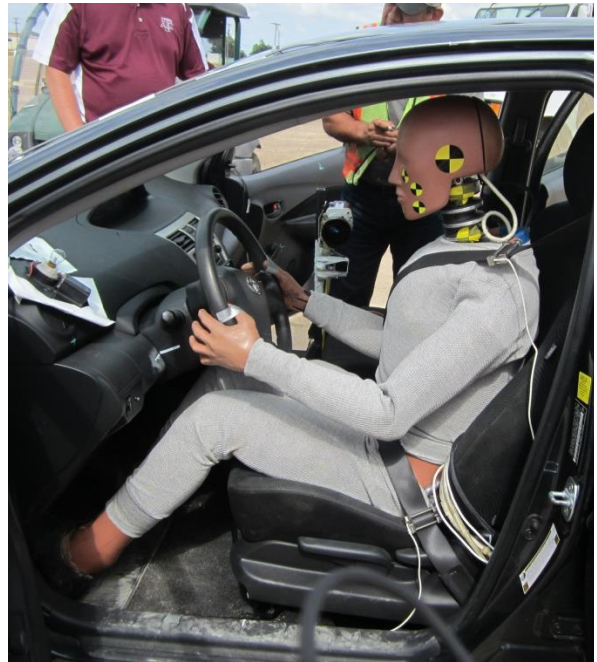


Figure 6-6 Continued

6.4.4 Photographic Instrumentation and Data Processing

Photographic coverage of the test included four high-speed digital cameras. one overhead with a field of view perpendicular to the ground and directly over the impact point; one perpendicular to the right side of the vehicle; one perpendicular to the left side of the vehicle; and one placed inside the vehicle aimed at the ATD. A flashbulb activated by pressure-sensitive tape switches was positioned on the impacting vehicle to indicate the instant of contact with the installation and was visible from each camera. The video from these high-speed cameras were analyzed using motion analyzer software to observe phenomena occurring during the collision and to obtain time-event, displacement, and angular data. A real-time video camera and still cameras recorded and documented conditions of the test vehicle and installation before and after the test.

6.5 Crash Test 602761-13

The crash test was performed the morning of May 27, 2015. Weather conditions at the time of testing were: wind speed: 5 mph (8 km/h); wind direction. 168⁰ with respect to the vehicle (vehicle was traveling in a northerly direction); temperature. 85⁰F (29.5⁰C); relative humidity: 71%.

6.5.1 Test Vehicle

Figure 6-7 and Figure 6-8 show the 2010 Toyota Yaris used for this crash test. Test inertia weight of the vehicle was 2415 lbs. (1095 kg), and its gross static weight was 2591 lbs. (1175 kg). The height to the lower edge of the vehicle front bumper was 11.25 in. (0.28 m), and the height to the upper edge of the front bumper was 21.25 in. (0.54 m). Additional dimensions and information on the vehicle are given in Appendix A.1. The vehicle was directed into the installation using the cable reverse tow and guidance system, and was released to be freewheeling and unrestrained just prior to impact.



Figure 6-7. Vehicle/Installation Geometries for Test No. 602761-13



Figure 6-8. Vehicle before Test No. 602761-13

6.5.2 Test Description

The 2010 Toyota Yaris, traveling at an impact speed of 34.7 mph (55.8 km/h), impacted the Rigid Wall at an impact angle of 90^0 with the centerline of the vehicle aligned with the centerline of the wall. At 0.017 s after impact, the ATD began moving toward the steering wheel, and at 0.020 s, the airbag deployed. The ATD's chin contacted the inflating airbag at 0.044 s, and the ATD's right hand lost contact with the steering wheel at 0.053 s. At 0.056 s, the ATD's right hand contacted the instrument panel, and at 0.060 s, the vehicle ceased forward motion. At 0.087 s, the ATD reached maximum

forward travel and began to move back toward the seat. The ATD's face lost contact with the airbag at 0.150 s, and the vehicle lost contact with the Rigid Wall at 0.219 s.

6.5.3 Test Article and Component Damage

Figure 6-9 show damage to the Rigid Wall. Other than gouges in the plywood face, no other damage was noted.



Figure 6-9. Vehicle/Rigid Wall Positions after Test No. 602761-13

6.5.4 Test Vehicle Damage

Figure 6-10 shows the damage to the vehicle after the test. The front bumper, grill, hood, radiator and support, right and left front fenders, firewall, and instrument panel were damaged. The airbags also deployed. Maximum crush to the exterior of the vehicle was 21.5 in. in the front plane at the center bumper height. Maximum occupant compartment

deformation was 1.0 in. (25.4 mm) along the entire firewall area. Figure 6-11 shows the interior of the vehicle.



Figure 6-10. Vehicle after Test No. 602761-13



Figure 6-11. Interior of Vehicle for Test No. 602761-13

6.6 Crash Test Results

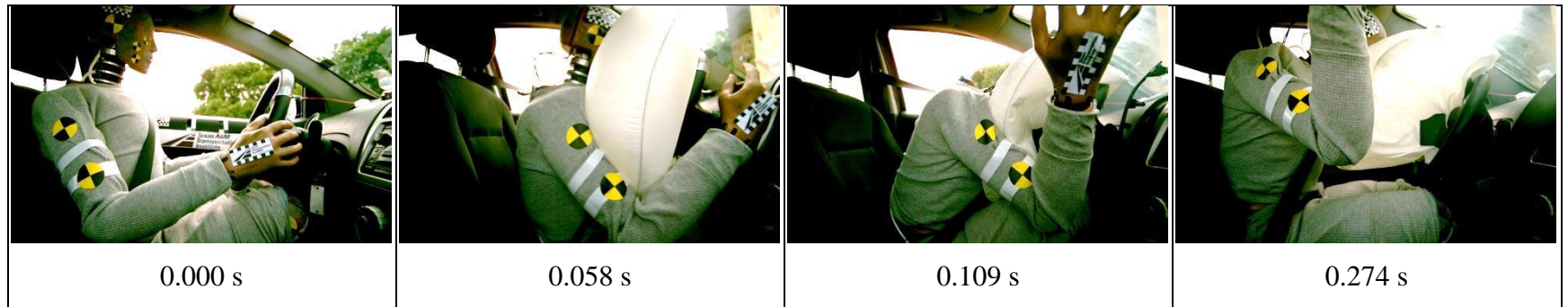
The results of the crash test are discussed in this section in two parts.

- i. Occupant Injury Risk values from vehicle dynamics - MASH,

6.6 Crash Test Results

The results of the crash test are discussed in this section in two parts.

- i. Occupant Injury Risk values from vehicle dynamics - MASH,
- ii. Injury Criteria from ATD Dynamics - FMVSS



General Information

Test Agency Texas A&M Transportation Institute (TTI)
Test Standard Test No.
TTI Test No. 602671-13
Date 2015-05-27

Test Article

Type Rigid Wall
Name Rigid Wall
Installation Length 10 ft (3.05 m) wide, 5 ft (1.02 m) tall, 2 ft (0.61 m) thick
Material or Key Elements... Structural steel brace assembly and concrete

Soil Type and Condition..... Concrete foundation, dry

Test Vehicle

Type/Designation..... 1100C
Make and Model 2010 Toyota Yaris
Curb 2318 lb (1051.5 kg)
Test Inertial..... 2415 lb (1095.5 kg)
ATD 176 lb (80 kg)
Gross Static..... 2591 lb (1175.3 kg)

Impact Conditions

Speed 34.7 mph (55.8 km/h)
Angle 90°
Location/Orientation Centerline to centerline

Exit Conditions

Speed Stopped
Angle NA

Occupant Risk Values

Longitudinal OIV 56.4 ft/s (17.2 m/s)
Lateral OIV 3.6 ft/s (1.1 m/s)
Longitudinal RDA 4.2 G
Lateral RDA 1.7 G
THIV 58.4 ft/s (17.8 m/s)
PHD 4.3 G
ASI 2.85

Max. 0.050-s Average

Longitudinal..... -30.6 G
Lateral..... -3.8 G
Vertical -4.7 G

Post-Impact Trajectory

Stopping Distance.....

Vehicle Stability

Maximum Yaw Angle 3°
Maximum Pitch Angle..... 7°
Maximum Roll Angle..... 3°
Vehicle Snagging No
Vehicle Pocketing..... No

Test Article Deflections

Dynamic NA
Permanent..... NA
Working Width..... NA
Vehicle Intrusion NA

Vehicle Damage

VDS..... 12FD6
CDC 12FDEW5
Max. Exterior Deformation 21.5 in. (0.546 m)
OCDI..... 1.0 in. (0.254 m)
Max. Occupant Compartment Deformation FS0010000

Figure 6-12. Summary of Results for Test No. 602671-13 on the Rigid Wall.

6.6.1 Occupant Risk Values as per Vehicle Dynamics

Data from the accelerometer, located at the vehicle center of gravity, were digitized for evaluation of occupant risk. In the longitudinal direction, the occupant impact velocity (OIV) was 56.4 ft/s (17.2 m/s) at 0.077 s, the highest 0.010 s occupant ridedown acceleration (RDA) was 4.2 G from 0.083 to 0.093 s, and the maximum 0.050 s average acceleration was -30.6 G between 0.013 and 0.063 s. In the lateral direction, the OIV was 3.6 ft/s (1.1 m/s) at 0.077 s, the highest 0.010 s occupant RDA was 1.7 G from 0.086 to 0.096 s, and the maximum 0.050 s average was -3.8 G between 0.023 and 0.073 s. Theoretical Head Impact Velocity (THIV) was 62.2 km/h or 17.3 m/s at 0.077 s; Post-Impact Head Decelerations (PHD) was 4.3 G between 0.083 and 0.093 s; and Acceleration Severity Index (ASI) was 2.85 between 0.046 and 0.096 s. Figure 6-12 summarizes these data and other pertinent information from the test.

6.6.2 Occupant Injury Criteria as per ATD Dynamics

The dynamics of the ATD have been analyzed from the data acquisition system by University of Michigan Transportation Research Institute. The results of accelerations, forces and moments have been summarized in Table 6-3. This will be used to calibrate the finite element model that is meant to nearly replicate the crash test dynamic and outcomes.

Table 6-3. Results of Accelerations, Forces and Moments in ATD and Loads in Shoulder and Lap Belts.

Head				
Head Acceleration	Maximum Positive (G)	Time (ms)	Maximum Negative (G)	Time (ms)
X	25.1	246	-53.9	84
Y	9.3	247	-29.5	89
Z	29.6	66	-7.2	95
Resultant Acceleration	58	84	-	-
HIC 15	264.1	-	-	-

Table 6-3 Continued

Chest				
Chest Acceleration	Maximum Positive (G)	Time (ms)	Maximum Negative (G)	Time (ms)
X	3.5	292	61.7	71
Y	5.3	57	3.8	93
Z	11.7	47	6.8	71
Resultant Acceleration	62	71	-	-
Chest Deflection	0.12 mm	12	50.9 mm	65
Pelvis				
Pelvis Acceleration	Maximum Positive (G)	Time (ms)	Maximum Negative (G)	Time (ms)
X	19.3	85	79.7	52
Y	15.2	61	16.3	54
Z	6.6	89	52	64
Resultant Acceleration	86.4	52	-	-
Upper Neck				
Forces	Maximum Positive (N)	Time (ms)	Maximum Negative (N)	Time (ms)
X	854.7	73	-272.3	296
Y	351.9	72	-155.4	107
Z	1822.8	66	-314.3	101
Resultant Force	1929.8	66		

Table 6-3 Continued

Moments	Maximum Positive (N-m)	Time (ms)	Maximum Negative (N-m)	Time (ms)
X	9.1	84	-15.7	120
Y	41.6	72	-25.5	294
Z	21.3	103	-13.2	165
Resultant moment	43.7	72	-	-
Femur				
Left femur Forces	Maximum Positive (N)	Time (ms)	Maximum Negative (N)	Time (ms)
X	1795.5	71	-459.1	48
Y	1089	55	-248.1	55
Z	3764.2	48	-1083.1	72
Right femur forces	Maximum Positive (N)	Time (ms)	Maximum Negative (N)	Time (ms)
X	1354.2	64	-259.4	54
Y	386.9	55	-584.4	47
Z	21226.3*	40	-5507.6	143
Belt Loads				
Lap/Shoulder Belt	Maximum Positive (N)	Time (ms)	Maximum Negative (N)	Time (ms)
Lap Belt	9521.3	60	-15.5	479
Shoulder Belt	520.9	50	-45.2	128

*A high value of right femur Z-force is due to transducer failure during the crash test.

Figure 6-13 through Figure 6-16 shows the head accelerations. Figure 6-17 shows the chest deflection. Figure 6-18 through Figure 6-21 shows chest accelerations. Figure 6-22 through Figure 6-25 shows the pelvis accelerations. Figure 6-26 through Figure 6-29

shows the upper neck forces. Figure 6-30 through Figure 6-33 shows the upper neck moments. Figure 6-34 through Figure 6-36 shows the Left Femur forces. Figure 6-37 through Figure 6-39 shows the Right Femur Forces. Figure 6-40 and Figure 6-41 shows the belt loads.

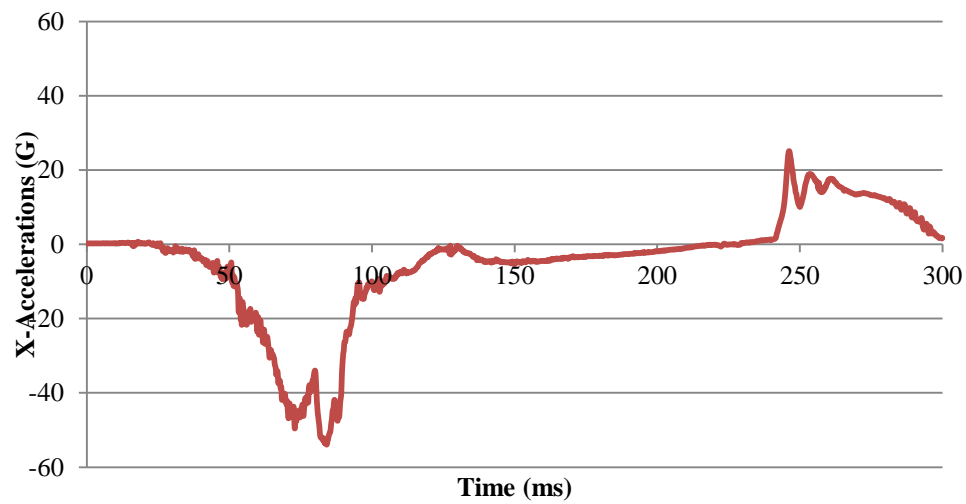


Figure 6-13. Head X-Accelerations

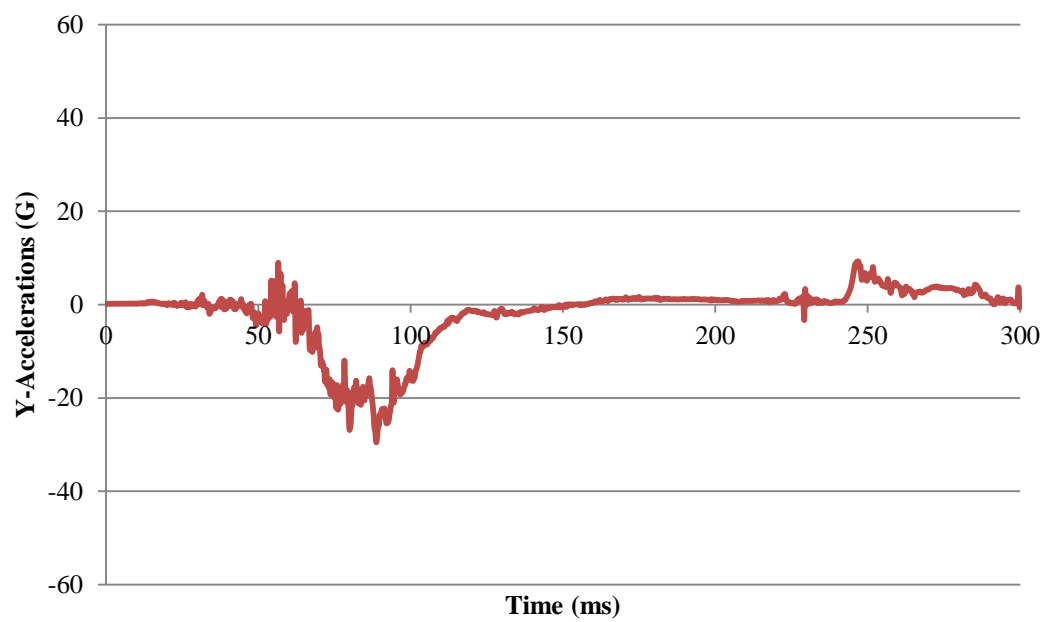


Figure 6-14. Head Y-Accelerations

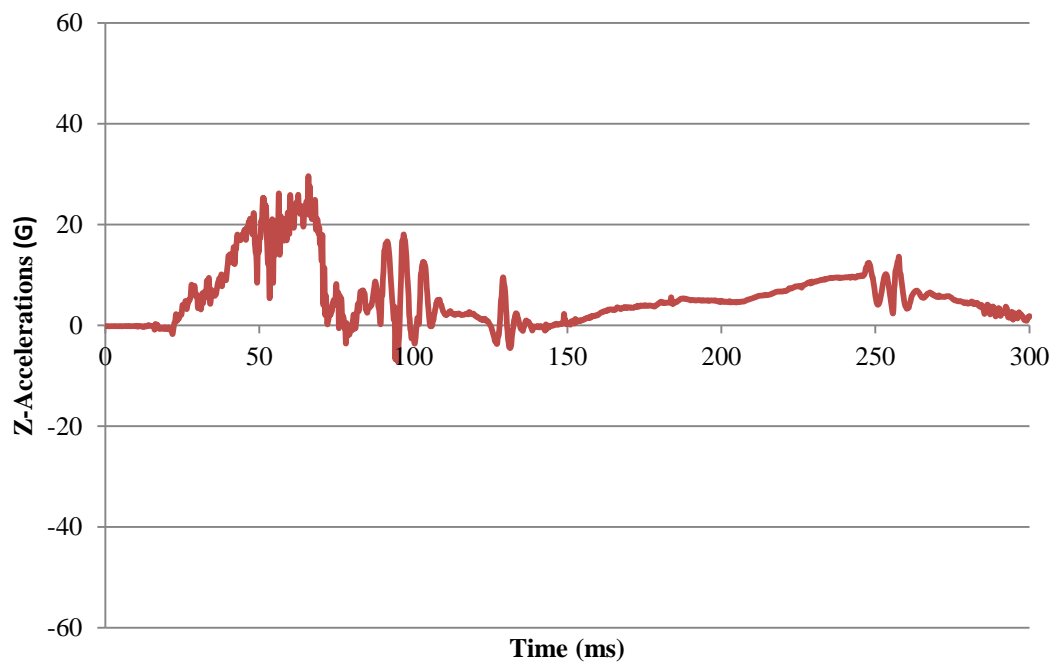


Figure 6-15. Head Z-Accelerations

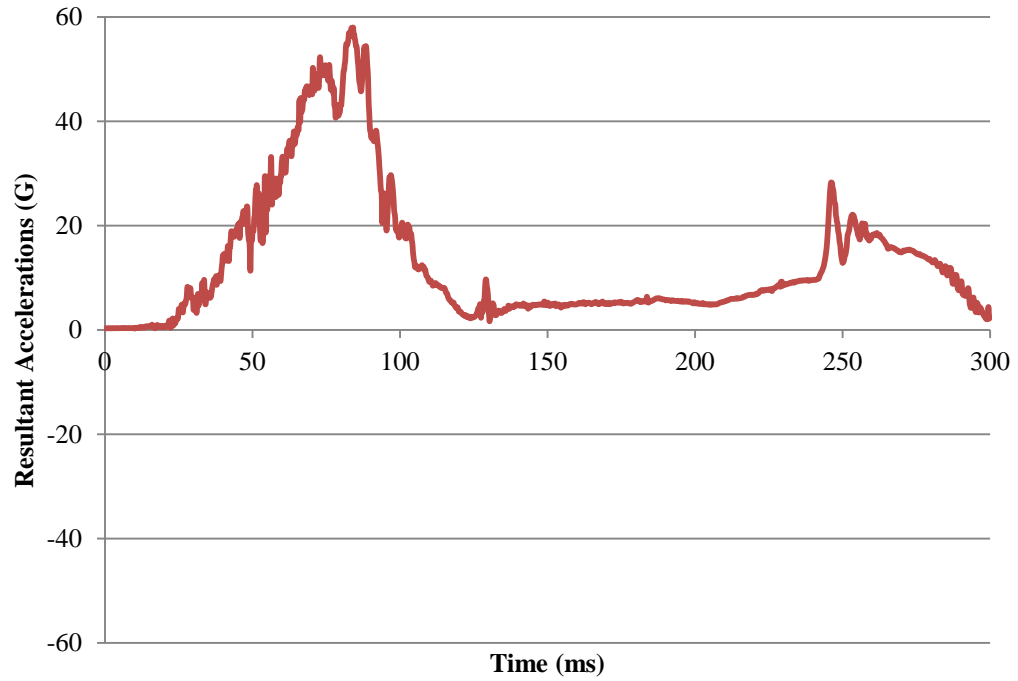


Figure 6-16. Resultant Head Accelerations

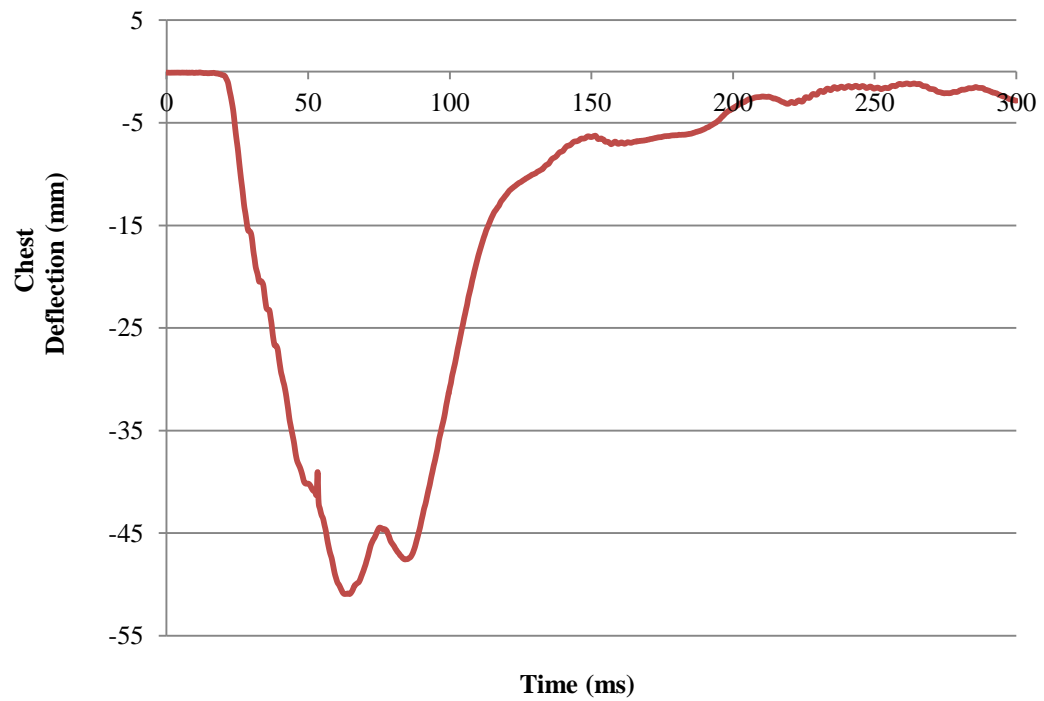


Figure 6-17. Chest Deflections

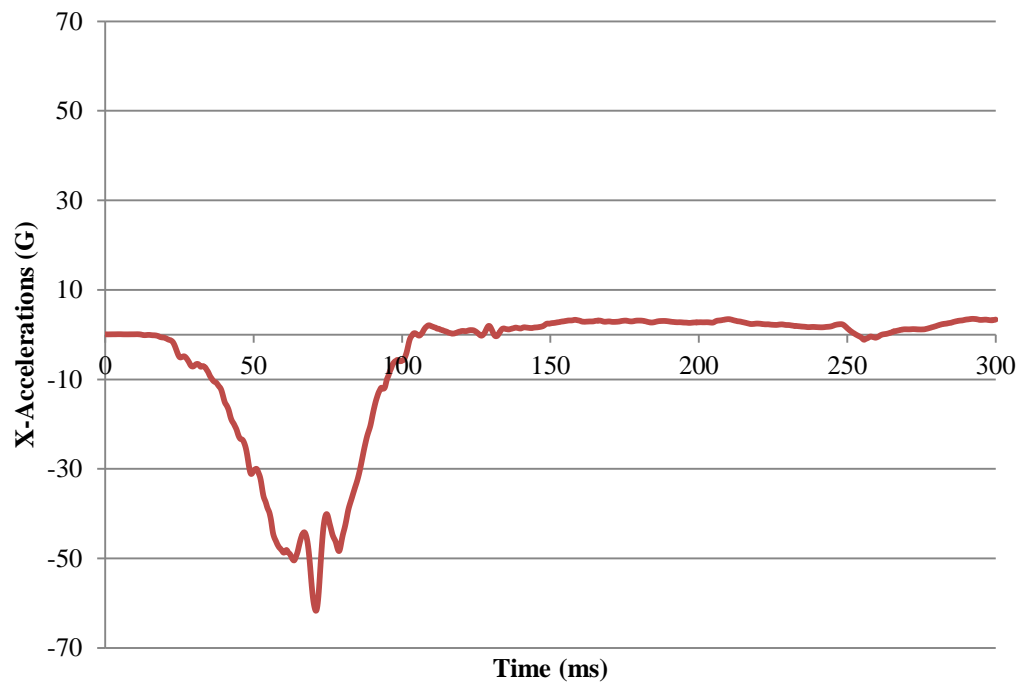


Figure 6-18. Chest X-Accelerations

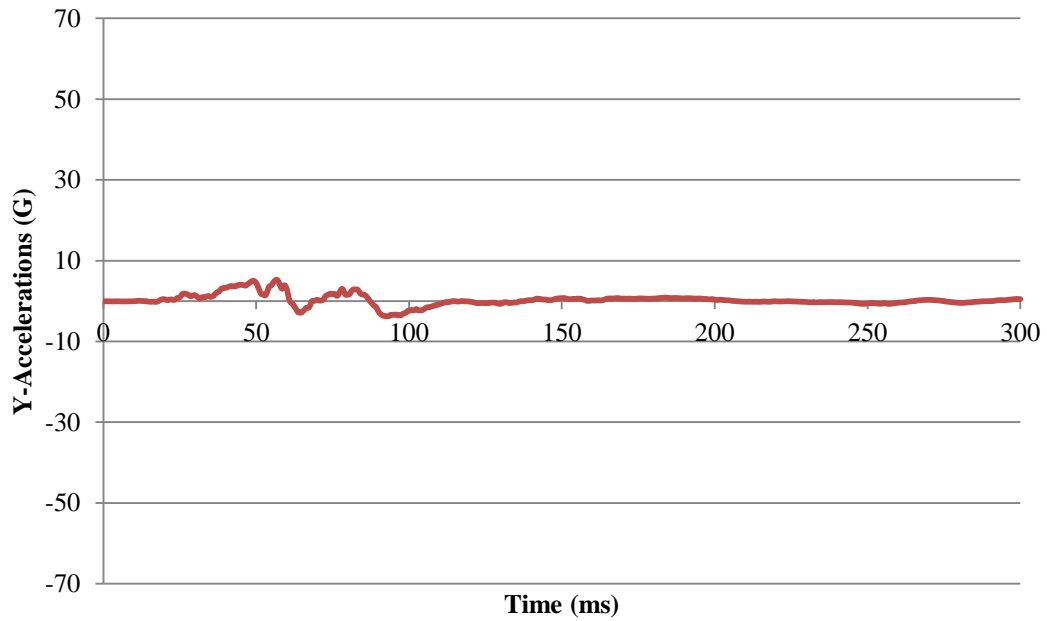


Figure 6-19. Chest Y- Accelerations

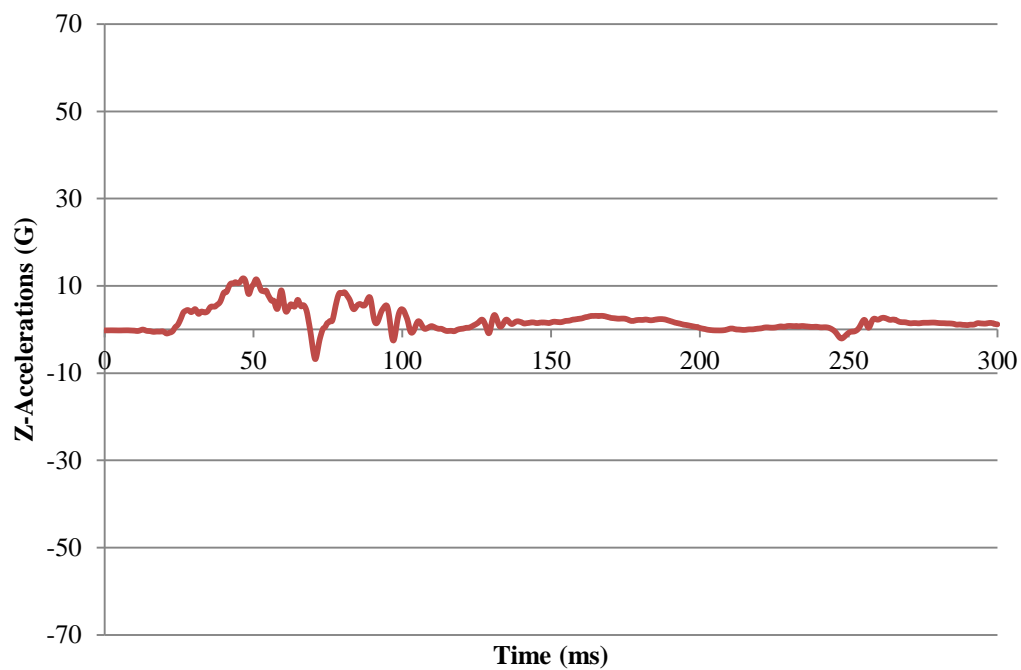


Figure 6-20. Chest Z-Accelerations

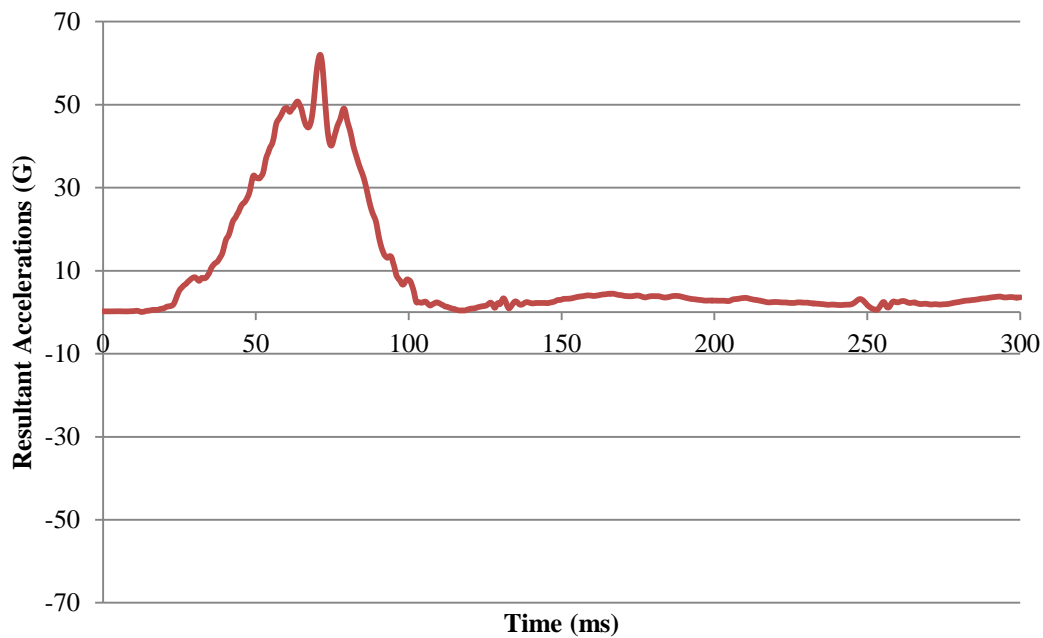


Figure 6-21. Chest Resultant Accelerations

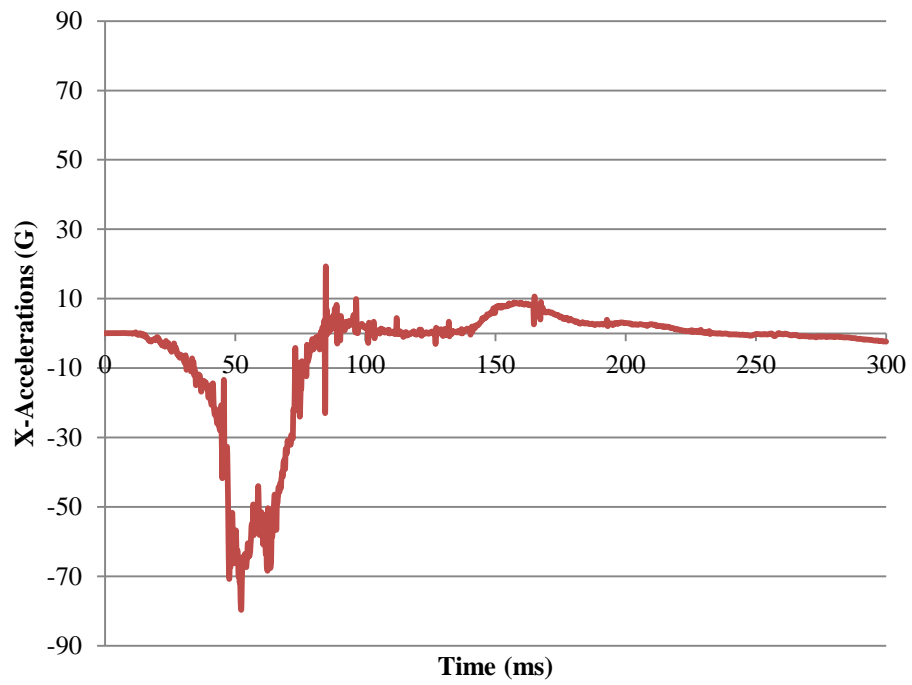


Figure 6-22. Pelvis X-Accelerations

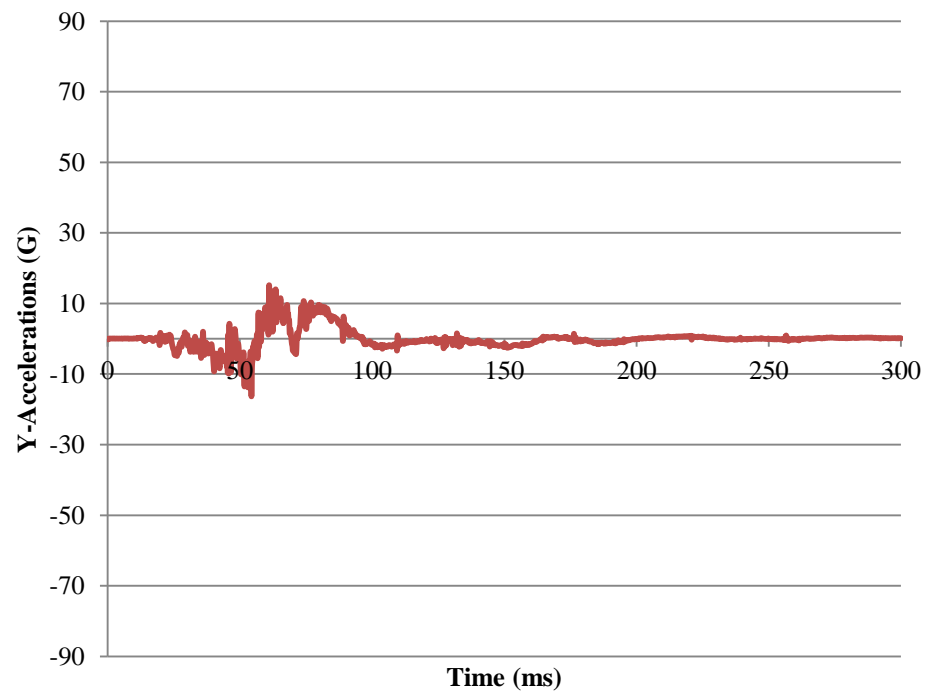


Figure 6-23. Pelvis Y-Accelerations

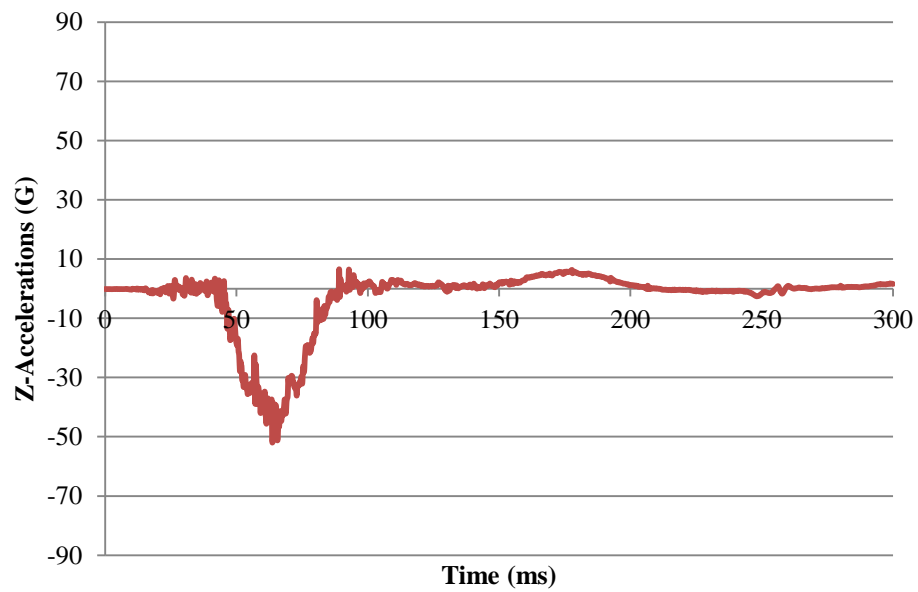


Figure 6-24. Pelvis Z-Accelerations

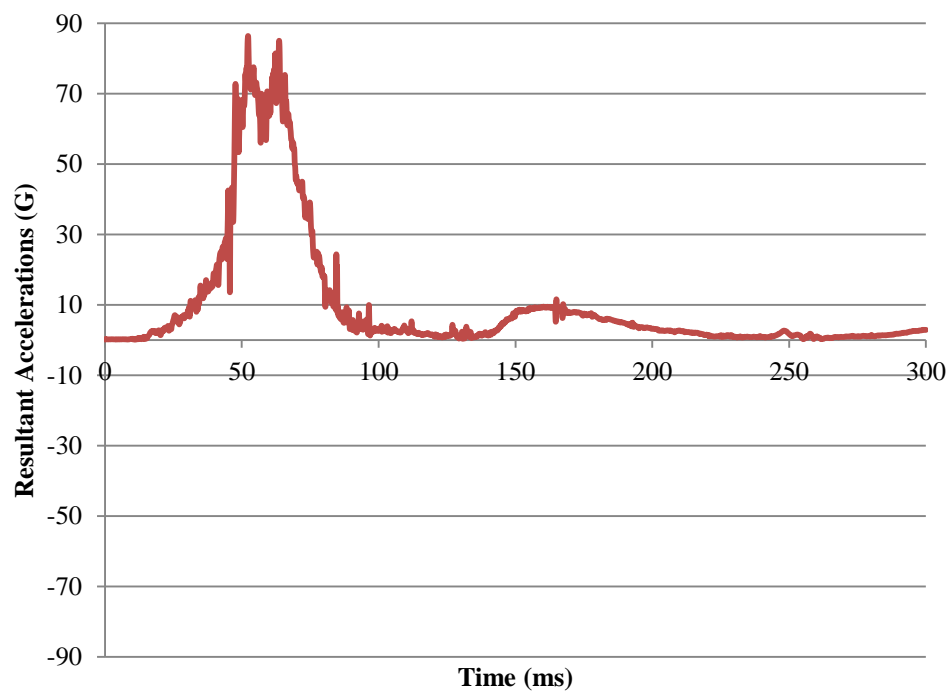


Figure 6-25. Pelvis Resultant Accelerations

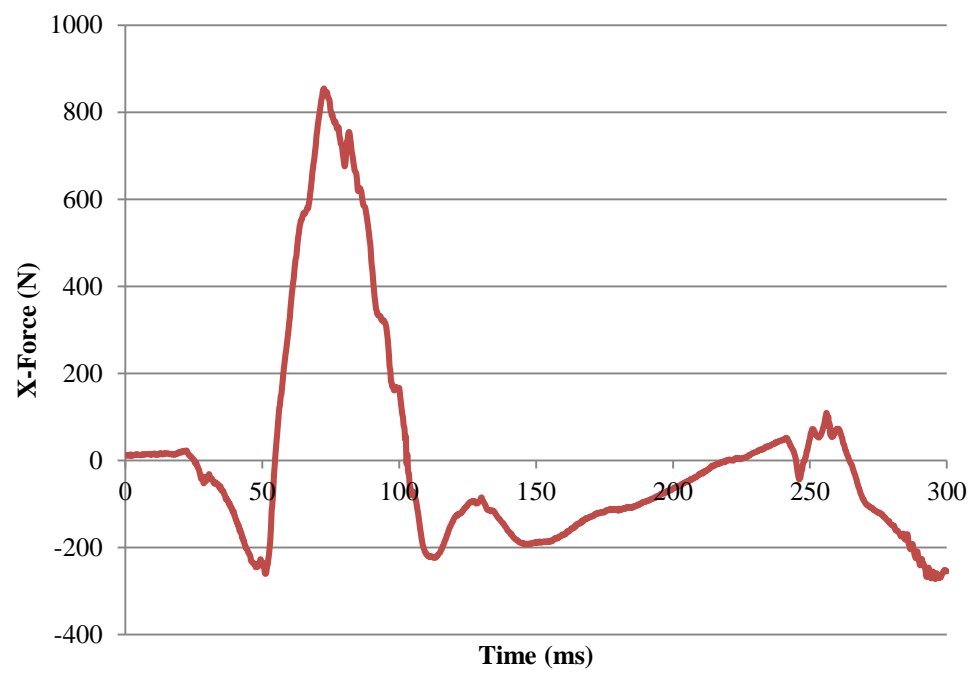


Figure 6-26. Upper Neck X-Forces

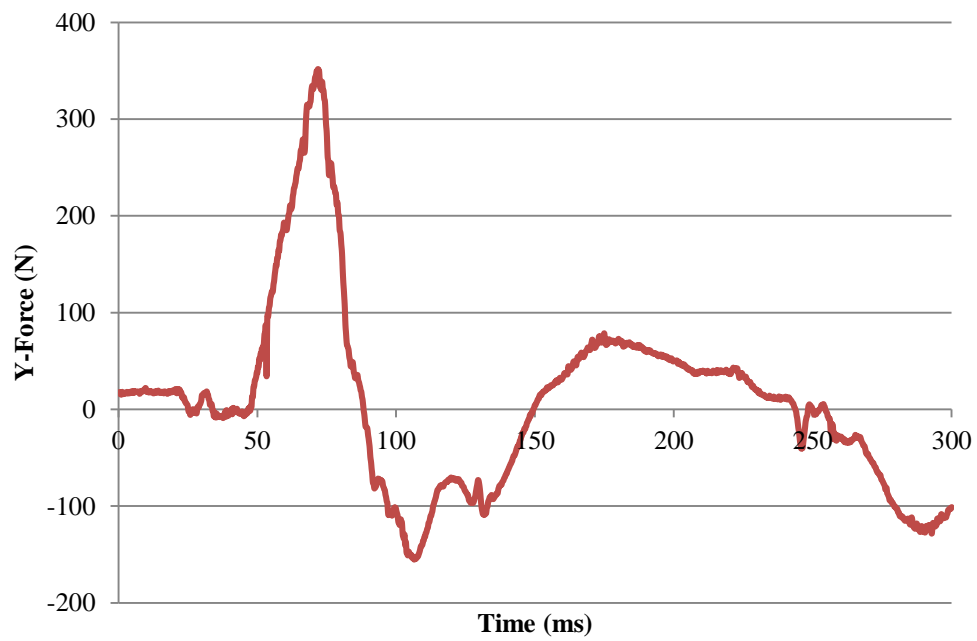


Figure 6-27. Upper Neck Y-forces

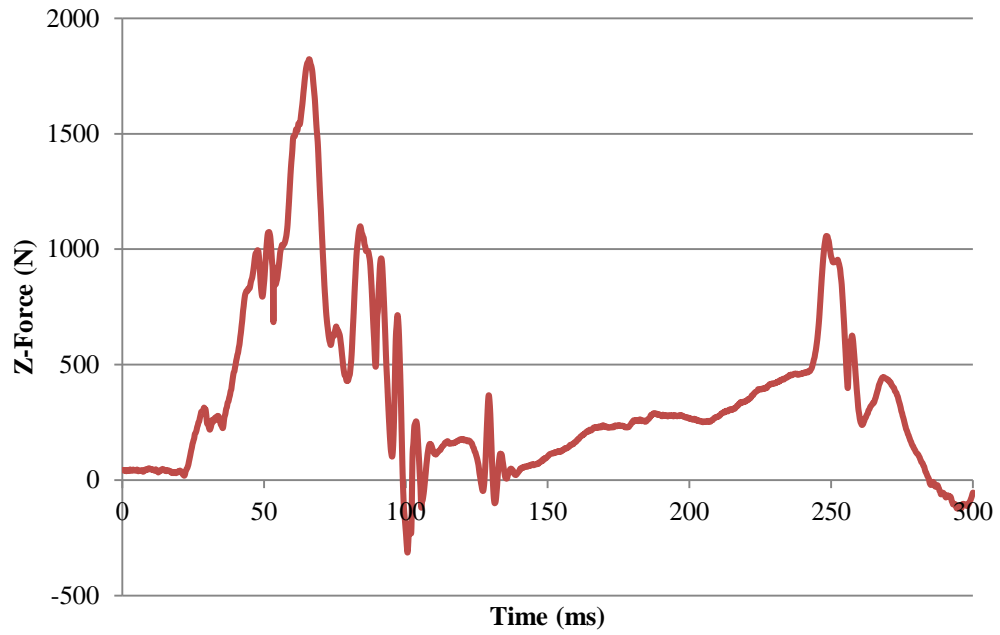


Figure 6-28. Upper Neck Z-Forces

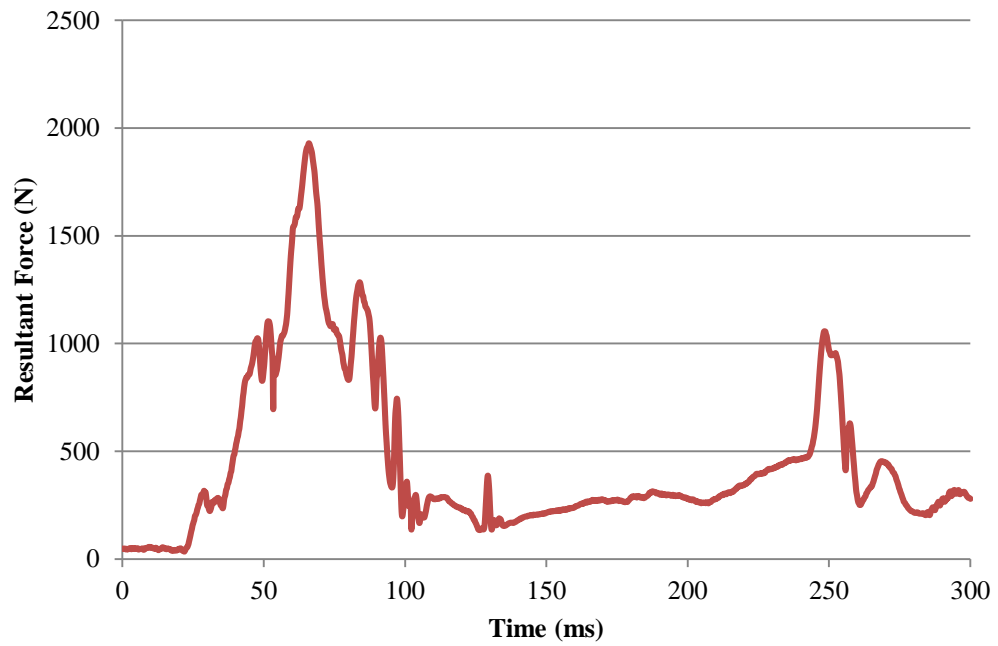


Figure 6-29. Upper Neck Resultant Forces

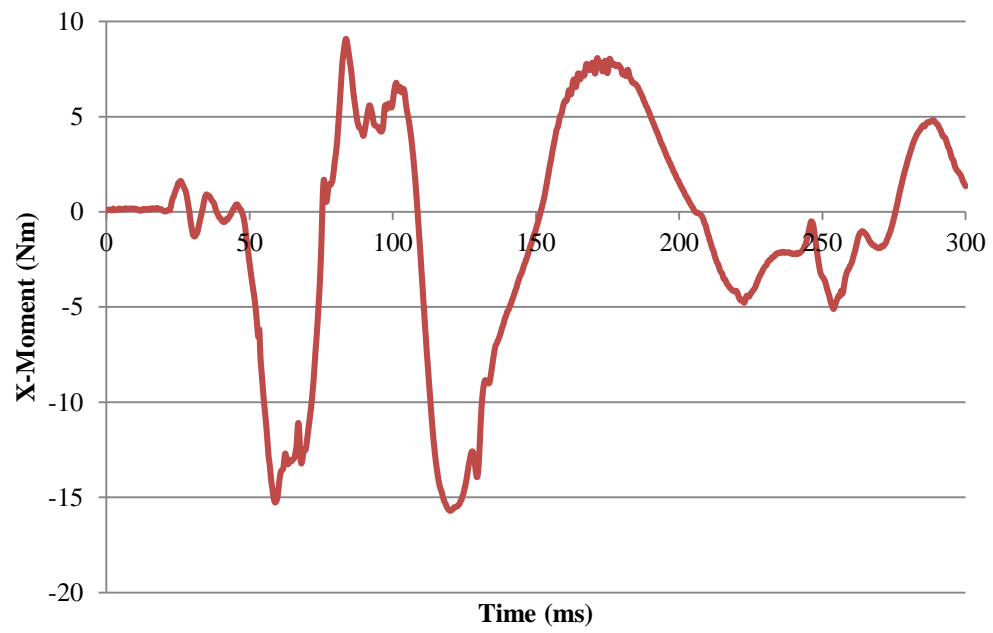


Figure 6-30. Upper Neck X-Moments

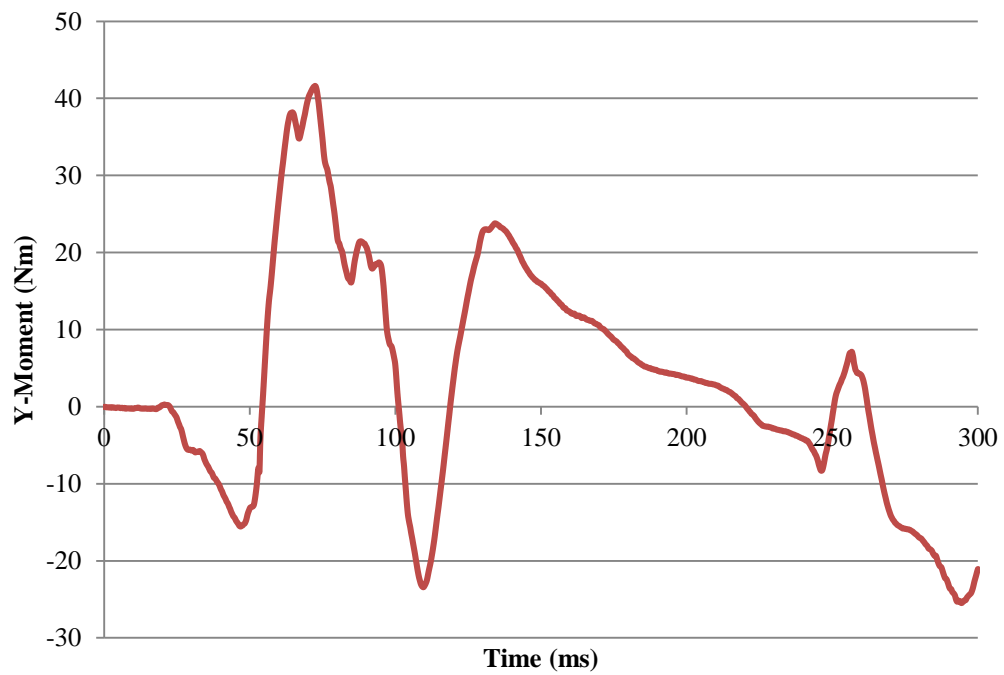


Figure 6-31. Upper Neck Y-Moments

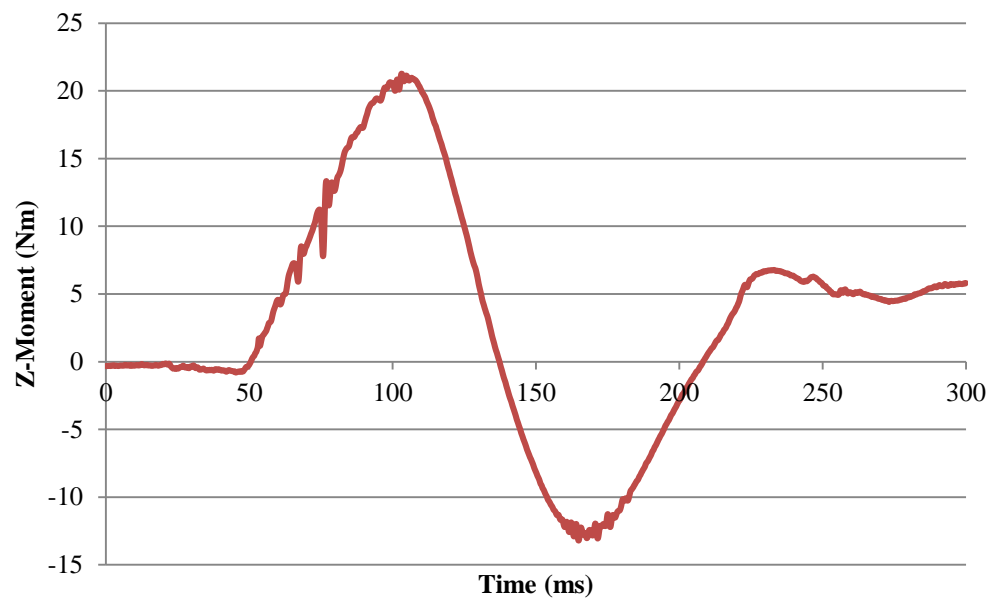


Figure 6-32. Upper Neck Z-Moments

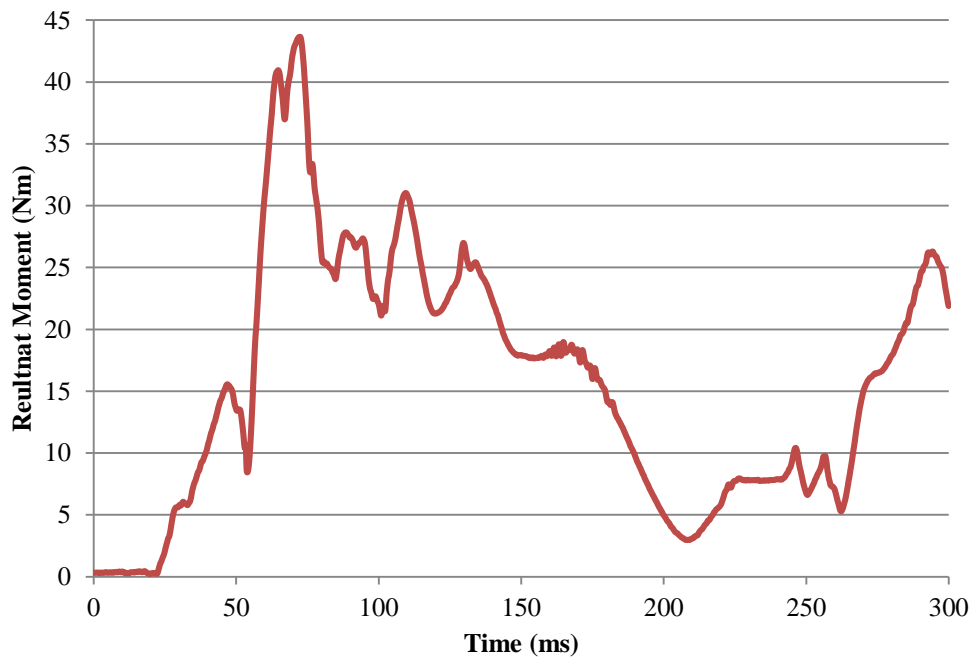


Figure 6-33. Upper Neck Resultant Moments

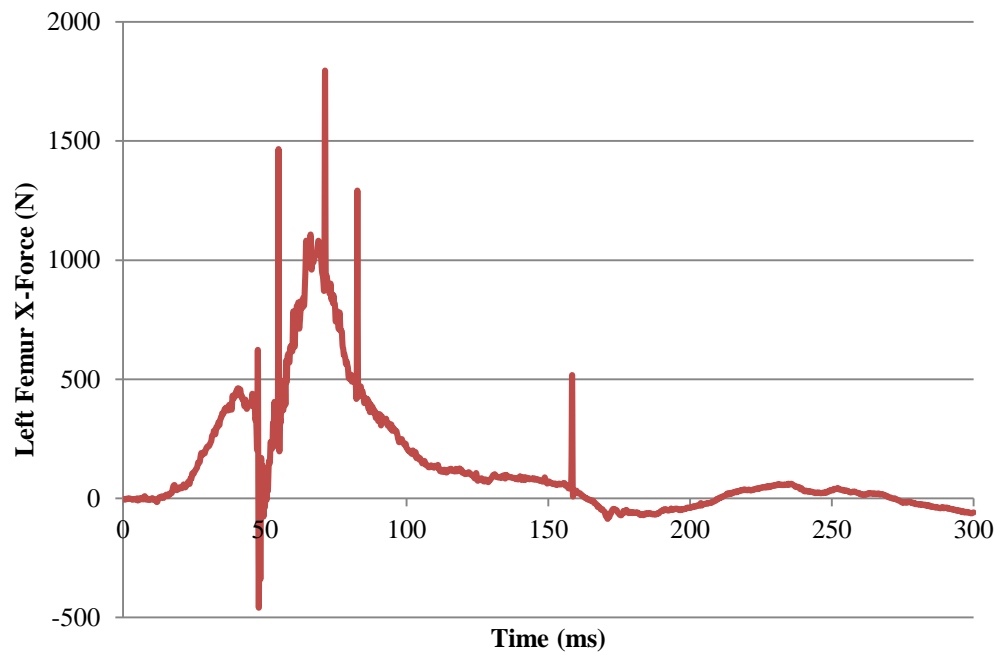


Figure 6-34. Left Femur X-Forces

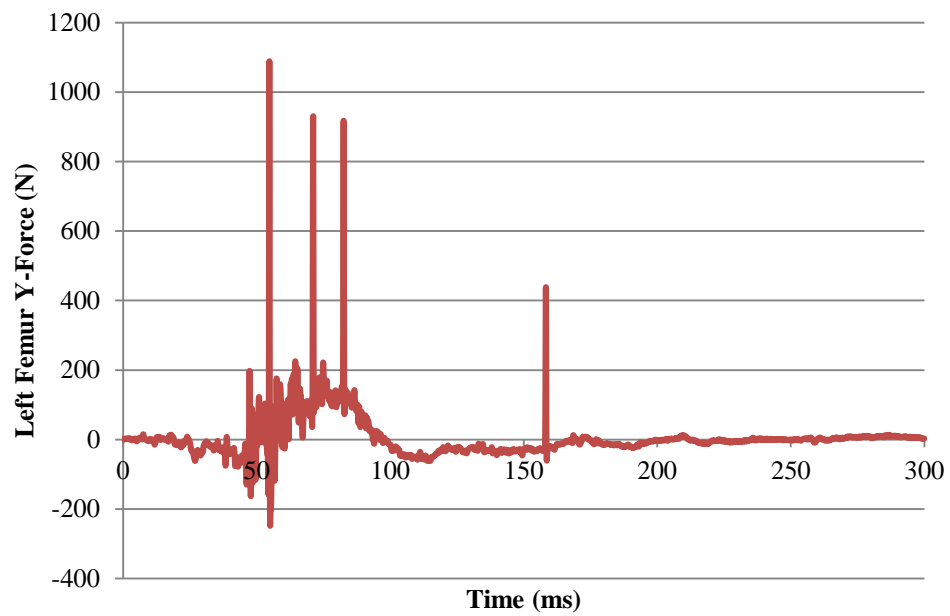


Figure 6-35. Left Femur Y-Forces

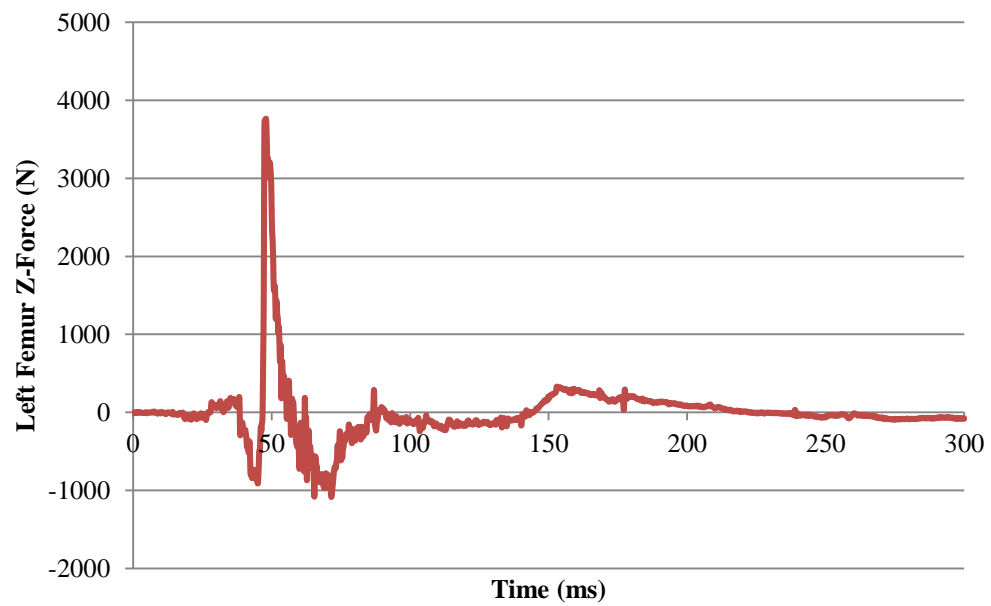


Figure 6-36. Left Femur Z-Forces

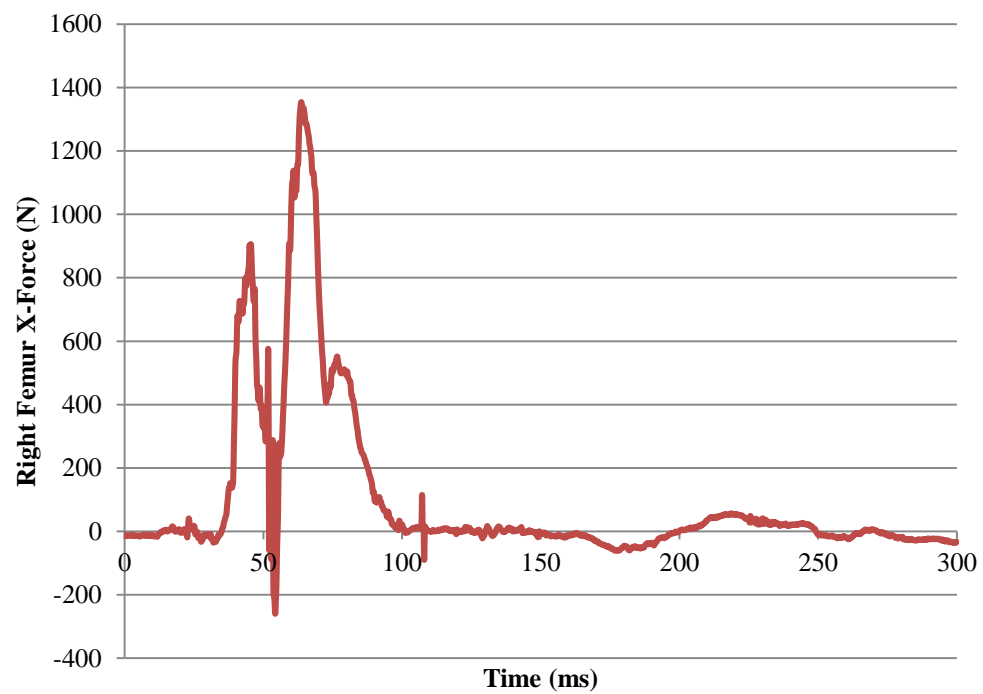


Figure 6-37. Right Femur X-Forces

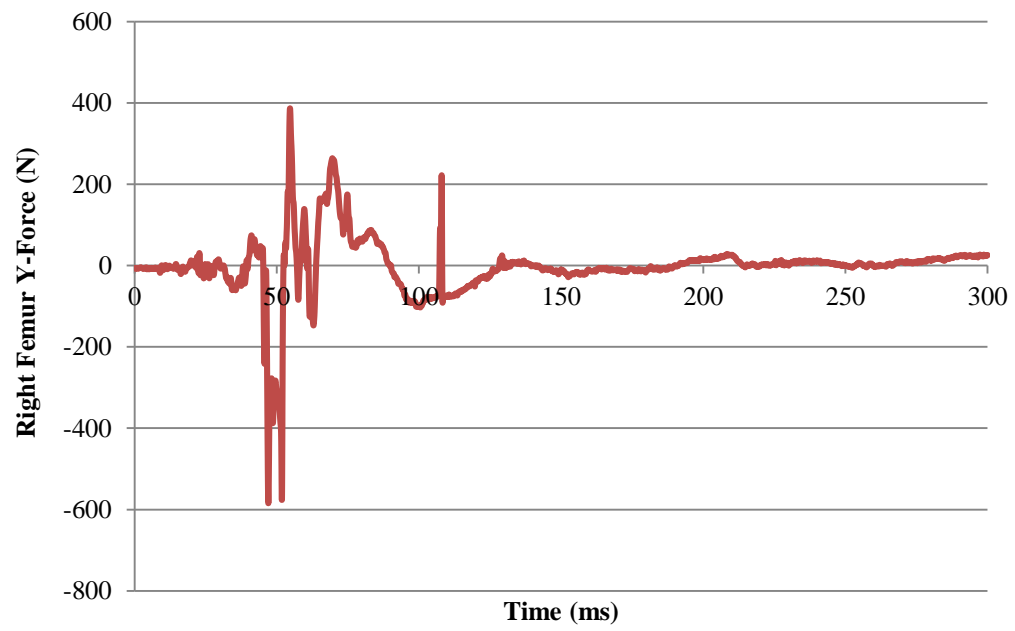


Figure 6-38. Right Y-Forces

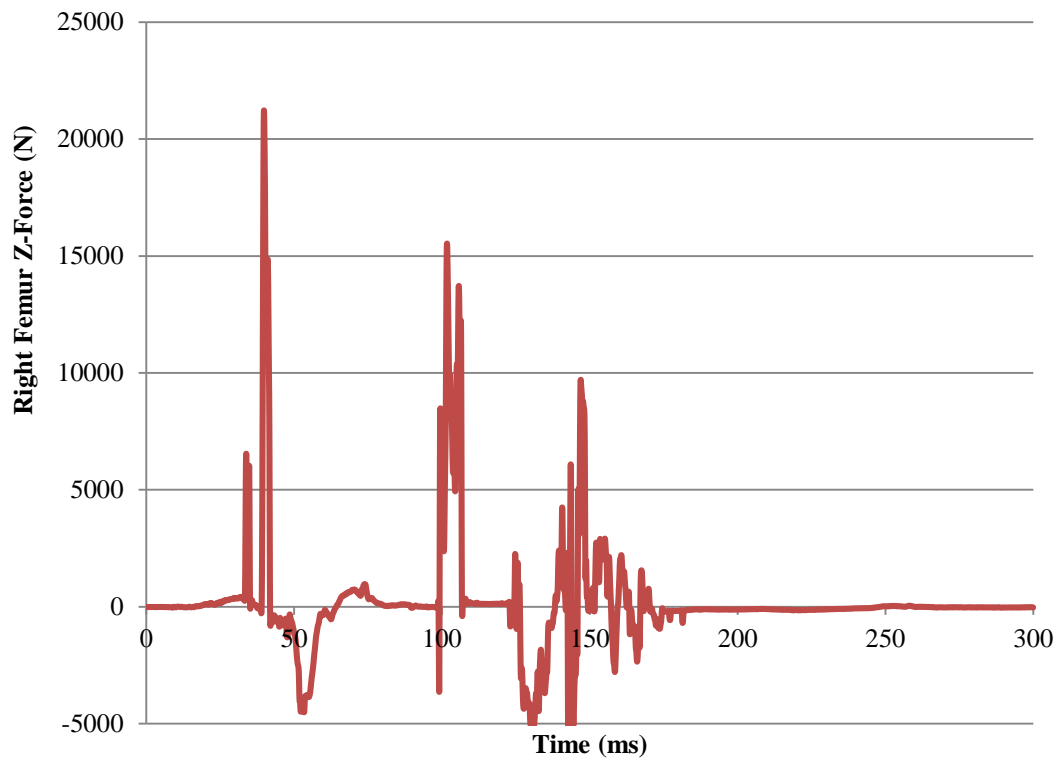


Figure 6-39. Right Z-Forces

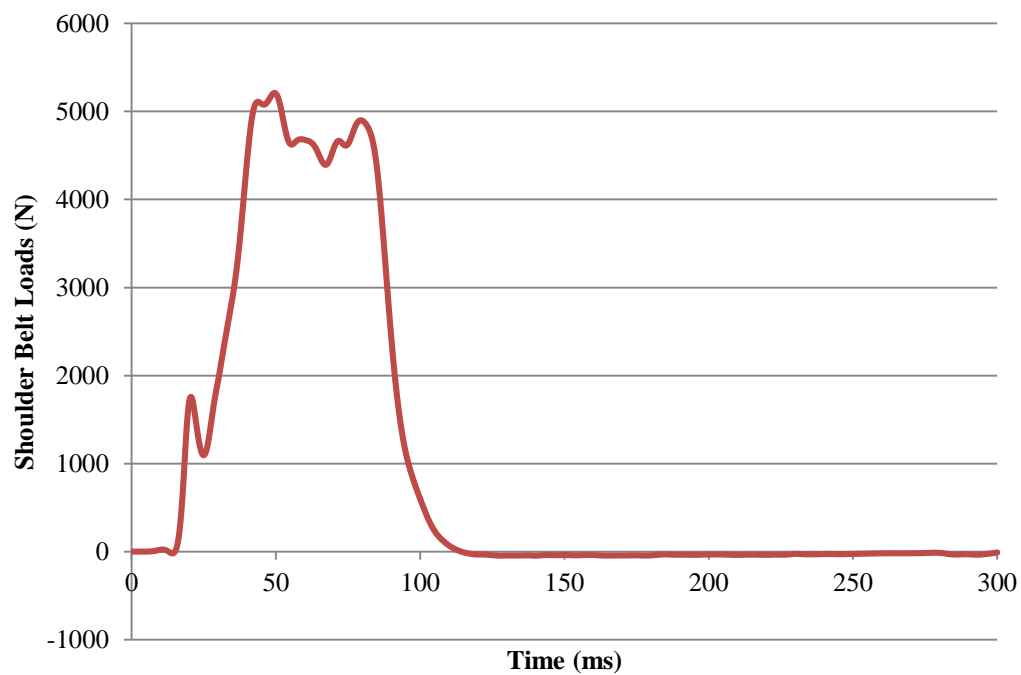


Figure 6-40. Shoulder Belt Loads

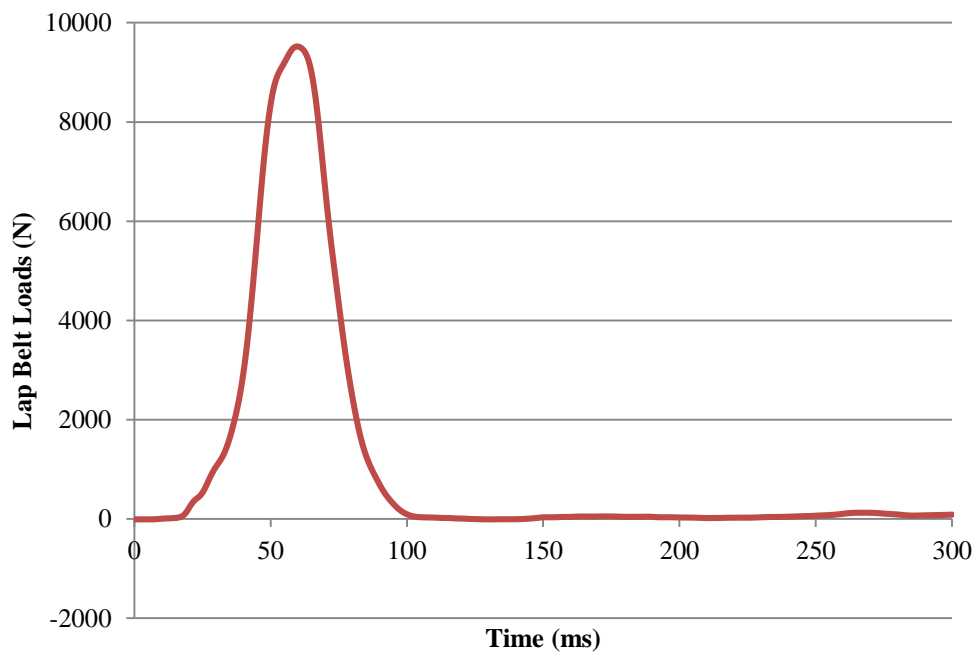


Figure 6-41. Lap Belt Loads

6.6.3 Assessment of Test Results as per Vehicle Dynamics

An assessment of the test based on the following applicable *MASH* safety evaluation criteria is presented below.

6.6.3.1 Structural Adequacy

- C. *Acceptable test article performance may be by redirection, controlled penetration, or controlled stopping of the vehicle.*

Results. The Rigid Wall brought the vehicle to a stop.

6.6.3.2 Occupant Risk

- D. *Detached elements, fragments, or other debris from the test article should not penetrate or show potential for penetrating the occupant compartment, or present an undue hazard to other traffic, pedestrians, or personnel in a work zone.*

Deformation of, or intrusions into, the occupant compartment should not exceed limits set forth in Section 5.3 and Appendix E of MASH. (roof ≤ 4.0 in. (101 mm); windshield = ≤ 3.0 in. (76.2 mm); side windows = no shattering by test article structural member; wheel/foot well/toe pan ≤ 9.0 in. (228 mm); forward of A-pillar ≤ 12.0 in. (300 mm); front side door area above seat ≤ 9.0 in (228 mm).; front side door below seat ≤ 12.0 in.; floor pan/transmission tunnel area ≤ 12.0 in. (300 mm)).

Results. No detached elements, fragments, or other debris were present to penetrate or to show potential for penetrating the occupant compartment, or to present hazard to others in the area. Maximum occupant compartment deformation was 1.0 in (25.4 mm). across the firewall area.

F. The vehicle should remain upright during and after collision. The maximum roll and pitch angles are not to exceed 75 degrees.

Results. The 1100C vehicle remained upright during and after the collision event. Maximum roll and pitch were 3 degrees and 4 degrees, respectively.

H. Occupant impact velocities should satisfy the following.

Longitudinal and Lateral Occupant Impact Velocity

Preferred

Maximum

30 ft/s (9 m/s)

40 ft/s (12 m/s)

Results. Longitudinal OIV was 56.4 ft/s (17.2 m/s), and lateral OIV was 3.6 ft/s (1.1 m/s). (FAIL)

I. Occupant ridedown accelerations should satisfy the following.

Longitudinal and Lateral Occupant Ridedown Accelerations

Preferred

Maximum

15.0 G

20.49 G

Results. Longitudinal RDA was 4.2 G, and lateral RDA was 1.7 G. (PASS)

6.6.4 Assessment of Test Results as per ATD Dynamics

The following section gives details of the assessment of occupant injury risk as per FMVSS and US-NCAP standards.

Injury risk curves were established with the help of the equations given in section 3.4 for computing the probability of injury risks of head, chest, neck and legs and certain reference values were set up for each occupant injury risk. These are known as Injury

Assessment risk values (IARV). A comparison of the maximum values from the test against the IARV is made to check if the test was a pass or a fail in Table 6-4.

Table 6-4. Comparison of Occupant Injury Risk Parameters to IARV

Injury Criteria	Values from crash test	Limits	Pass/Fail
HIC-15	264.1	700	Pass
Chest Deflection, in. (mm)	2 (50.9)	2.5 (63)	Pass
Neck Tension Force, lbf (N)	434 (1929.8)	1058 (4710)	Pass
Femur (Left) Axial Force, lbf (N)*	843 (3764.2)	2248 (10000)	Pass

* During the crash test, wires connected to the right femur accelerometer got loose; therefore the obtained data was not realistic and could not be used for the purpose of this project.

From the above table it can be seen that the test is pass from point of view of head neck and chest injury criteria.

7. FINITE ELEMENT MODEL CALIBRATION

The finite element model of the 2010 Toyota Yaris along with inclusion of ATD and passive restraint systems was used to replicate the full-scale crash event. Some modifications were applied to the geometry and characteristics of the model to more accurately replicate the recorded kinematics and results from the impact event.

7.1 Seat Adjustment and Steering Wheel Data

As an initial step towards this attempt, the driver's seat of the FE model of the Toyota Yaris was adjusted to replicate general position, and angles of back rest and head rest recorded for the full-scale crash preparation. Similarly, the inclination angle of the FE model of the steering wheel was adjusted to replicate the condition observed in the full-scale test. Both seat and steering wheel were previously position as in the full-scale test as per US-NCAP requirements. Figure 7-1 shows the position of the finite element model of the driver's seat and steering wheel.

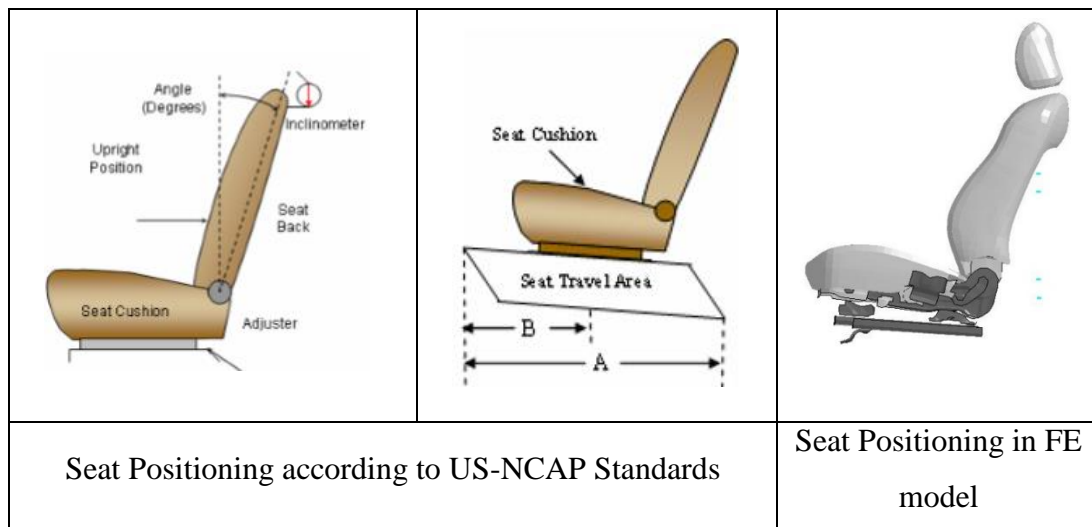


Figure 7-1. Position of Drivers' Seat and Steering Wheel Adjusted as per US-NCAP Regulations

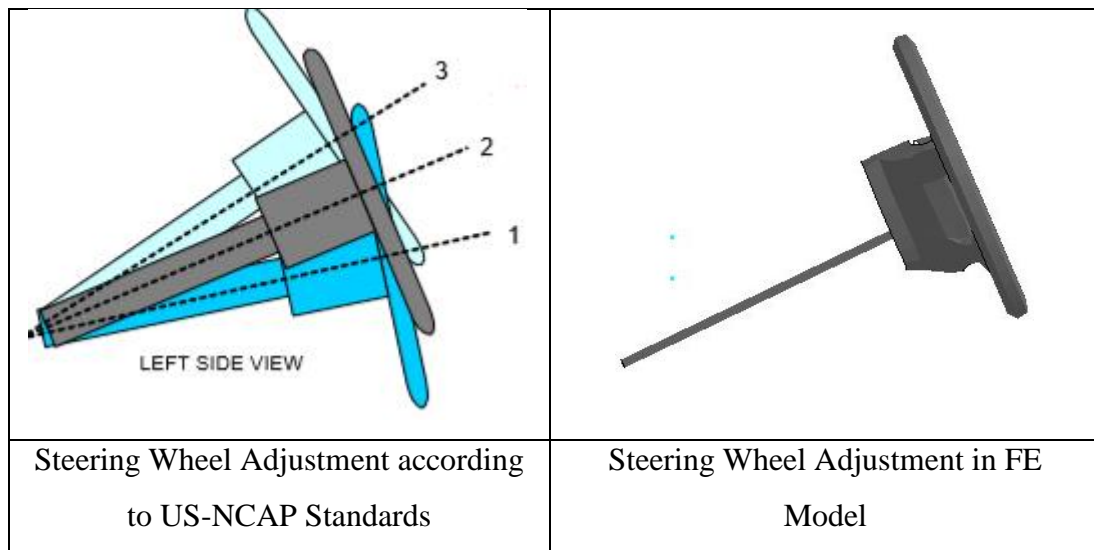


Figure 7-1. Continued

7.2 Anthropomorphic Test Device Position

The position of the ATD as per US-NCAP regulations plays a vital role in its behavior and dynamics. The FE model of the ATD was placed in position as per US-NCAP requirements by adjusting its fore arms, shoulders, position of hands on steering wheel, angles of lower body part such as ankle, feet, knees. A crucial part was to adjust the FE model of the ATD on the driver's seat with approximately the same distance between the head and the vehicle roof (referred as HZ as per US-NCAP) that was recorded in the full-scale test preparation. To achieve this, preliminary simulations were performed to place the ATD in the driver's seat applying gravity to the model.

7.3 Airbag Adjustment

One of the most important issues for the finite element model was the adjustment of the airbag model. NCAC developed a working FE model of a steering wheel and airbag that is publicly available for download on their website. This airbag model was used in this research to analyze the effects of an airbag restraint system on occupant injury criteria.

In finite element simulations, the inflation, deployment and deflation mechanisms are achieved using an inflation-deflation curve. Attempts were made in this research to best achieve the highest correlation between test and simulation airbag behavior through adjustments of the inflation and deflation curves. The original model obtained from the NCAC website had an inflation curve with a mass flow rate vs. time ranging between 0 to 1 second. Figure 7-2 shows the original mass flow rate vs. time of the airbag.

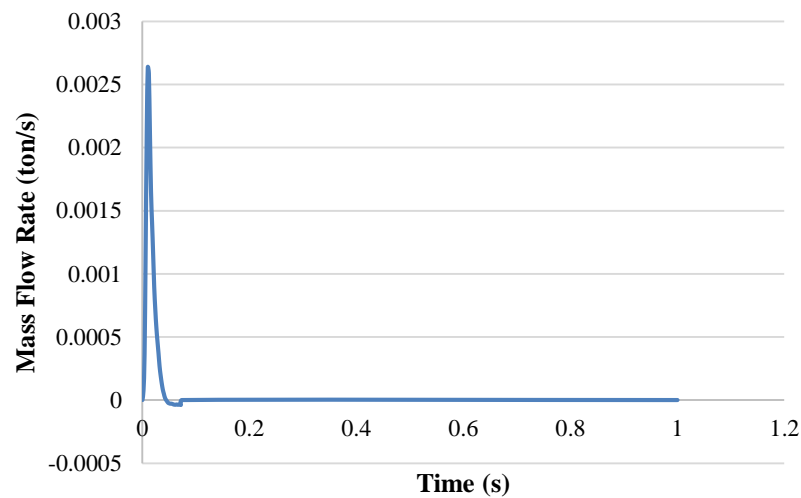


Figure 7-2. Original Mass Flow Rate vs. Time Curve for Airbag Inflation

After running preliminary simulations to evaluate the airbag inflation and deflation behavior and comparing it to the recorded behavior during the full-scale crash test, some curve adjustments were applied. A new deflation curve was developed using the existing inflation curve and modifying it by decreasing the mass flow rate. The peak value of deflation curve was initially considered as the same as the peak value of inflation curve. Parametric simulations were performed by decreasing the deflation peak value to 80%, 60%, 50%, and 40% of the initial peak value. To match it to the crash test results, the inflation curve was tailored with a time lag. The modified curves are shown in Figure 7-3.

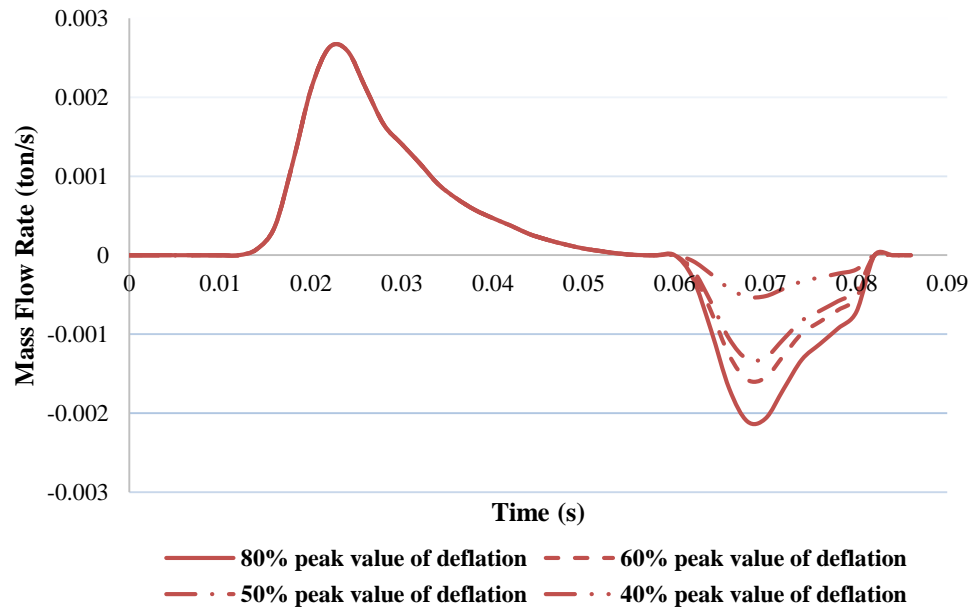


Figure 7-3. Airbag Curve Tailored Slope with Different Deflation Peaks (Mass Flow Rate vs. Time)

Table 7-1 shows sequential images of the FE computer simulations for different cases of deflation curve considered (inflation curve was maintained the same).

Table 7-1. Sequential Images of Airbag Deflation in Different Cases

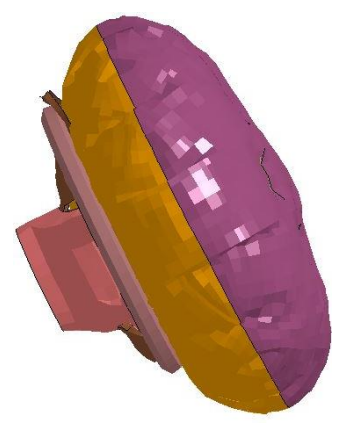
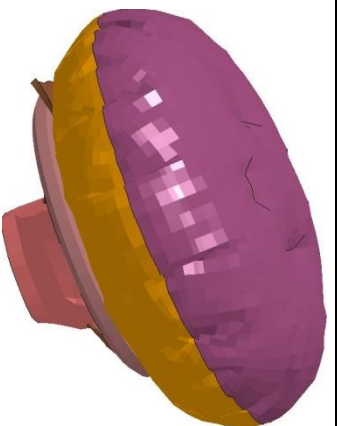
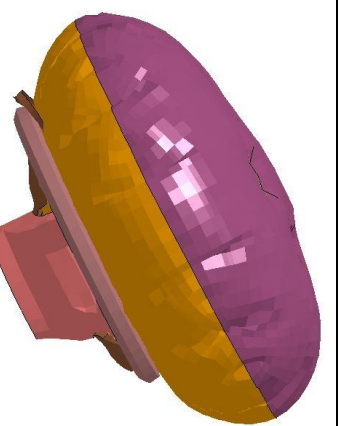

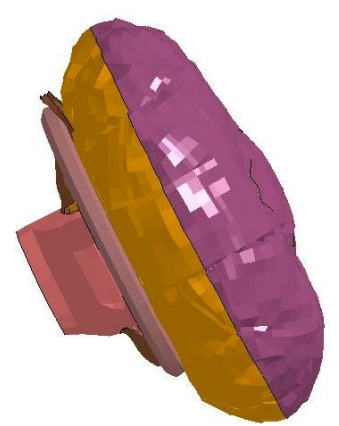
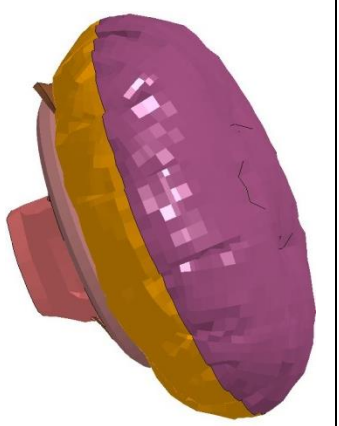
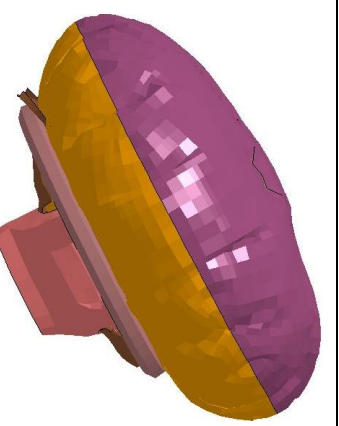

Time	80% of peak value of inflation curve	60% of peak value of inflation curve	50% of peak value of inflation curve	40% of peak value of inflation curve
0.07				
0.072				

Table 7-1 Continued

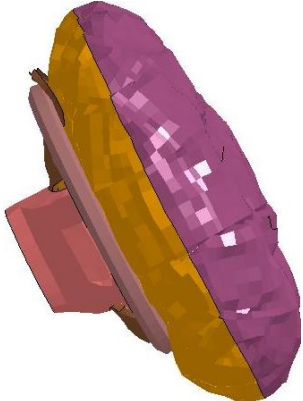
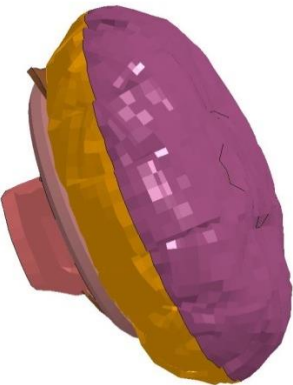


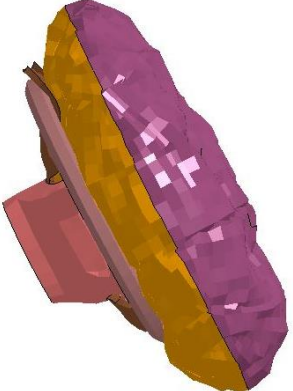
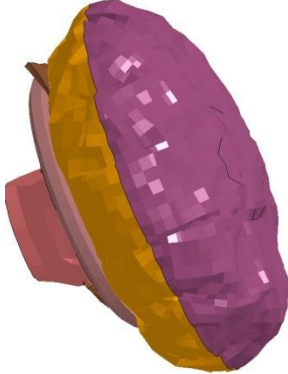

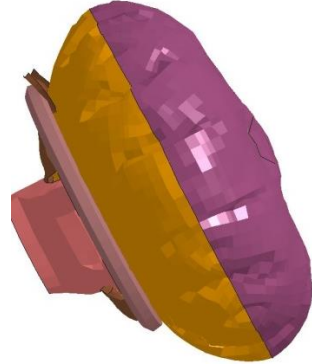
Time	80% of peak value of inflation curve	60% of peak value of inflation curve	50% of peak value of inflation curve	40% of peak value of inflation curve
0.074				
0.076				

Table 7-1 Continued


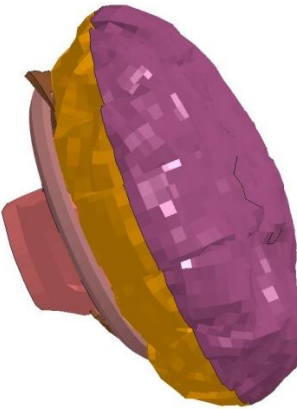


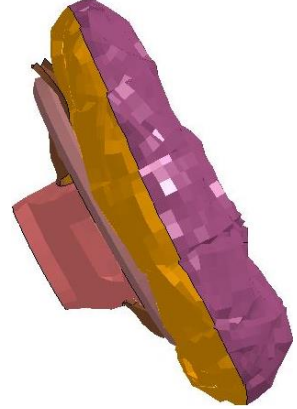




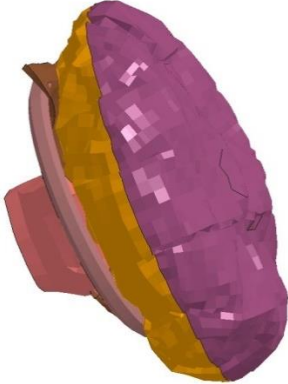
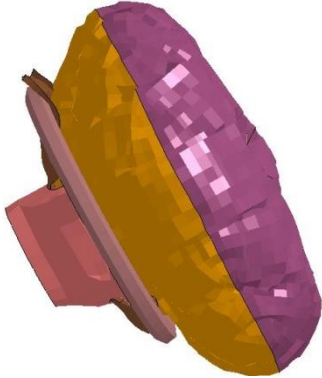


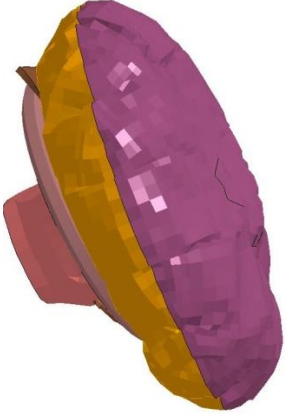
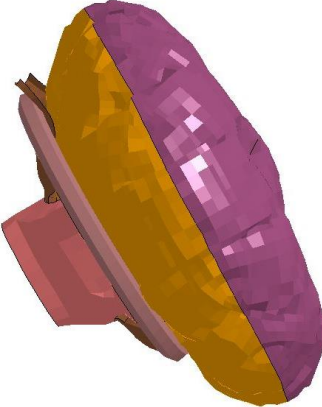
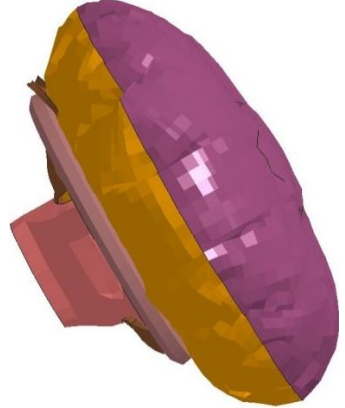
Time	80% of peak value of inflation curve	60% of peak value of inflation curve	50% of peak value of inflation curve	40% of peak value of inflation curve
0.078				
0.08				

Table 7-1 Continued

Time	80% of peak value of inflation curve	60% of peak value of inflation curve	50% of peak value of inflation curve	40% of peak value of inflation curve
0.082				
0.092				

As seen in Table 7-1, the airbag deflation for case #1 happens too quickly. This behavior was proven to allow the ATD to hit the steering wheel during a complete model simulation, which caused a major head injury value. On the other hand, the deflation of airbag in case #4 appeared to be too slow, leading to a “bouncing” type reaction when the ATD hit the airbag during the complete model run, and causing high head injury value once again. It was observed that reasonable values of HIC were achieved in the second and the third case where the highest value of deflation mass flow rate with time was 60% and 50% of the highest inflation mass flow rate, respectively. The third case was selected to be a reasonable value as it was best replicating the recorded dynamic and results from the full-scale crash test scenario.

7.4 Simulation of FE Model Frontal Crash

With all applied adjustments to ATD and seat positioning, and to the airbag model, the complete FE model was employed to replicate the rigid barrier frontal test with a speed of 34.7 mph (55.8 km/h). Figure 7-4 and Figure 7-5 shows the sequential images of FE simulations at the initial nominal conditions of the full-scale test.


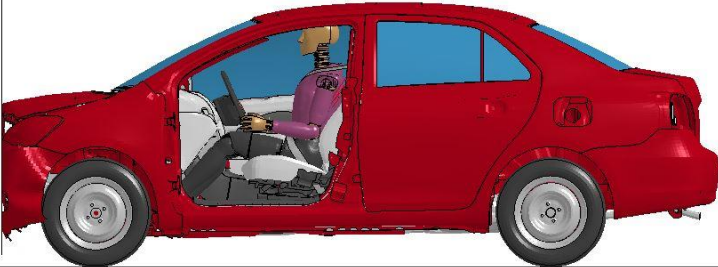
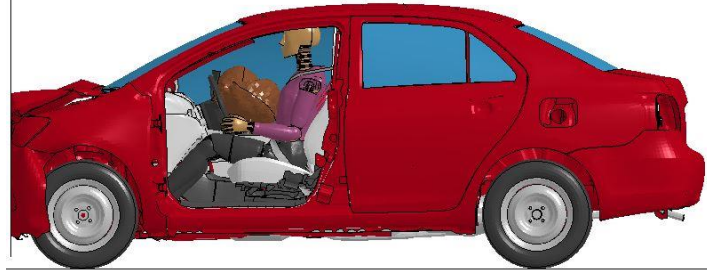

Time (s)	FE Model of Car, ATD and Restraints (34.7 mph i.e., 55.8 km/h)
0.000	
0.02	
0.03	
0.04	

Figure 7-4. Sequential Images of Simulations of Crash Test at 34.7 mph (Side View)

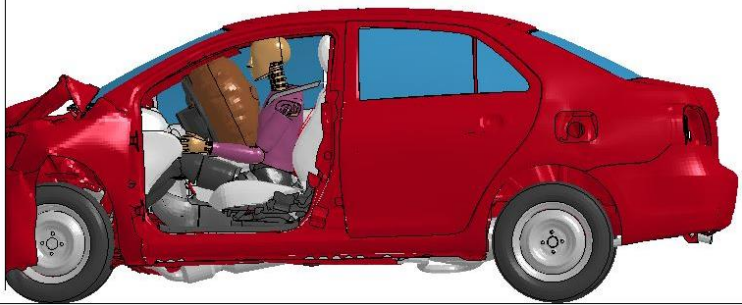


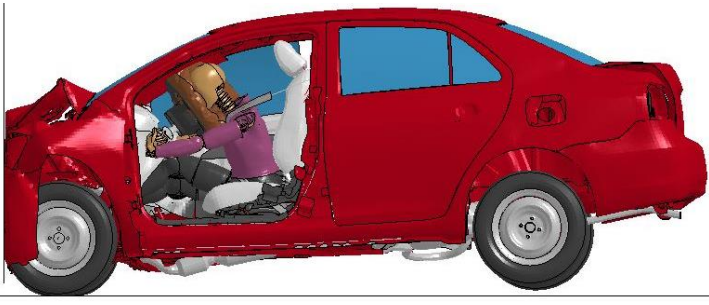
Time (s)	FE Model of Car, ATD and Restraints (34.7 mph i.e., 55.8 km/h)
0.05	
0.06	
0.07	
0.08	

Figure 7-4 Continued




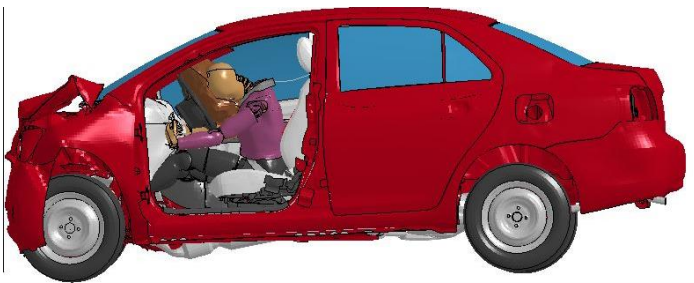
Time (s)	FE Model of Car, ATD and Restraints (34.7 mph i.e., 55.8 km/h)
0.09	
0.1	
0.11	
0.12	

Figure 7-4 Continued

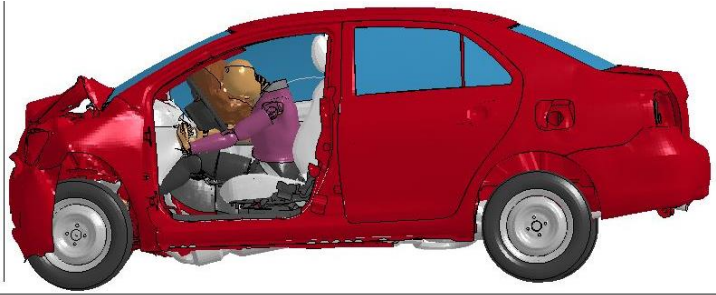
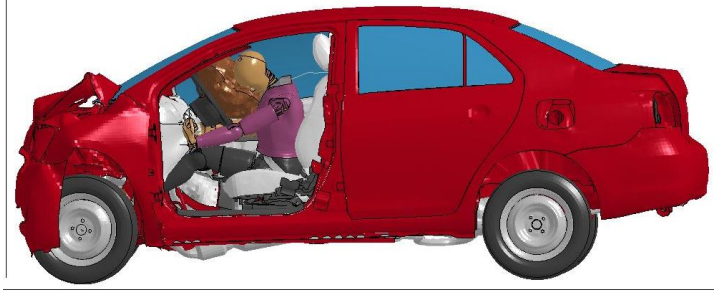

Time (s)	FE Model of Car, ATD and Restraints (34.7 mph i.e., 55.8 km/h)
0.13	 A side-view finite element model of a red sedan. The driver-side airbag is deployed, shown as a large, inflated, light-colored cushion. The driver's head and torso are visible, positioned behind the airbag. The car's front end shows some deformation, and the wheels are visible.
0.14	 A side-view finite element model of a red sedan, similar to the previous frame. The driver-side airbag is deployed. The driver's head and torso are visible, positioned behind the airbag. The car's front end shows some deformation, and the wheels are visible.
0.15	 A side-view finite element model of a red sedan, similar to the previous frames. The driver-side airbag is deployed. The driver's head and torso are visible, positioned behind the airbag. The car's front end shows some deformation, and the wheels are visible.

Figure 7-4 Continued

Figure 7-5 shows the sequential images of simulation of crash test from top view.


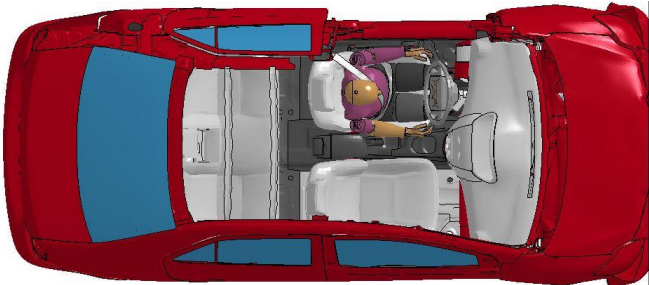

Time (s)	FE Model of Car, ATD and Restraints (34.7 mph i.e., 55.8 km/h)
0.000	
0.01	
0.02	
0.03	

Figure 7-5. Sequential Images of Simulations of Crash Test at 34.7 mph (Top View)




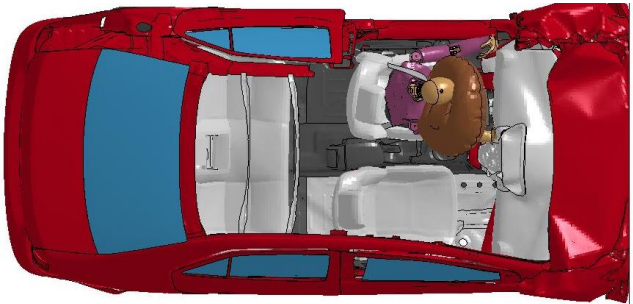
Time (s)	FE Model of Car, ATD and Restraints (34.7 mph i.e., 55.8 km/h)
0.04	
0.05	
0.06	
0.07	

Figure 7-5 Continued


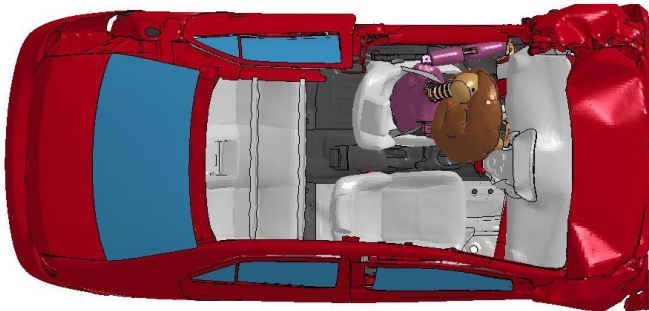


Time (s)	FE Model of Car, ATD and Restraints (34.7 mph i.e., 55.8
0.08	
0.09	
0.1	
0.11	

Figure 7-5 Continued


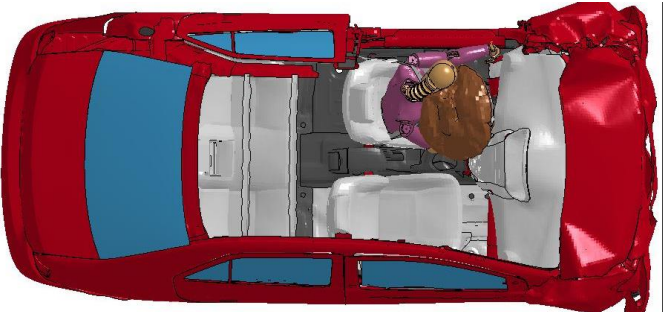


Time (s)	FE Model of Car, ATD and Restraints (34.7 mph i.e., 55.8 km/h)
0.12	
0.13	
0.14	
0.15	

Figure 7-5 Continued

7.5 Finite Element Simulation Results

The following section discusses the occupant injury risk from FE simulations.

7.5.1 Occupant Risk Values as per Vehicle Dynamics

The TRAP program was used to evaluate occupant risk factors based on the applicable *MASH* safety evaluation criteria. The modeled Toyota Yaris remained upright during and after the modeled collision event. Data from the accelerometer, located at the FE model of the vehicle center of gravity, were used in TRAP program for evaluation of occupant risk. For post processing, SAE Class 180 filter on acceleration data and angular velocity/displacement data. In the longitudinal direction, the occupant impact velocity (OIV) was 56.4 ft/s (17.2 m/s) at 0.0736 s, the highest 0.010 s occupant ridedown acceleration (RDA) was 4.8 G from 0.0812 to 0.0912 s, and the maximum 0.050 s average acceleration was -33.1 G between 0.0205 and 0.0705 s. In the lateral direction, the OIV was 0.6 ft/s (0.18 m/s) at 0.0736 s, the highest 0.010 s occupant RDA was 2.5 G from 0.1116 to 0.1216 s, and the maximum 0.050 s average was -1.4 G between 0.068 and 0.1108 s. Theoretical Head Impact Velocity (THIV) was 60 km/h (18.3 m/s) at 0.0736 s; Post-Impact Head Decelerations (PHD) was 5 G between 0.0812 and 0.0912 s; and Acceleration Severity Index (ASI) was 2.76 between 0.0205 and 0.0705 s.

Table 7-2 gives the comparison of occupant risk assessment values from crash test and computer FE model simulation.

Table 7-2. Comparison of Occupant Risk Assessment Values from Crash Test and Computer Simulation

Occupant Risk Parameters	From Test	From Simulation
Longitudinal		
OIV, ft/s (m/s)	56.4 (17.2)@0.077 s	56.4 (17.2)@0.0736s
RDA (G)	4.2@0.083s-0.093s	4.8@0.0812s-0.0912s
Max. 0.05 s Avg Accl (G).	-30.6@0.013s-0.063s	-33.1@0.0205s-0.0705s
Lateral		
OIV, ft/s (m/s)	3.6 (1.1)@0.077s	0.6 (0.18) @0.0736s
RDA (G)	1.7@0.086s-0.096s	5@0.1116s to 0.1216s
Max. 0.05 s Avg Accl. (G)	-3.8@0.023-0.073s	-1.4@0.068s-0.1108s
THIV, mph (km/h or m/s)	38.6 (62.2 or 17.3)@0.077s	41 (66 or 18.3)@0.0736s
PHD(G)	4.3@0.083s-0.093s	5@0.0812s-0.0912s
ASI	2.85@0.046s-0.096s	2.76@0.0205s-0.0705s

7.5.2 Occupant Injury Criteria as per ATD Dynamics

The dynamics of the model of the anthropomorphic test device have been analyzed with the help of acceleration and force data. This data is given by the accelerometers placed in various locations of the ATD such as head, neck, chest and femur. The accelerations in head, pelvis and neck, chest deflections and the forces and moments of neck and femur are plotted and compared with those of the crash tests from Figure 7-6 to Figure 7-32. Table 7-3 shows the comparison of head, chest, neck and femur injury risk between the crash test and FE Simulation.

Table 7-3. Comparison of Head, Chest, Neck and Femur Injury Criteria from the Crash Test and FE Simulation

Injury Criteria	Values from crash test	Values from FE simulation
HIC-15	264.1	312.15
Chest Deflection(mm)	50.9	46.6
Neck Force (N)	1929.8	2318.7
Femur Axial Force (N)	-3764.2	-4735.39

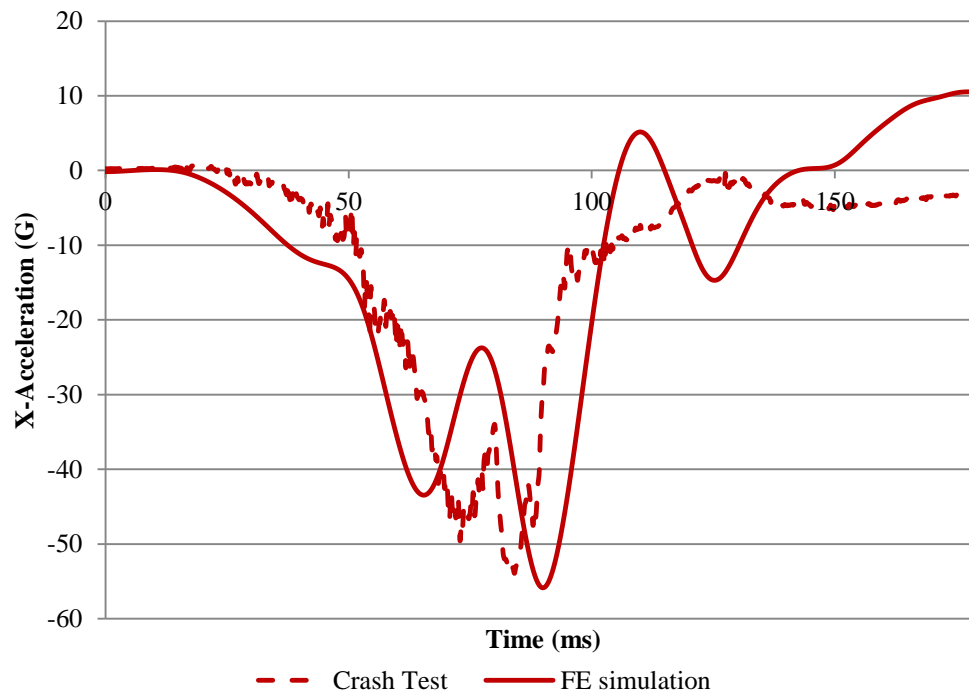


Figure 7-6. Head X-Accelerations vs. Time

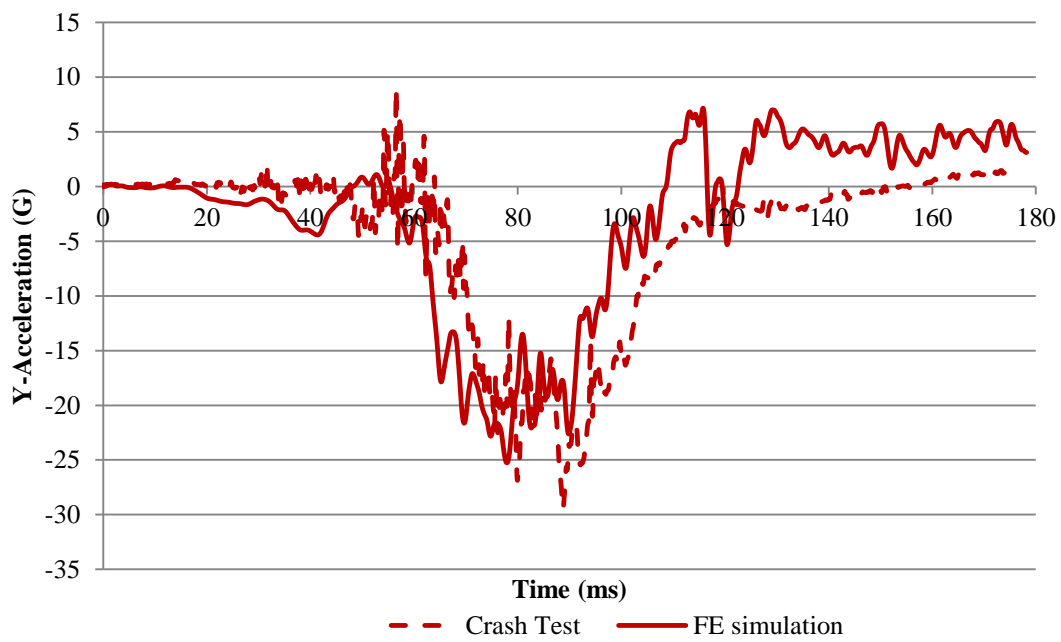


Figure 7-7. Head Y-Accelerations vs. Time

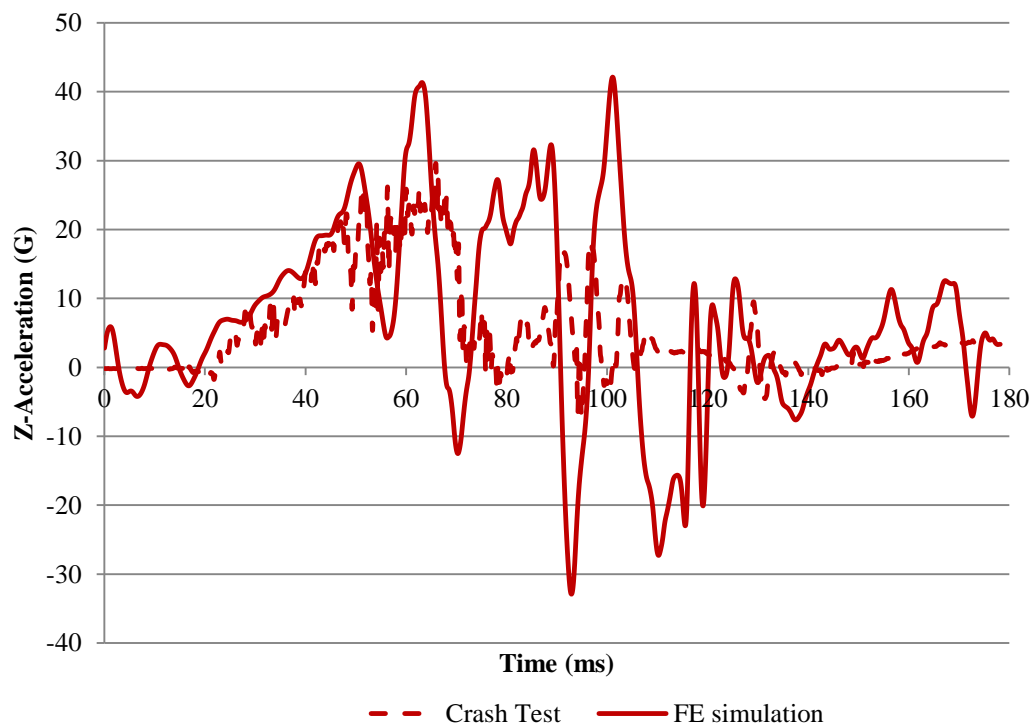


Figure 7-8. Head Z-Accelerations vs. Time

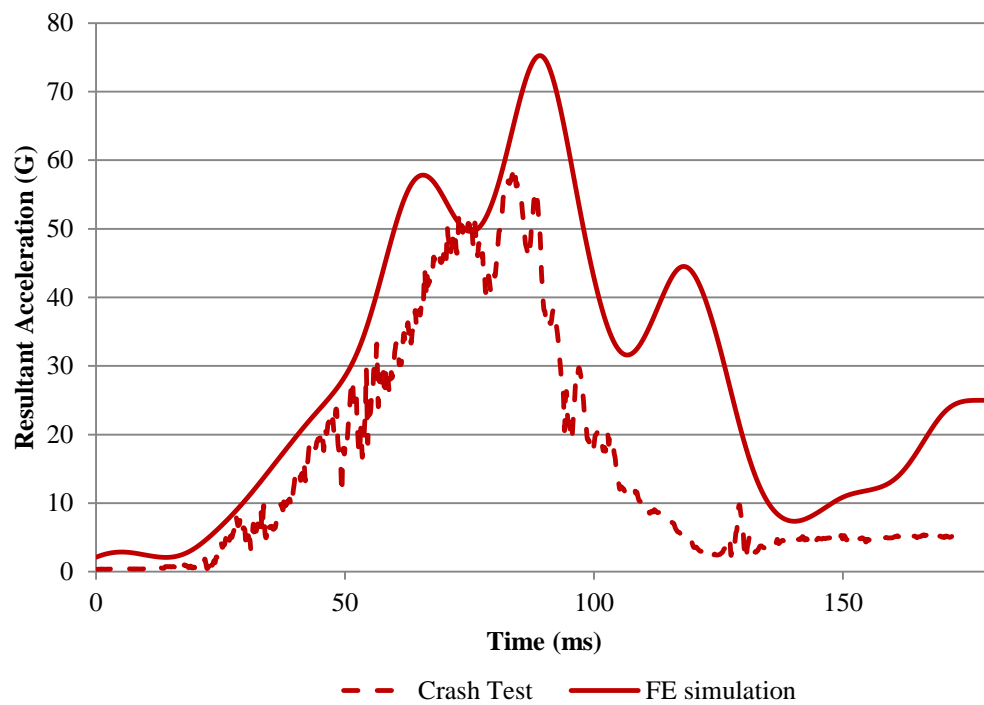


Figure 7-9. Resultant Head Accelerations vs. Time

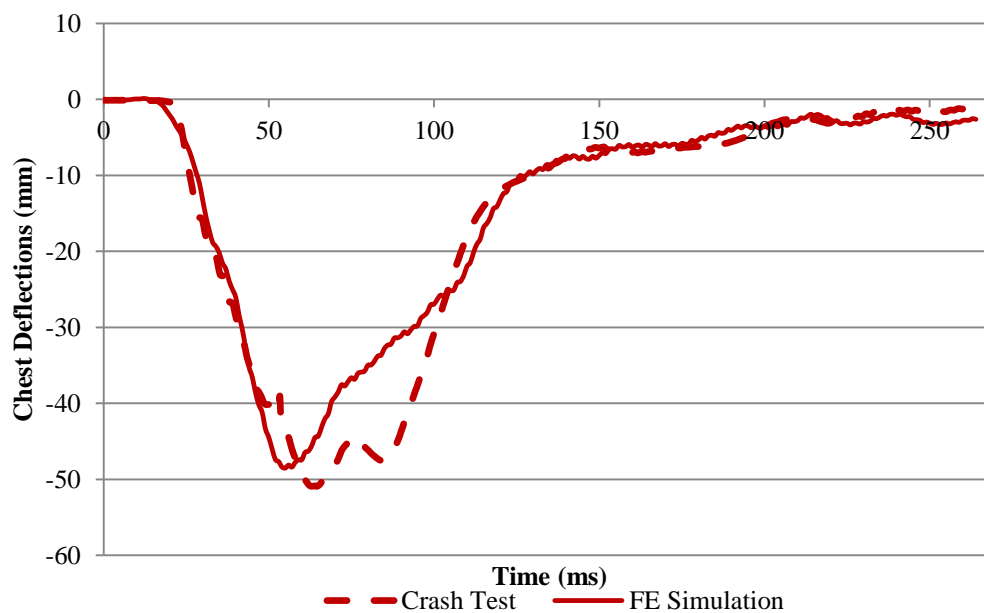


Figure 7-10. Chest Deflections vs. Time

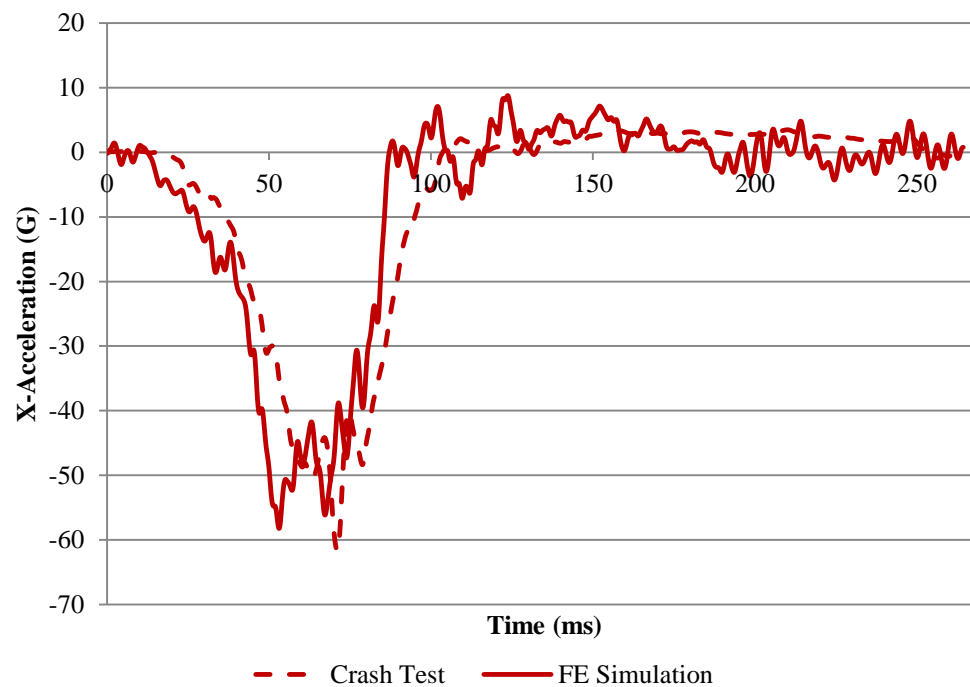


Figure 7-11. Chest X-Accelerations vs. Time

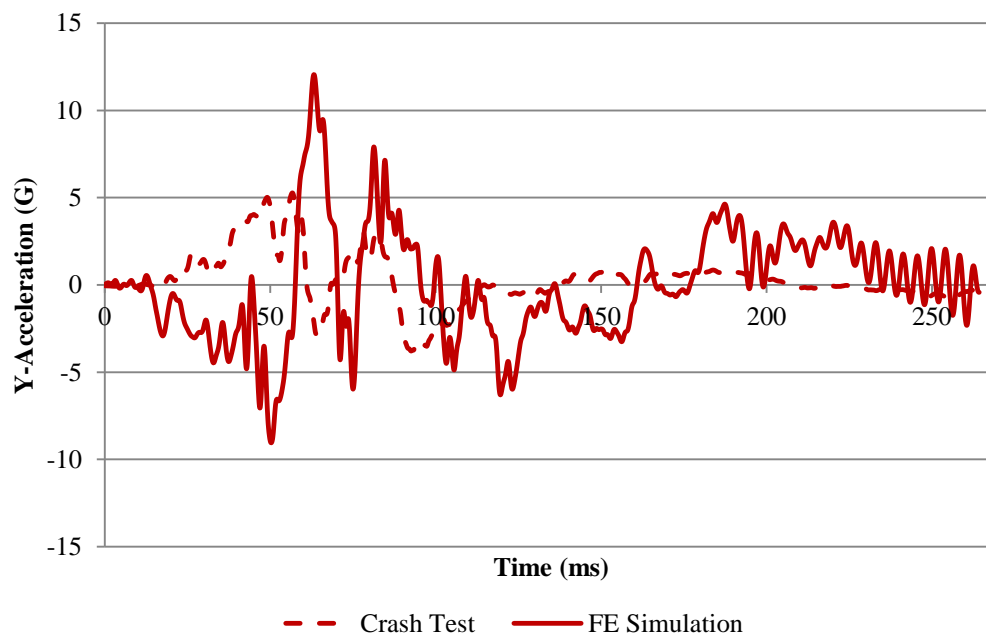


Figure 7-12. Chest Y-Accelerations vs. Time

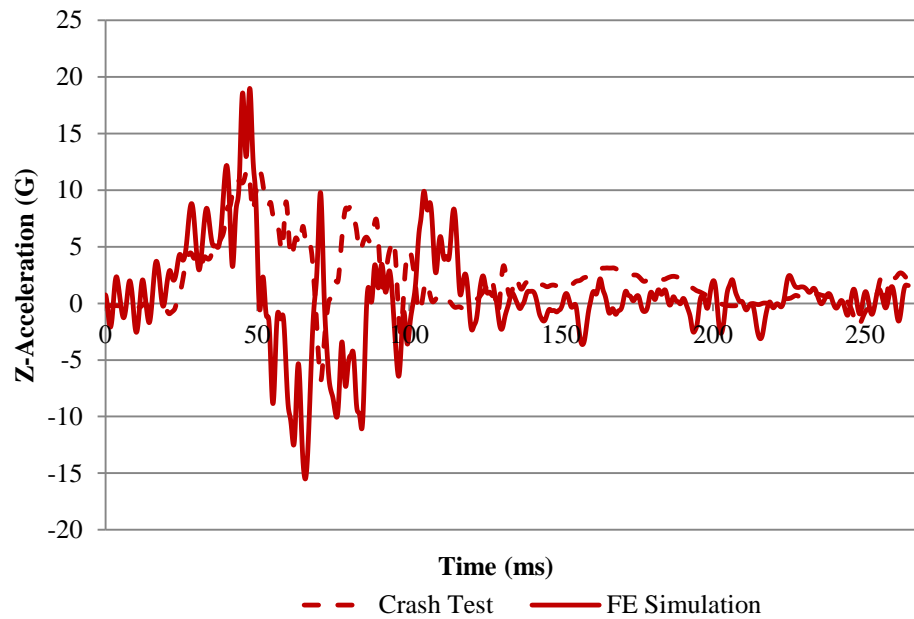


Figure 7-13. Chest Z-Acceleration vs. Time

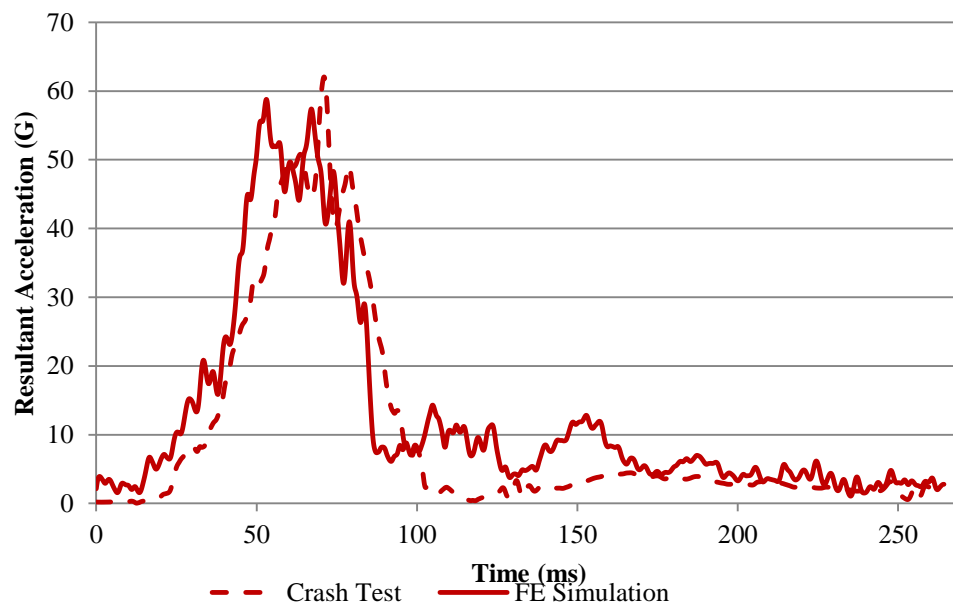


Figure 7-14. Chest Resultant Accelerations vs. Time

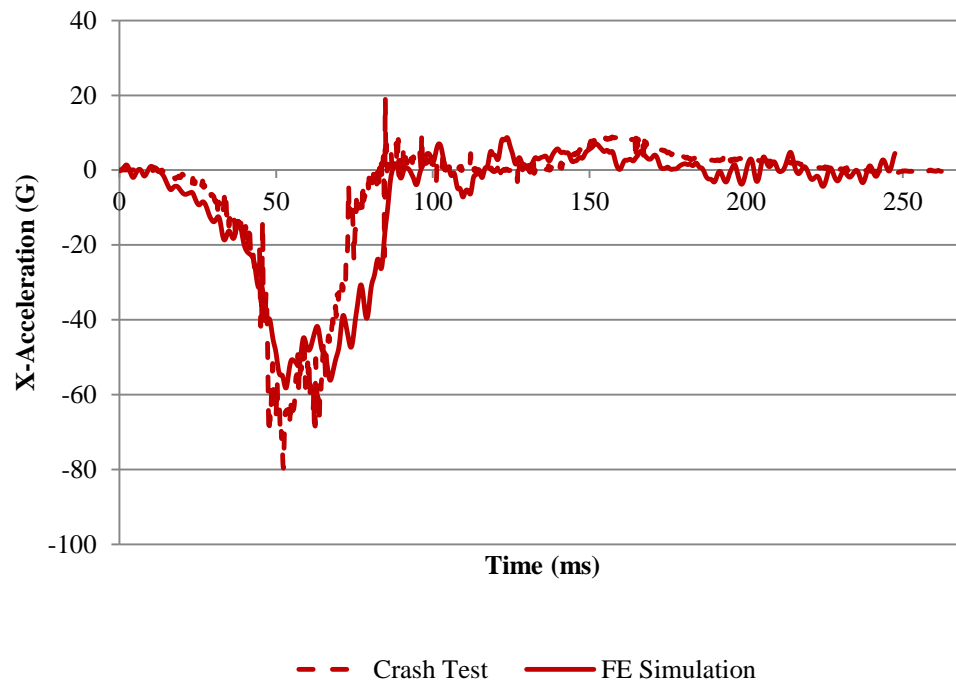


Figure 7-15. Pelvis X-Acceleration vs. Time

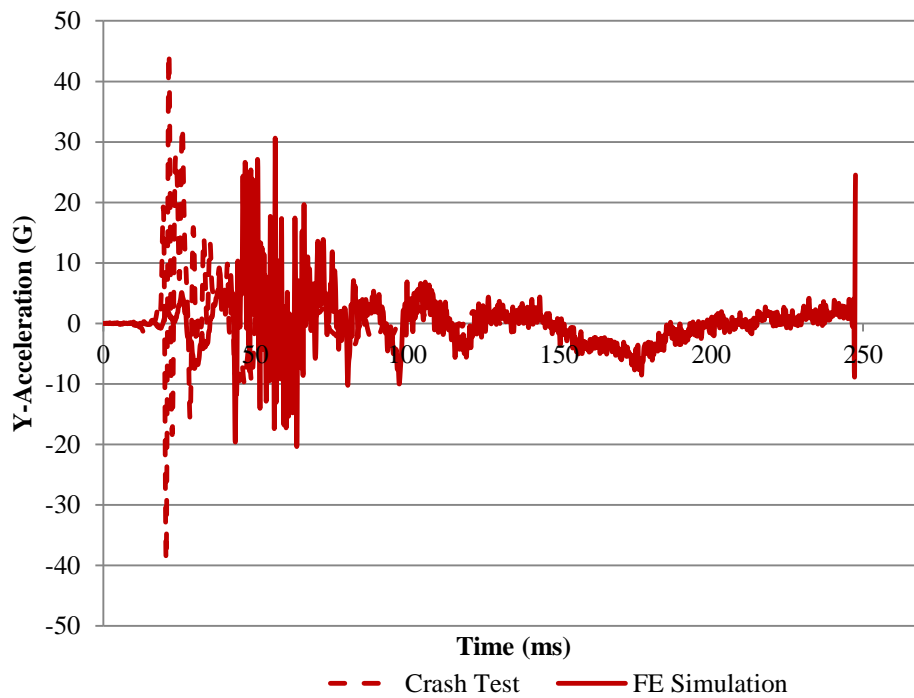


Figure 7-16. Pelvis Y-Acceleration vs. Time

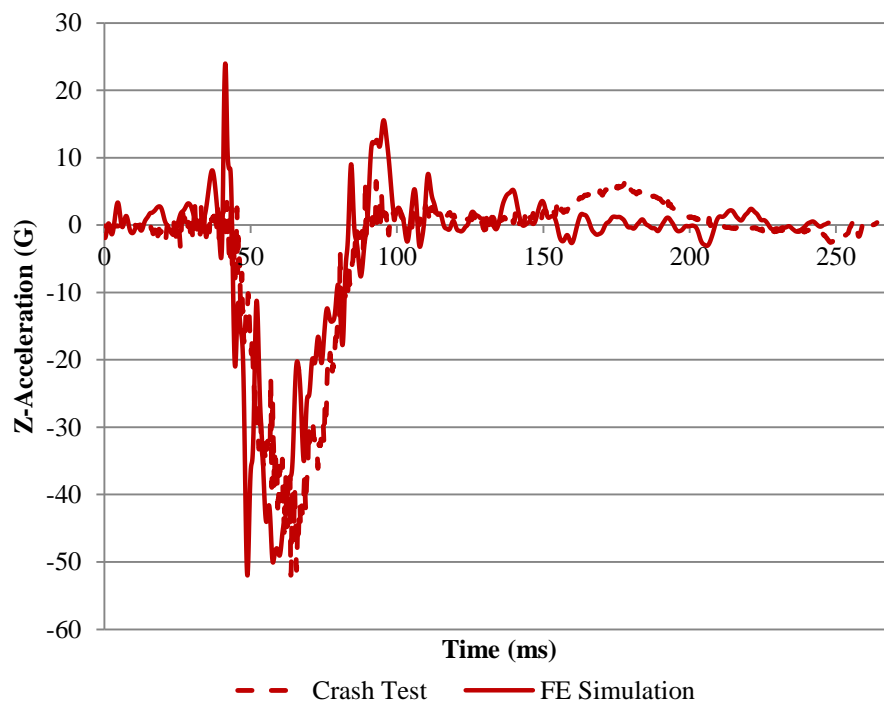


Figure 7-17. Pelvis Z-Acceleration vs. Time

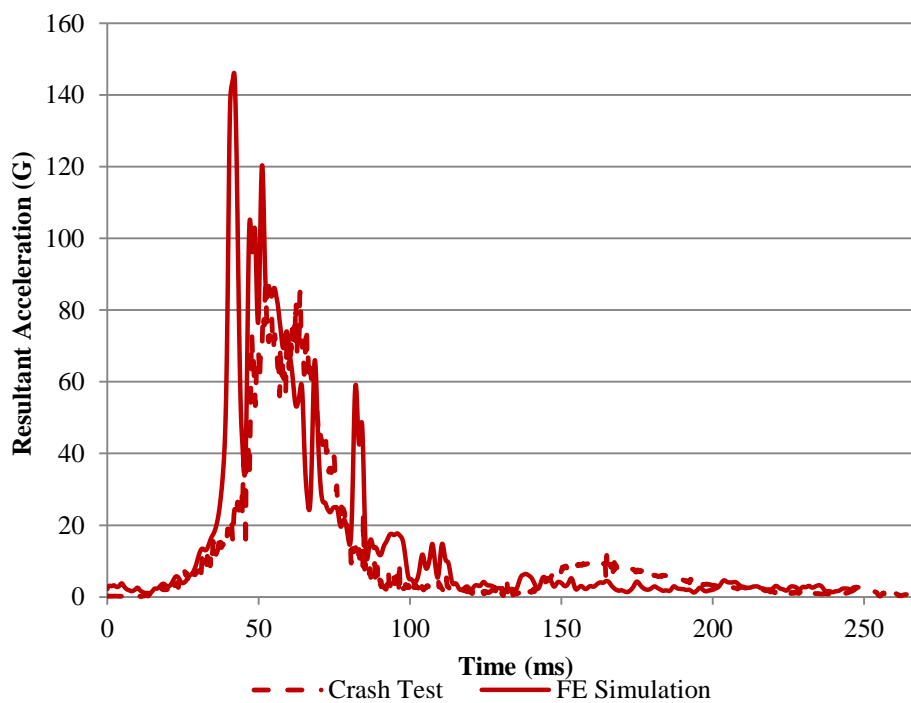


Figure 7-18. Resultant Pelvis Acceleration vs. Time

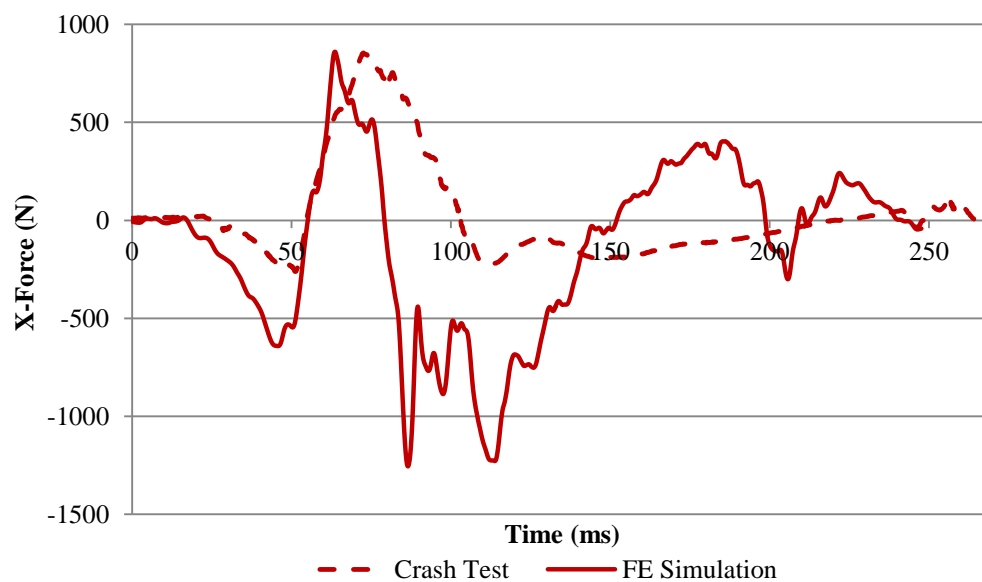


Figure 7-19. Upper Neck X-Force vs. Time

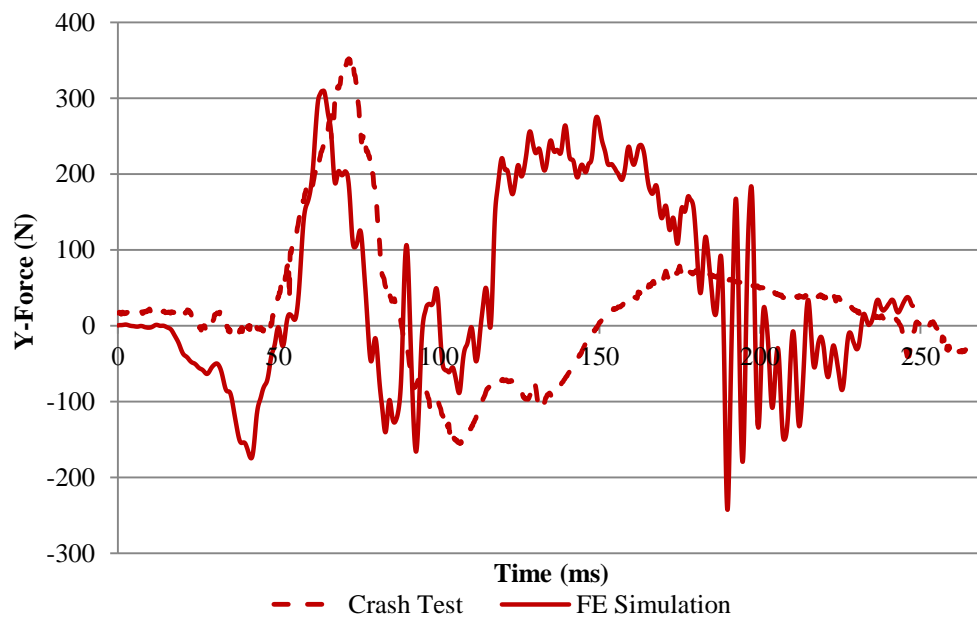


Figure 7-20. Upper Neck Y-Forces vs. Time

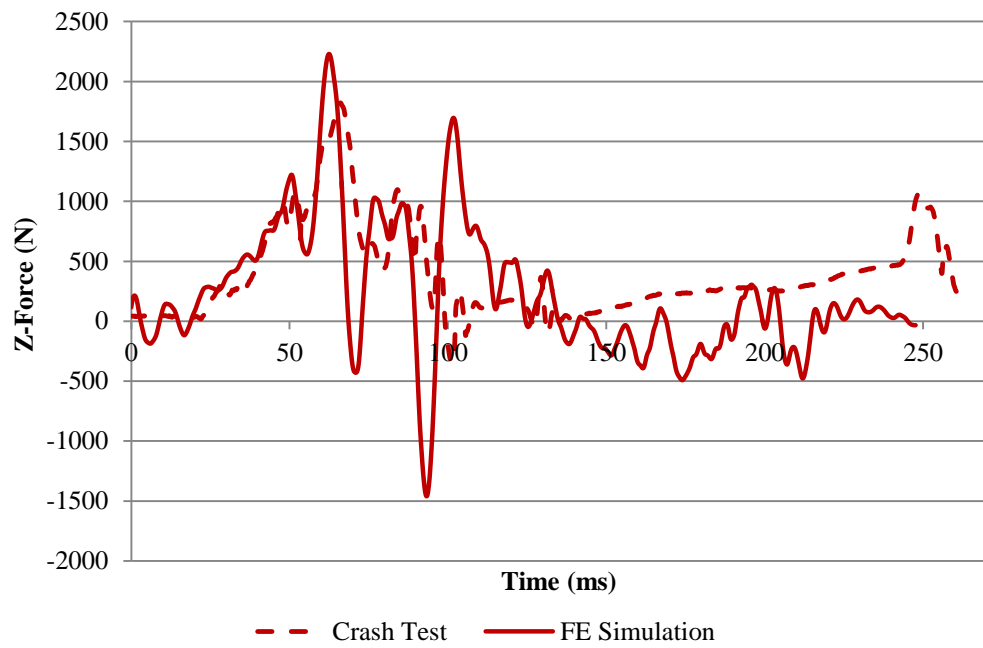


Figure 7-21. Upper Neck Z-Forces vs. Time

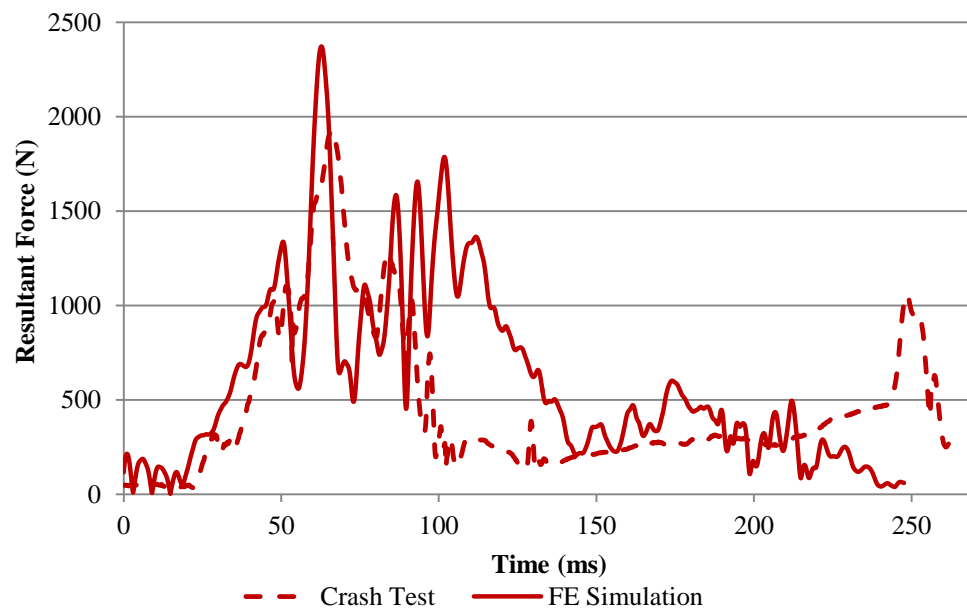


Figure 7-22. Resultant Neck Force vs. Time

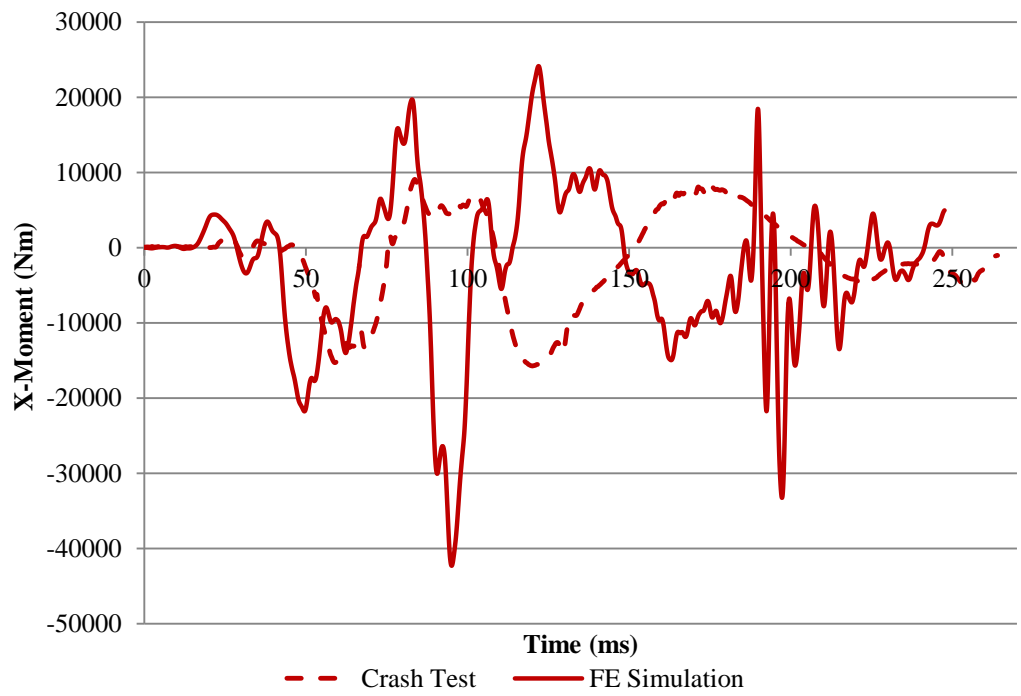


Figure 7-23. Upper Neck X-Moments vs. Time

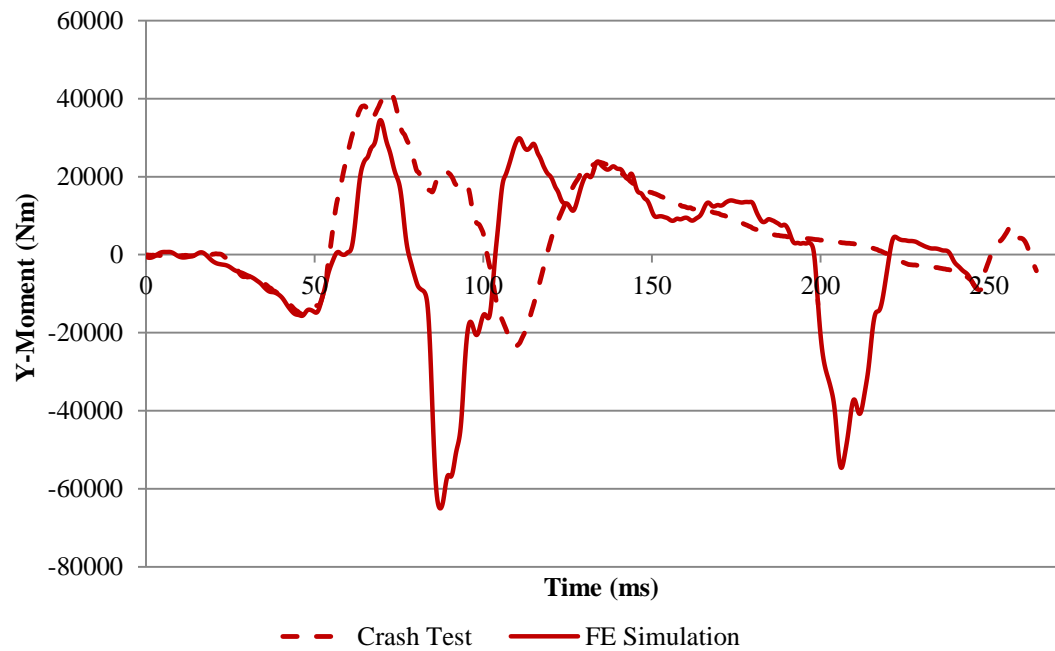


Figure 7-24. Upper Neck Y-Moments vs. Time

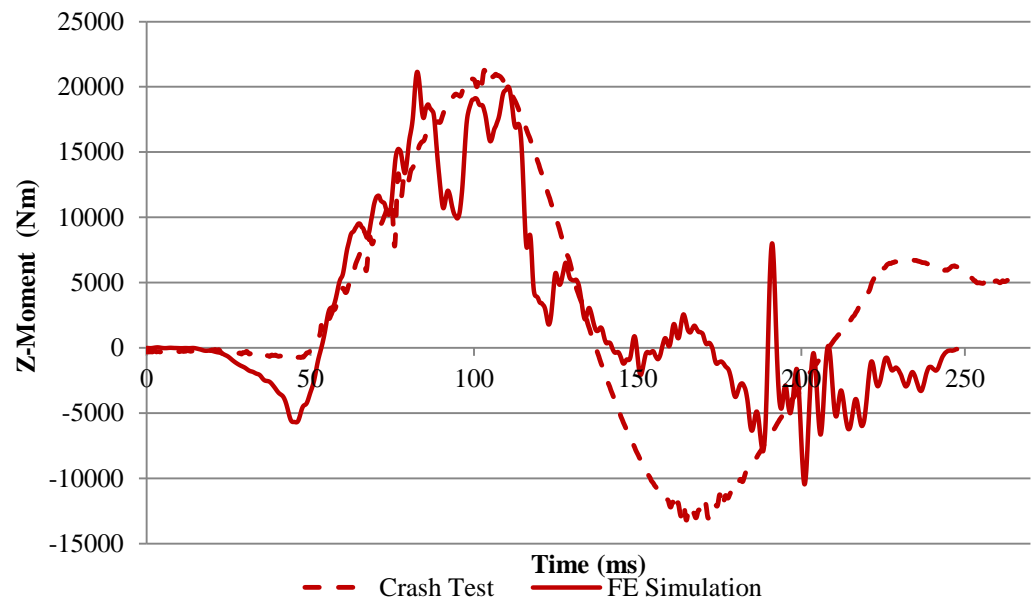


Figure 7-25. Upper Neck Z-Moment vs. Time

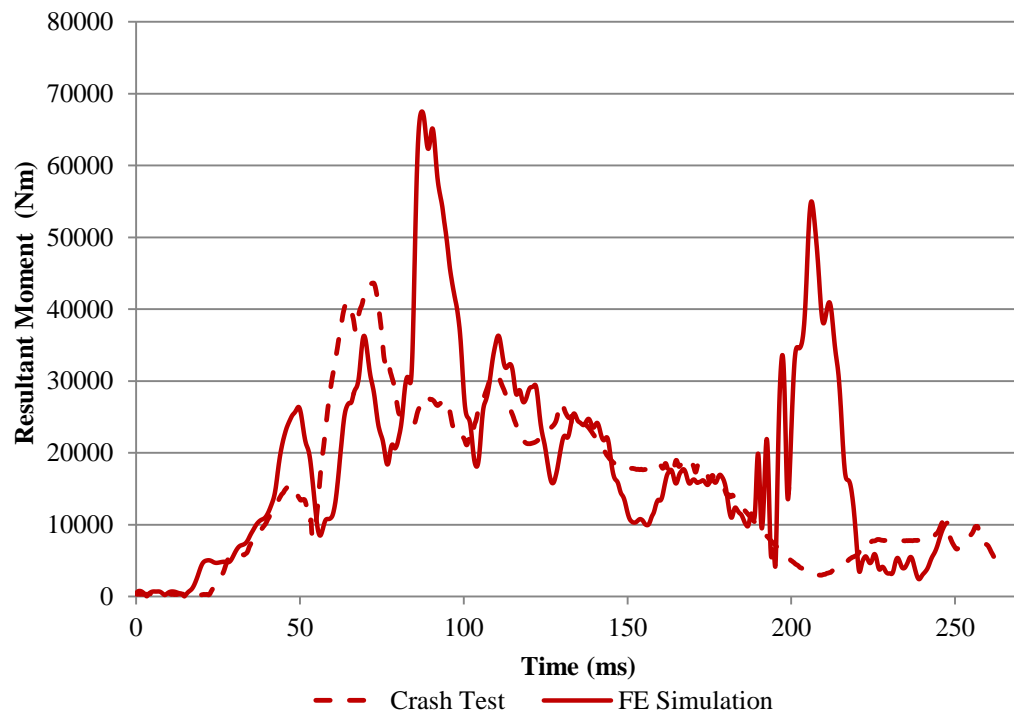


Figure 7-26. Upper Neck Resultant Moment vs. Time

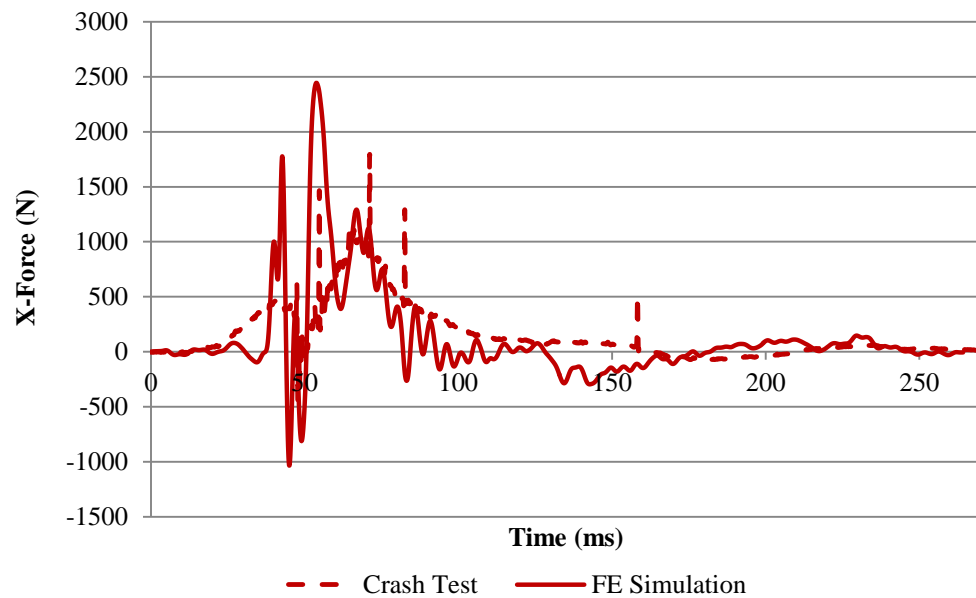


Figure 7-27. Left Femur X-Force vs. Time

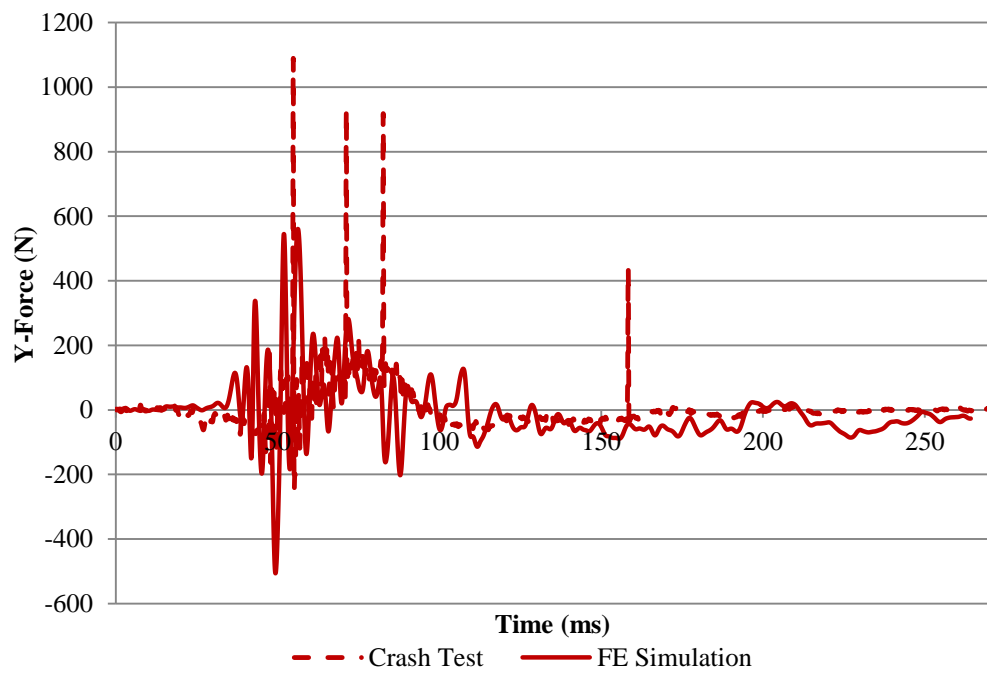


Figure 7-28. Left Femur Y-Force vs. Time

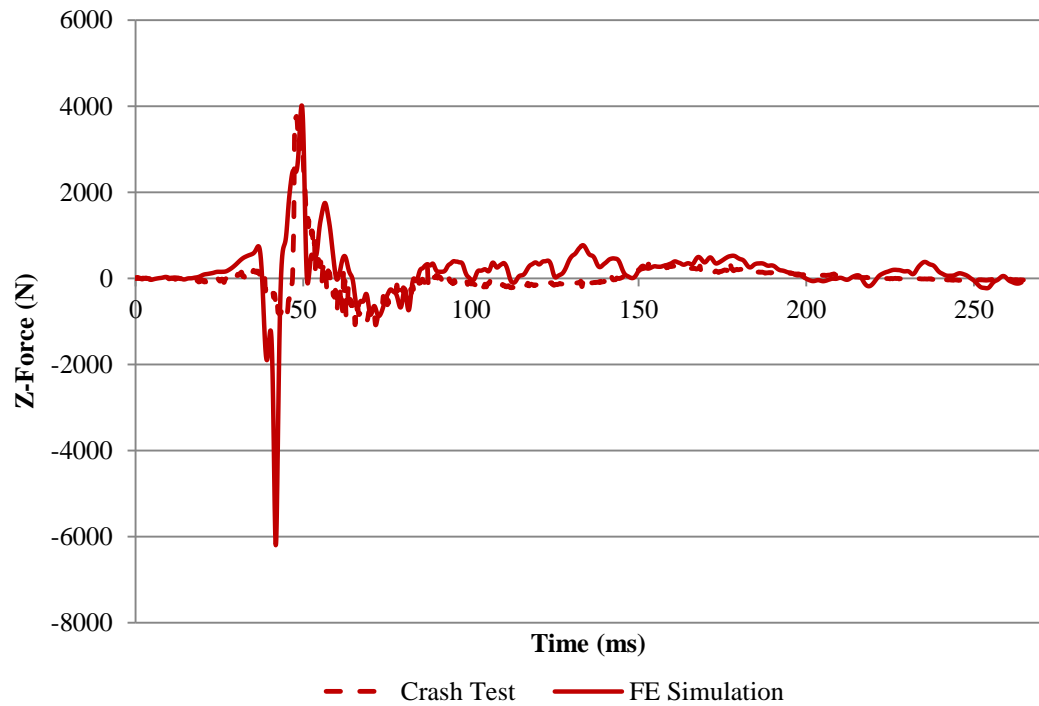


Figure 7-29. Left Femur Z-Forces vs. Time

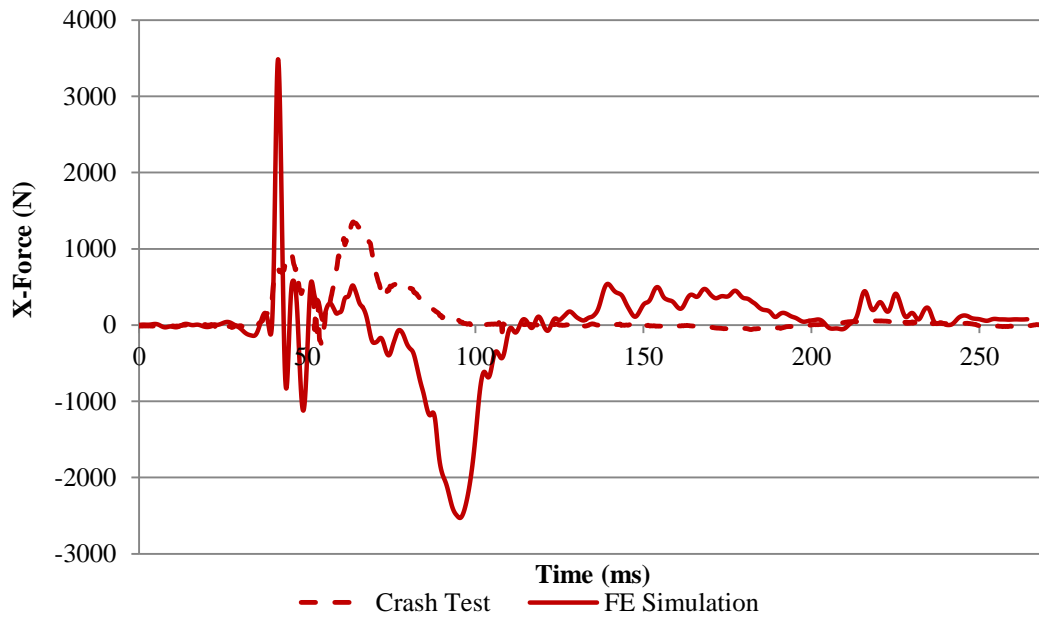


Figure 7-30. Right Femur X-Force vs. Time

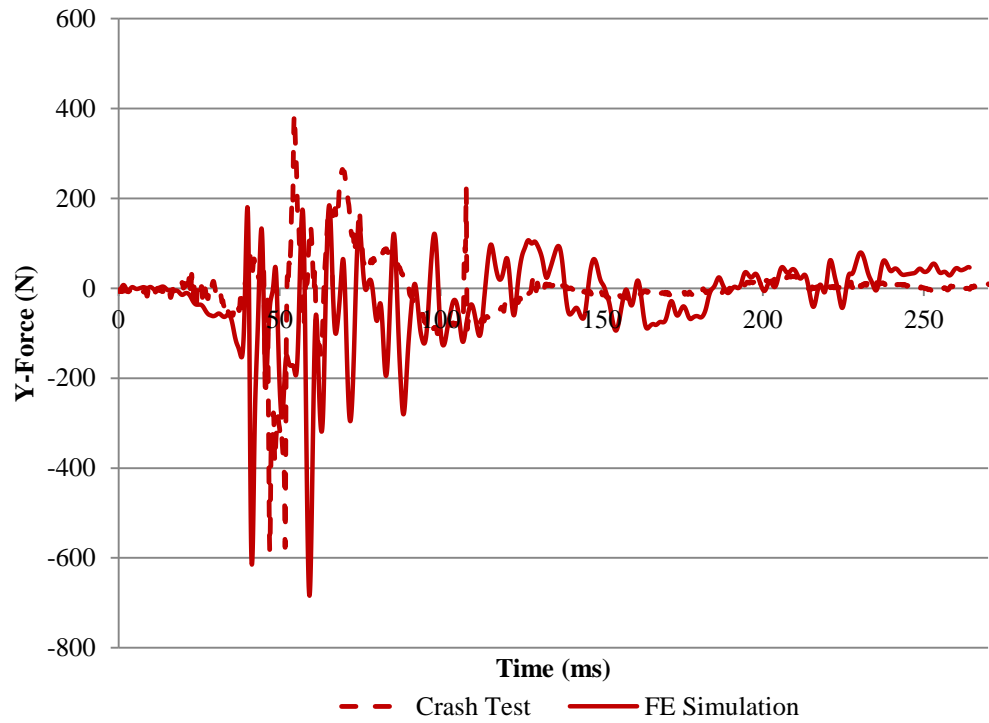


Figure 7-31. Right Femur Y-Force vs. Time

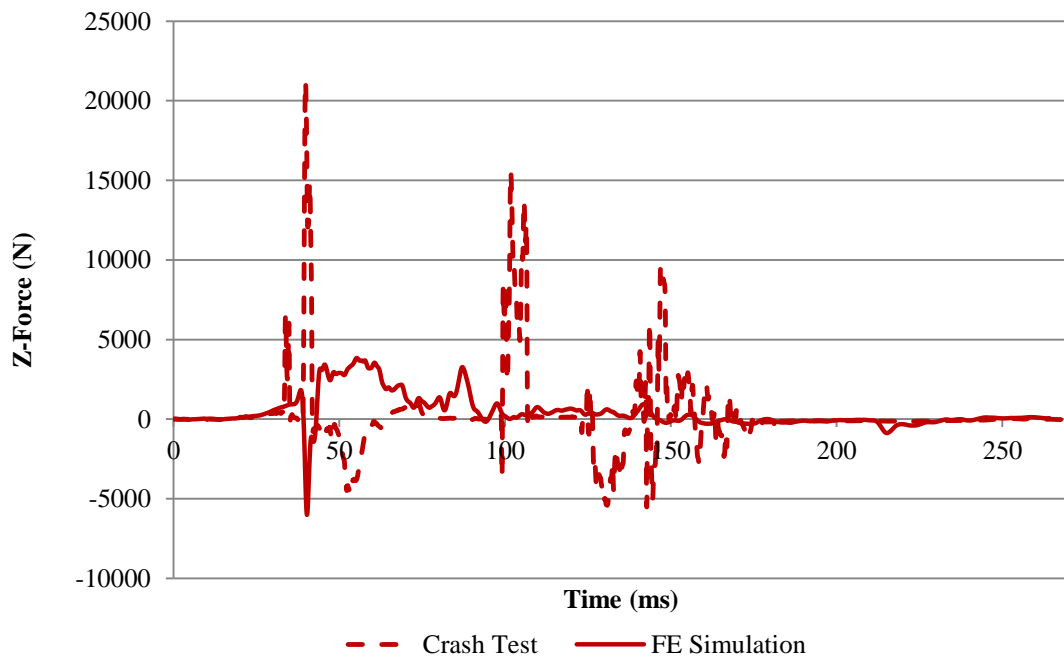


Figure 7-32. Right Femur Z-Force vs. Time

The probability of occupant risk is calculated using the following relation.

$$P(AIS \geq 3) = 1 - \left((1 - P(head)) * (1 - P(neck)) * (1 - P(chest)) * (1 - P(femur)) \right) = 77\%$$

The probability of injury of head, neck, chest and femur are calculated using the formulae listed in Table 3-8 through Table 3-10

7.5.3 Seatbelt Forces

The following section shows the loads attained in the shoulder and the lap belt. A pretensioner is used to control seatbelt elements from initial slack. Shortly after the retractor engages and locks, the pretensioner fires and engages and pulls in belt material to create 1.8 kN of tension in the belt. Once the tension in the belt reaches 1.8 kN the pretensioner disengages and the retractor takes over again. The retractor induces force into the seatbelt as per the pull-out until the maximum force in the retractor is reached. Figure 4-5 shows the force vs. pull-out curve on which the seatbelt lengthening is based on. The maximum force has been determined to be 3kN with an estimated maximum force in seatbelt as 5kN from the crash test. Figure 7-33 and Figure 7-34 shows the loads developed in the shoulder and the lap belt and compared with that in the crash test.

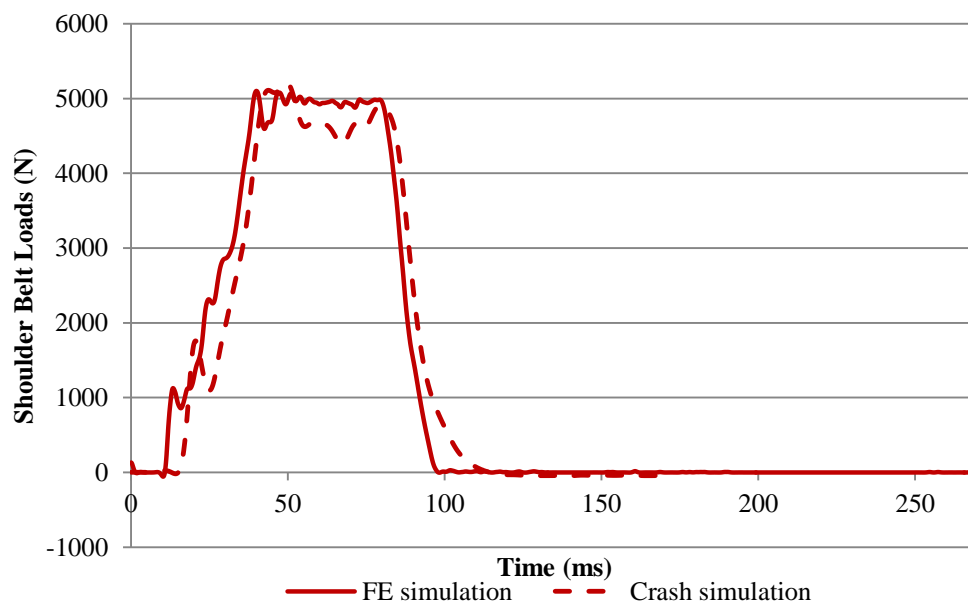


Figure 7-33. Shoulder Belt Loads vs. Time

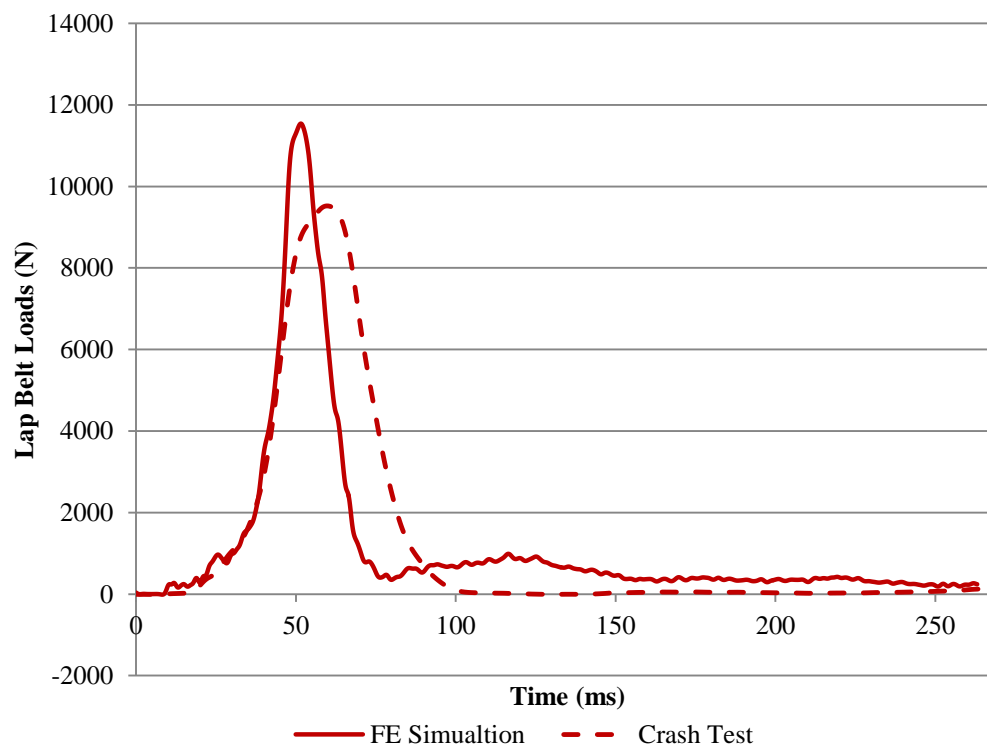


Figure 7-34. Lap Belt Loads vs. Time

7.6 Conclusions

The finite element models of the 2010 Toyota Yaris along with inclusion of ATD and passive restraint systems were used to replicate the full-scale crash event. The driver's seat of the FE model of the Toyota Yaris was adjusted to replicate general position, and angles of back rest and head rest recorded for the full-scale crash preparation. The FE model of the ATD was placed in position as per US-NCAP requirements by adjusting its fore arms, shoulders, position of hands on steering wheel, angles of lower body part such as ankle, feet, knees. Preliminary simulations were performed to place the ATD in the driver's seat applying gravity to the model to ensure that the distance between the head of ATD and the roof of the car is approximately equal to that in the test. Attempts were made to best achieve the highest correlation between test and simulation airbag behavior through adjustments of the inflation and deflation curves. The force vs. payout retractor curve has been modified with a peak value of force of 3kN in order to achieve a maximum shoulder belt load of 5.21kN.

With the above modifications made, the seatbelt and airbag behavior was found to be adequately matching with the crash test. The chest deflections, neck forces and femur forces are also found to be in good agreement with those of the test. However, it is observed that the Head Injury Criteria, though in limits as per FMVSS Standard No. 208, is found to be deviating with an error of 21.6%. This error is due to the fact that HIC is non-linear in nature and a small change in head acceleration shall result in large deviations. Efforts were made by the researchers to best replicate the inflation and deflation scenario of the airbag from the crash test with the help of a deflation curve. A plausible explanation for a higher value of HIC is that the reaction forces when the head of ATD hits the airbag could be higher due to the fact that the airbag material model was not validated.

8. CORRELATION OF EVALUATION CRITERIA OF MASH AND FMVSS

The risk of occupant in a vehicle subjected to crash test is measured in terms of occupant impact velocity and occupant ride down acceleration according to MASH (MASH, 2009). The maximum limit of occupant impact velocity as per MASH evaluation criteria is set to 40ft/s. The result of OIV from the crash test was 56.4 ft/s which is higher than the required maximum limit (Table 8-1). However, the recorded injury criteria of the ATD head, chest and neck are well below the limits as per FMVSS Standard No. 208 (Table 8-2). For instance, the HIC 15 limit is 700 and the recorded HIC value during the crash test was found to be 264.1.

Table 8-1: Recorded MASH Occupant Risk Parameters from Full-Scale Crash Test

Occupant Risk	Recorded Values from Crash Test	MASH Limits		Pass/Fail
		Preferred	Maximum	
Occupant Impact Velocity, ft/s (m/s)				
Longitudinal	56.4 (17.2)	30 (9)	40 (12)	Fail
Lateral	3.6 (1.1)	30 (9)	40 (12)	Pass
Ridedown Acceleration (G)				
Longitudinal	4.2	15	20.49	Pass
Lateral	1.7	15	20.49	Pass
Maximum 0.05 s average acceleration (G)				
Longitudinal	-30.6	-	-	-
Lateral	-3.8	-	-	-
Vertical	-4.7	-	-	-

Table 8-2: Recorded FMVSS Occupant Injury Risk Parameters from Full-Scale Crash Test

Injury Criteria	Recorded Values from Crash Test	IARV Limits	Pass/Fail
HIC-15	264.1	700	Pass
Chest Deflection(mm)	50.9	63	Pass
Neck Tension Force (N)	1929.8	4710	Pass
Femur (Left) Axial Force (N)*	3764.2	10000	Pass

* During the crash test, wires connected to the right femur accelerometer got loose; therefore the obtained data was not realistic and could not be used for the purpose of this project.

MASH values suggest a failure of the test with respect to occupant risk. At the same time, however, all recorded ATD injury values were well below the allowable limits, which indicate that the occupant was not at risk of serious, life-threatening injuries. These results and comparisons suggest that MASH evaluation criteria are conservative in nature.

In specific situations, the researchers suggest that when the recorded occupant injury velocity is beyond the value of 40 ft/s (12 m/s), attention should be given to the recorded maximum 50 ms acceleration average. The researchers would recommend setting an allowable limit of 31 G to the maximum 50 ms acceleration average. The decision of this value is directly related to the recorded results from the performed crash test: the 50 ms acceleration average in the longitudinal direction was found to be -30.6 G. Therefore, researchers suggest that if the longitudinal component of the 50 ms acceleration average is below the proposed 31 G limit, the occupant would not be at risk for serious, life-threatening injuries and the test should be considered a pass. However, it is suggested to perform more crash tests with different impact conditions with other vehicle models to verify for the repeatability of the value and check if 31 G is an allowable number for 50 ms average acceleration.

9. SUMMARY AND CONCLUSIONS

MASH specifies guidelines for crash tests and gives evaluation criteria for safety devices. As per MASH, the risk of injury to the occupant is assessed based on the concept of the Flail Space Model. The occupant impact velocity and occupant ridedown acceleration are used for assessing the injury criteria of an occupant.

It is assumed that the model is an “unrestrained” point mass which can move as a free projectile. There is a growing usage of restraints such as seatbelts and airbags. Hence, attempts are made in this study to assess real-world occupant injury risk associated with current MASH criteria using crash tests performed with instrumented seat belt and airbag restrained ATD’s and comparing them with injury criteria provided by US-NCAP regulations.

Finite element models for a passenger car, passive restraint systems (seatbelt and airbags), and anthropomorphic test ATD were calibrated against a full-scale frontal crash test. The crash test was conducted with a passenger car impacting a rigid wall at 90° angle, and with 34.7 mph (55.6 km/h) impact speed. The vehicle was instrumented according to MASH requirements, and an instrumented ATD was included as required by US-NCAP standards. The full-scale crash test was designed to replicate to the maximum extent possible testing criteria from MASH and US-NCAP testing standards.

The ATD dynamics show that the values of injury criteria are well below the limits set by FMVSS Standard No. 208. However the occupant injury risk as per vehicle dynamics, namely OIV (56.4 ft/s i.e., 17.2 m/s) is exceeding the limits set by MASH (the maximum OIV is 40 ft/s i.e., 12 m/s), suggesting that the maximum limits set by MASH are conservative when compared to the occupant injury risk calculated as per FMVSS Standard No. 208 for belt and airbag restrained occupants.

Occupant injury risk results calculated using FEA are found to be in good agreement with those of the crash test. The chest deflections, neck forces and femur forces are also found to be in good agreement with that of the test. However, it is observed that the

Head Injury Criteria, though in limits as per FMVSS Standard No: 208, is found to be deviating. Efforts were made by the researchers to best replicate the inflation and deflation scenario of the airbag from the crash test with the help of a deflation curve. A plausible explanation for a higher value of HIC is that the reaction forces when the head of ATD hits the airbag could be higher as the material properties are also not validated. Also, it is important to maintain the angle of the steering wheel as it affects the way the ATD hits the airbag. As the interiors of the Yaris model used are not validated, the steering column characteristics should be tuned to maintain the angle during the crash event.

The forces in shoulder belt could be best replicated from the crash test in the FE model of the seatbelt. This was done by modifying the maximum force in the retractor to 3 kN in the Force vs. Payout curve. The maximum force in the lap belt is found to be 21.2% higher in the FE simulation as compared to the crash test. It is caused by the body weight and friction between the ATD and the seat.

The maximum limit of occupant impact velocity as per MASH evaluation criteria is set to 40 ft/s (12 m/s). The result of OIV from the crash test was 56.4 ft/s (17.2 m/s) which is higher than the required maximum limit. However, the recorded injury criteria of the ATD head, chest and neck were well below the limits as per FMVSS Standard No. 208.

MASH values suggest a failure of the test with respect to occupant risk. At the same time, however, all recorded ATD injury values were well below the allowable limits, which indicate that the occupant was not at risk of serious, life-threatening injuries. These results and comparison suggest that MASH evaluation criteria are conservative in nature. In specific situations, the researchers suggest that when the recorded occupant injury velocity is beyond the value of 40ft/s, attention should be given to the recorded maximum 50 ms acceleration average. The researchers would recommend setting an allowable limit of 31G to the maximum 50 ms acceleration average, for which the occupant would not be at risk for serious, life-threatening injuries and the test should be considered a pass.

10. FUTURE WORK

The researchers conducted this study as a pilot project to attempt developing a correlation between the roadside safety hardware and vehicle safety standards evaluation criteria. Following are some suggestions for future research developments:

1. Further efforts are suggested to calibrate /validate the developed complete FE model of the occupant /vehicle /restraint systems. The FE model can become a valuable for use in parametric simulations for future studies, in support of a crash testing program.
2. Enhancement of the airbag model can be achieved in terms of material properties and inflation /deflation dynamic to more closely replicate the behavior recorded during the full-scale crash test. Researchers believe that a closer replication of the airbag dynamic would also help with a better replication of the ATD injury criteria, especially for the head and neck regions.
3. Researchers suggest investigating occupant injury risk correlation for cases with different speeds and different impact angles.
4. Researchers suggest conducting a similar study to determine correlation for occupant injury risk in frontal impacts with employment of a pickup truck vehicle to verify if similar correlation results are obtained.
5. Crash tests and simulations can be performed considering impacts of passenger vehicles against roadside safety devices to determine occupant injury risk and correlate it to the pertinent evaluation criteria.

REFERENCES

- American Association of State Highway and Transportation Officials, 2009, Manual for Assessing Safety Hardware.
- Association for the Advancement of Automotive Medicine, 2001, The Abbreviated Injury Scale: 1990 Revision, Update 98.
- Blamey, C., 1964, "Results for Impact Tests on Telegraphic Poles," Highways and Bridges, Vol 32, pp. 7, 8, 13.
- Chi, M., 1976, Assessment of injury in Roadside Barrier Tests. Federal Highway Administration, U.S., Department of Transportation.
- Council, F. M., and Stewart, R. J., 1993, "Attempt to define the relationship between forces to crash-test vehicles and occupant injury in similar real-world crashes," Transportation Research Record 1419, Transportation Research Board, National Research Council, Washington, D.C., pp 78–85.
- Eppinger, R., Sun, E., Kuppa, S., and Saul, R., 2000. "Development of Improved Injury Criteria for the Assessment of Advanced Automotive Restraint Systems – II," National Highway Traffic Safety Administration Vehicle Research & Test Center.
- Gabauer, D.J., and Gabler, H.C., 2004, "A comparison of roadside crash test occupant risk criteria using event data recorder technology." In: Proceedings of the 2004 International IRCOBI Conference on the Biomechanics of Impact, Graz, Austria.
- Gabauer, D.J., and Gabler, H.C., 2005, "Evaluation of Threshold values of acceleration severity index by using event data recorder technology." Transportation Research Record 1904, pp. 37–45.
- Gabauer, D.J., and Gabler, H.C., 2006, "Comparison of the Delta-V and occupant impact velocity crash severity metrics using event data recorders." In: Proceedings of the 50th Annual Association for the Advancement of Automotive Medicine Conference, Chicago, IL.

- Gabauer, D.J., and Gabler, H.C., 2008a, "Comparison of roadside and vehicle crash test injury criteria in frontal crash tests." *International Journal of Vehicle Safety*, Vol. 3, No. 2, pp. 135–148.
- Gabauer, D.J., and Gabler, H.C., 2008b, "Methodology to Evaluate the Flail Space Model by Using Event Data Recorder Technology" *Transportation Research Record*.
- Kornhauser, M., and Gold A., 1961, "Application of Impact Sensitivity Method to Animate Structures," *Impact Acceleration Stress*, pp. 333–344.
- Mertz, H. J., Kroll, C. K., and Patrick, L. M., 1967, "Knee, Chest and Head impact Loads," 11th Stapp Car Crash Conference, SAE, pp. 116.
- Michie, D. J., 1981, "Collision Risk Assessment Based on Occupant Flail-Space Model," *Transportation Research Record*, pp. 1–9.
- National Highway Transport and Safety Administration (NHTSA), 2004, *Federal Motor Vehicle Safety Standards: Occupant Crash Protection*, 49 C.F.R., Part 571.208, 1 October.
- Ray, M.H., Michie, J.D., and Hargrave, M., 1986, "Events that Produce Occupant Injury in Longitudinal Barrier Accidents." *Transportation Research Record* 1065: 19–30.
- "New Car Assessment Program (US-NCAP) Frontal Barrier Impact Test Toyota Motor Corporation, Toyota Yaris Le 5-Door Hatchback, Report Number: US-NCAP-KAR-12-032, 2012, U.S. Department of Transportation, National Highway Traffic Safety Administration Safety Performance Standards, NHTSA Number: MC5106, Office of Crashworthiness Standards.
- Ross, H.E., Sicking, D.L., Zimmer, R.A. and Michie, J.D., 1993, *Recommended Procedures for the Safety Performance Evaluation of Highway Features*. NCHRP Report 350, Transportation Research Board, National Research Council, Washington, D.C.
- Shoemaker, N. E., 1961, *Summary Report of Highway Barrier Analysis and Test Program*. Cornell Aeronautical Laboratory, Cornell University, Buffalo, NY.

- Southwest Research Institute, 1974, Recommended Procedures for Vehicle Crash Testing of Highway Appurtenances. NCHRP Report 153.
- Southwest Research Institute, 1980, Recommended Procedures for the Safety Performance Evaluation of Highway Safety Appurtenances. NCHRP Report 230.
- Tamanini, F. J., and Viner, J. G., 1970, "Energy Absorbing Roadside Crash Barriers," Civil Engineering, pp. 63–67.
- Thomson, R., and Gabauer, D, 2005, "Correlation of Vehicle and Roadside Crash Test Injury Criteria". Rowan University U.S., Chalmers University, Sweden, Paper Number 05-0283.
- Versace, J., 1971, "Review of the severity Index, SAE 710881," Proceeding of 15th Stapp Car Crash Conference, pp. 771–796.

APPENDIX A

CRASH TEST NO: 602761-13

A.1 VEHICLE PROPERTIES AND INFORMATION

Table A-1. Vehicle Properties for Test No. 602761-13

Date:	<u>2015-05-27</u>	Test No.:	<u>602671-13</u>	VIN No.:	<u>JTDBT4K31A1393565</u>
Year:	<u>2010</u>	Make:	<u>Toyota</u>	Model:	<u>Yaris</u>
Tire Inflation Pressure:	<u>32 psi</u>	Odometer:	<u>98535</u>	Tire Size:	<u>P185/60R15</u>

Describe any damage to the vehicle prior to test:

None

• Denotes accelerometer location.
NOTES: None

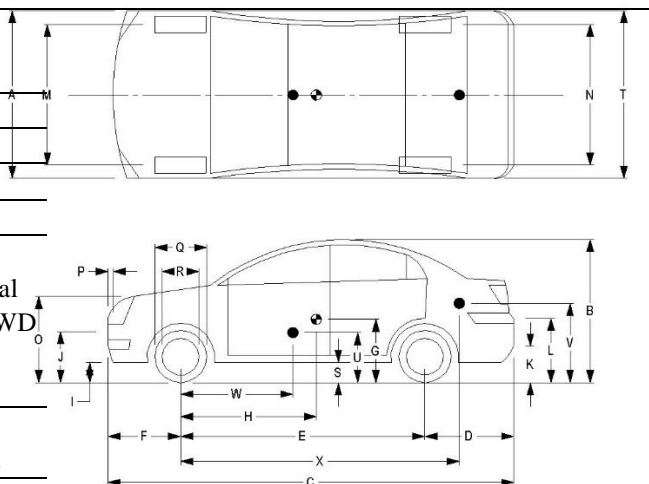
Engine Type: 4 cylinder
Engine CID: 1.5 liter
Transmission Type:
x Auto or Manual
x FWD RWD 4WD
Optional Equipment:
None

ATD Data:

Type: 50th percentile male

Mass: 176 lb

Seat Position: Driver side



Geometry: in.																	
A	67.00			F	28.50			K	15.00			P	1.50			U	15.00
B	57.88			G				L	27.00			Q	23.50			V	21.25
C	169.30			H	38.37			M	58.25			R	16.25			W	44.50
D	36.50			I	7.50			N	57.50			S	8.50			X	107.00
E	100.40			J	21.25			O	32.00			T	66.25				
Wheel Center Ht Front					11.25		Wheel Center Ht Rear					11.50					

RANGE LIMIT: A = 65 ± 3 in.; C = 168 ± 8 in.; E = 98 ± 5 in.; F = 35 ± 4 in.; G = 39 ± 4 in.; O = 24 ± 4 in.; M+N/2 = 56 ± 2 in.

GVWR Ratings:		Mass: lb	<u>Curb</u>	<u>Test Inertial</u>	<u>Gross Static</u>
Front	1840	M _{front}	1425	1492	1591
Back	1820	M _{rear}	893	923	1000
Total	3300	M _{Total}	2318	2415	2591

Allowable TIM = 2420 lb ± 55 lb | Allowable GSM = 2585 lb ± 55 lb

Mass Distribution: LF: 761 RF: 731 LR: 457 RR: 466

Table A-2. Exterior Crush Measurements for Test No. 602761-13.

Date: 2015-05-27 Test No.: 602671-13 VIN No.: JTDBT4K31A1393565

Year: 2010 Make: Toyota Model: Yaris

VEHICLE CRUSH MEASUREMENT SHEET¹

Complete When Applicable	
End Damage	Side Damage
Undeformed end width _____ Corner shift: A1 _____ A2 _____ End shift at frame (CDC) (check one) < 4 in. _____ ≥ 4 in. _____	Bowing: B1 _____ X1 _____ B2 _____ X2 _____ Bowing constant $\frac{X1 + X2}{2} = \underline{\hspace{2cm}}$

Note: Measure C₁ to C₆ from Driver to Passenger Side in Front or Rear impacts – Rear to Front in Side Impacts.

Specific Impact Number	Plane* of C-Measurements	Direct Damage		Field L**	C ₁	C ₂	C ₃	C ₄	C ₅	C ₆	±D
		Width** (CDC)	Max*** Crush								
1	Front plane at bumper ht	54.50	21.50	54.50	15.25	19.50	21.50	21.50	19.50	15.75	0
	Measurements recorded										
	in in.										

¹Table taken from National Accident Sampling System (NASS).

*Identify the plane at which the C-measurements are taken (e.g., at bumper, above bumper, at sill, above sill, at beltline, etc.) or label adjustments (e.g., free space).

Free space value is defined as the distance between the baseline and the original body contour taken at the individual C locations. This may include the following: bumper lead, bumper taper, side protrusion, side taper, etc.

Record the value for each C-measurement and maximum crush.

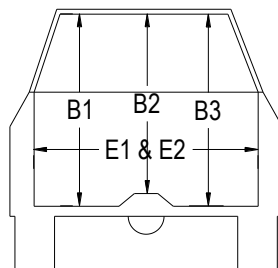
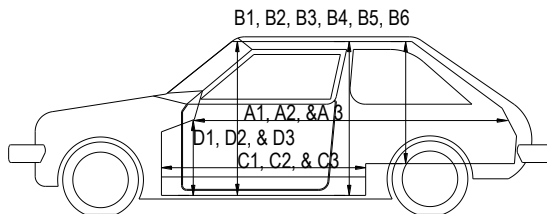
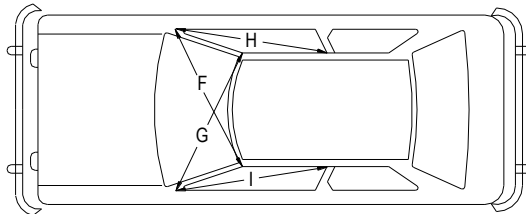
**Measure and document on the vehicle diagram the beginning or end of the direct damage width and field L (e.g., side damage with respect to undamaged axle).

***Measure and document on the vehicle diagram the location of the maximum crush.

Note: Use as many lines/columns as necessary to describe each damage profile.

Table A-3. Occupant Compartment Measurements for Test No. 602761-13.

Date: 2015-05-27 Test No.: 602671-13 VIN No.: JTDBT4K31A1393565
 Year: 2010 Make: Toyota Model: Yaris



OCCUPANT COMPARTMENT DEFORMATION MEASUREMENT		
	Before	After
	(in.)	(in.)
A1	71.50	71.00
A2	78.50	78.25
A3	71.50	71.00
B1	40.12	40.12
B2	37.00	37.00
B3	40.12	40.12
B4	35.25	35.25
B5	35.00	35.00
B6	35.25	35.25
C1	25.25	24.25
C2	-----	-----
C3	25.25	24.25
D1	9.75	9.75
D2	-----	-----
D3	9.25	9.25
E1	52.75	52.75
E2	49.75	49.75
F	49.50	49.50
G	49.50	49.50
H	38.00	38.00
I	38.00	38.00
J*	51.50	51.50

*Lateral area across the cab from driver's side kickpanel to passenger's side kickpanel.

A.2 SEQUENTIAL PHOTOGRAPHS



0.000 s



0.030 s



0.060 s



0.090 s



Figure A-1. Sequential Photographs for Test No. 602761-13 (Overhead and Frontal Views).



0.120 s



0.150 s



0.180 s



0.210 s



**Figure A-1. Sequential Photographs for Test No. 602761-13 (Overhead and Frontal Views)
(Continued).**



0.000 s



0.120 s



0.030 s



0.150 s



0.060 s



0.180 s

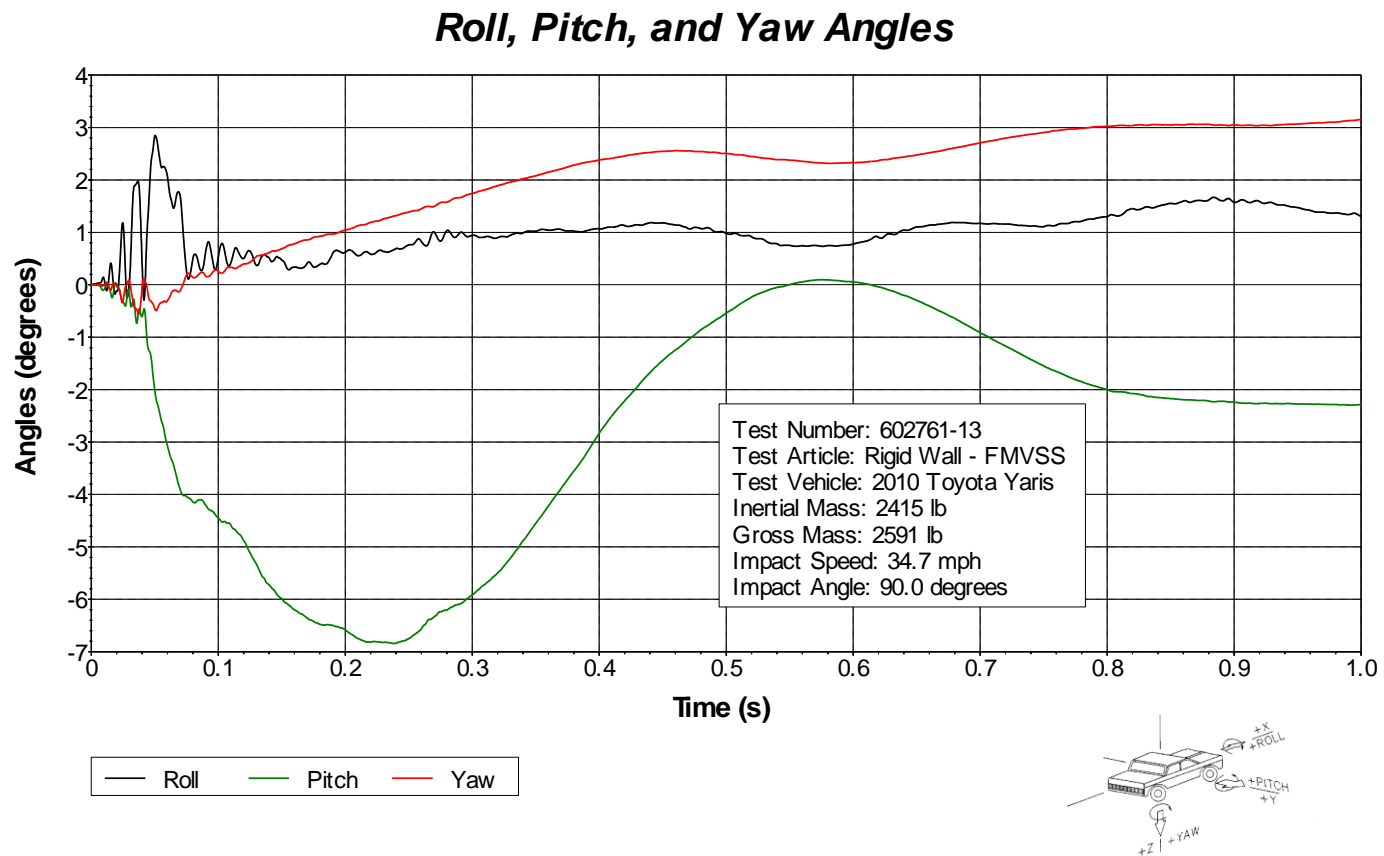


0.090 s



0.210 s

Figure A-2. Sequential Photographs for Test No. 602761-13 (Rear View).

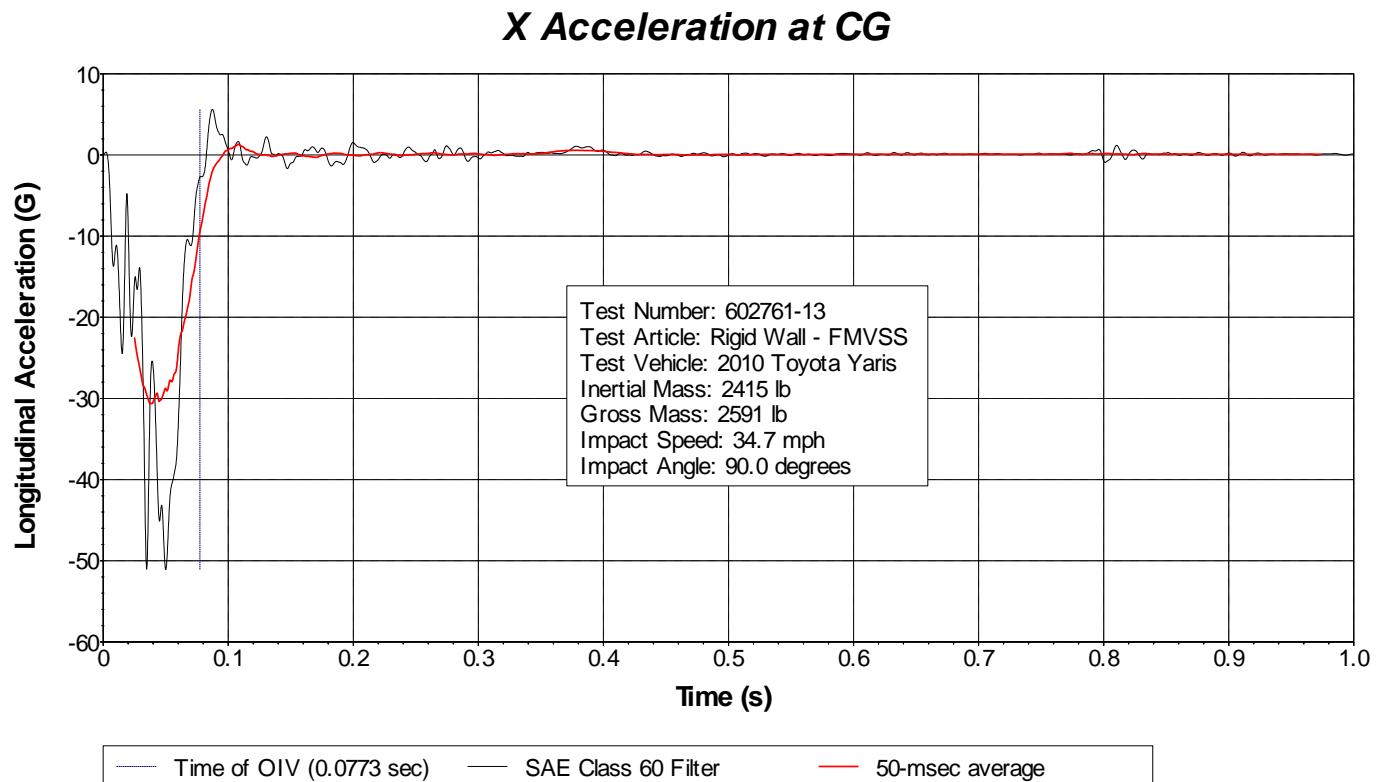


Axes are vehicle-fixed.

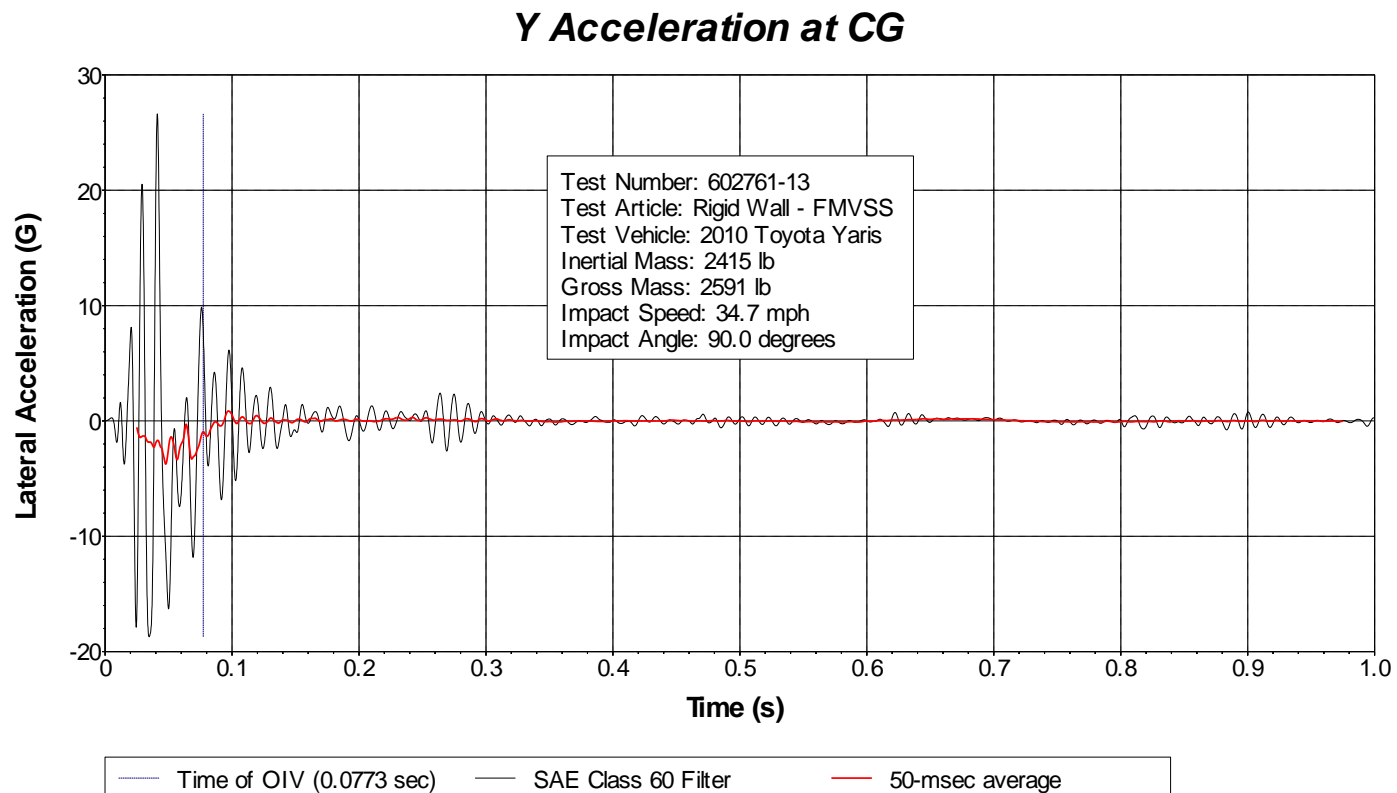
Sequence for determining
orientation:

1. Yaw.
2. Pitch.

Figure A-3. Vehicle Angular Displacements for Test No. 602761-13.

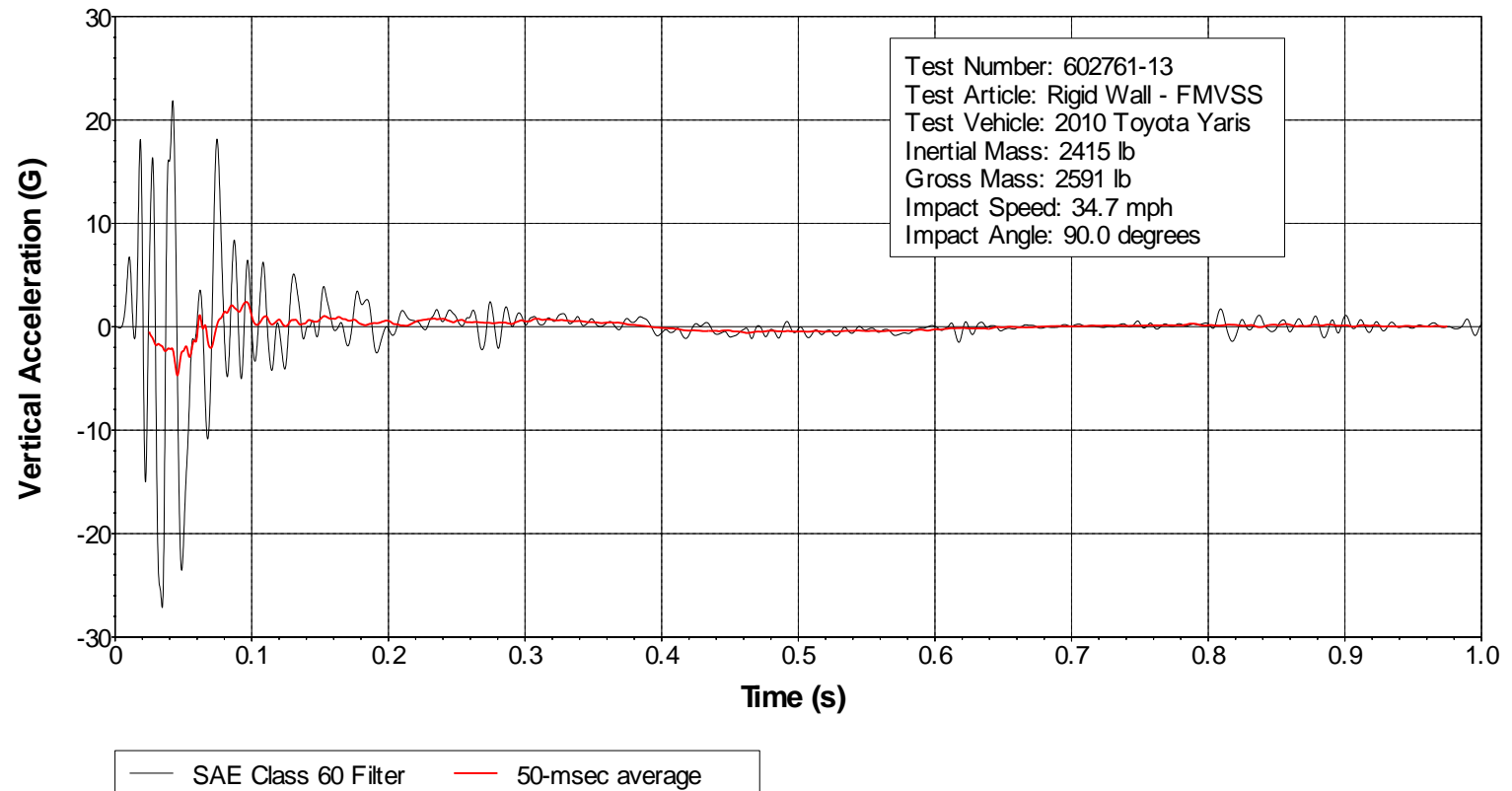


**Figure A-4. Vehicle Longitudinal Accelerometer Trace for Test No. 602761-13
(Accelerometer Located at Center of Gravity).**

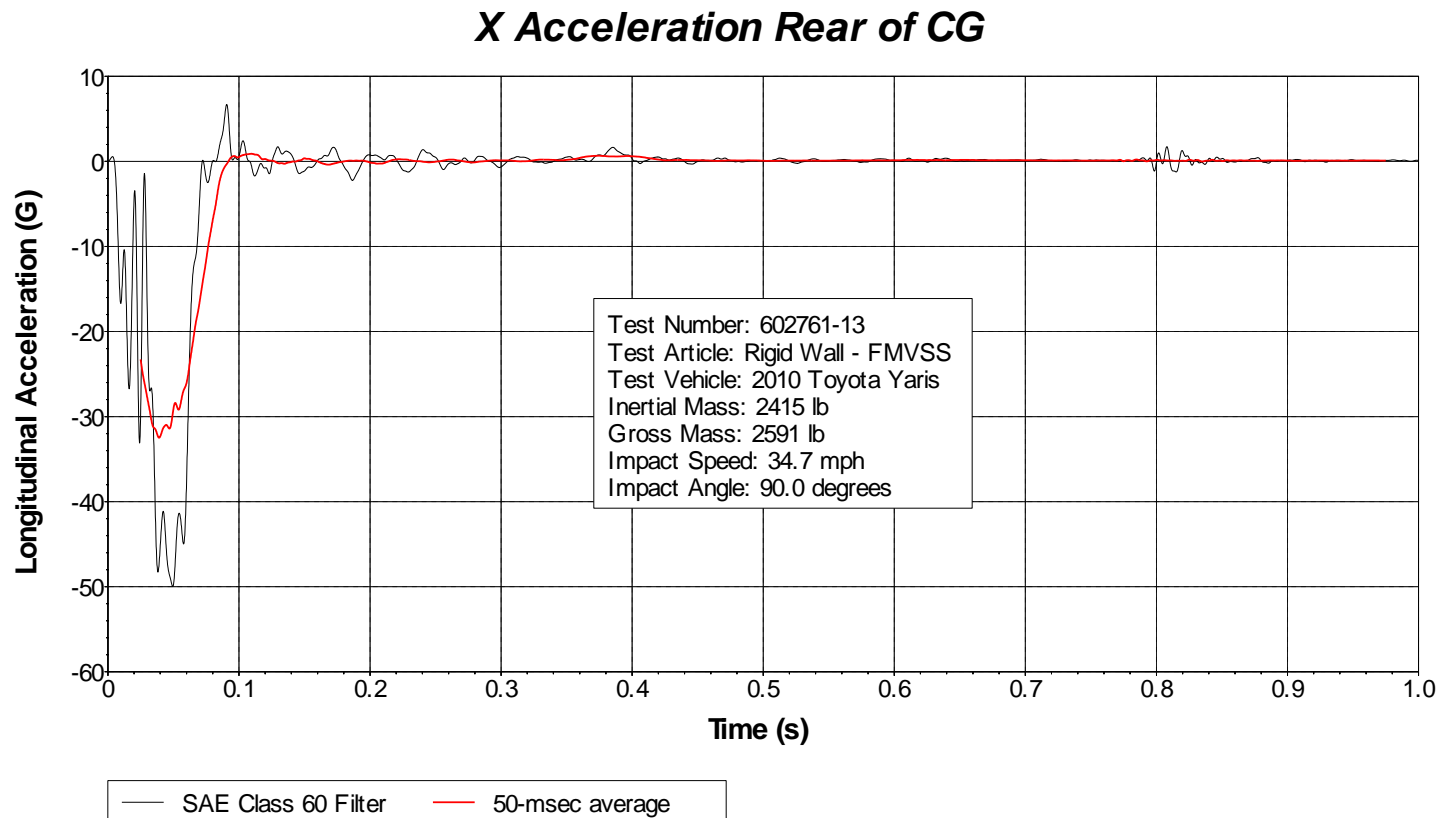


**Figure A-5. Vehicle Lateral Accelerometer Trace for Test No. 602761-13
(Accelerometer Located at Center of Gravity)**

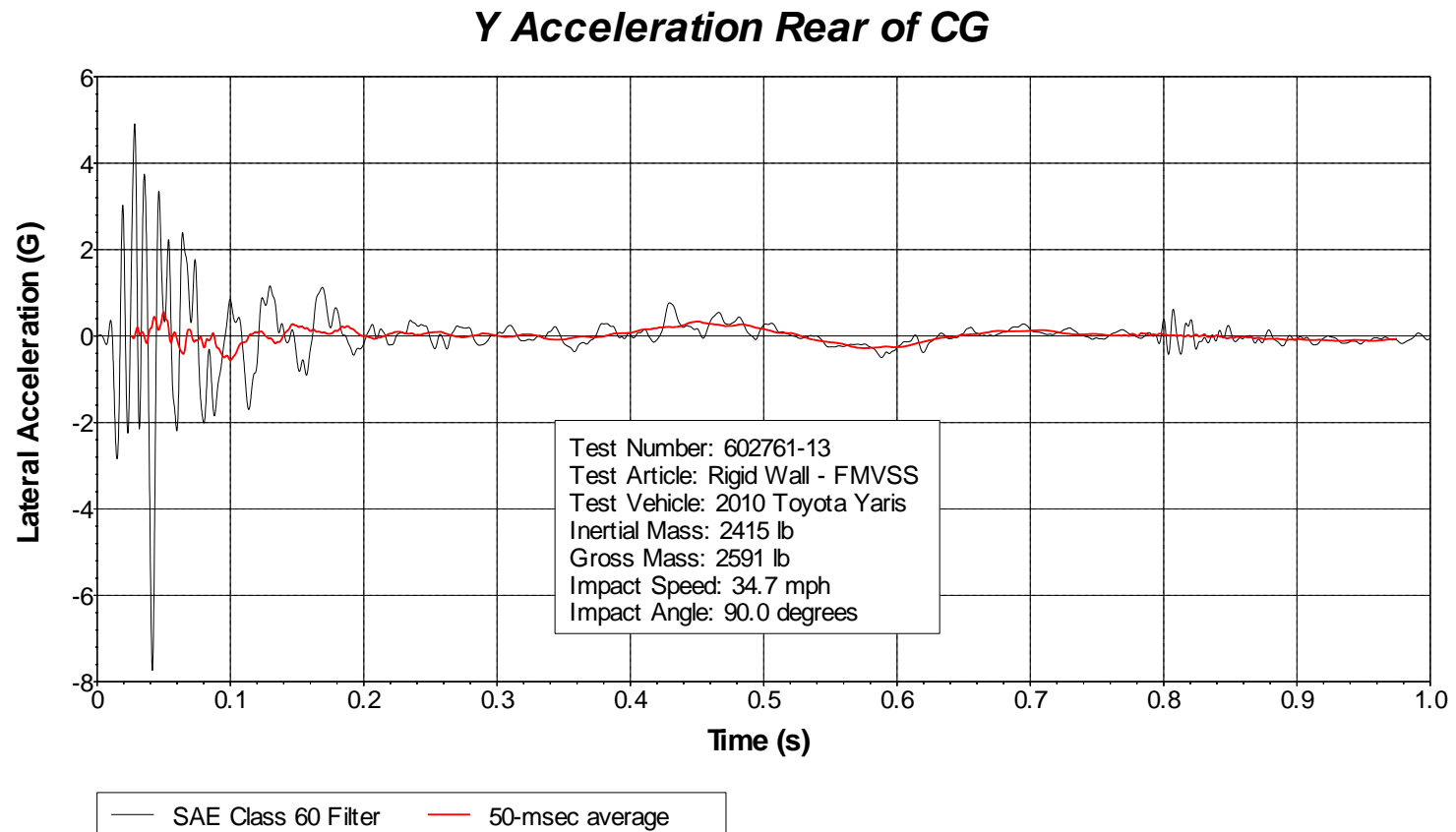
Z Acceleration at CG



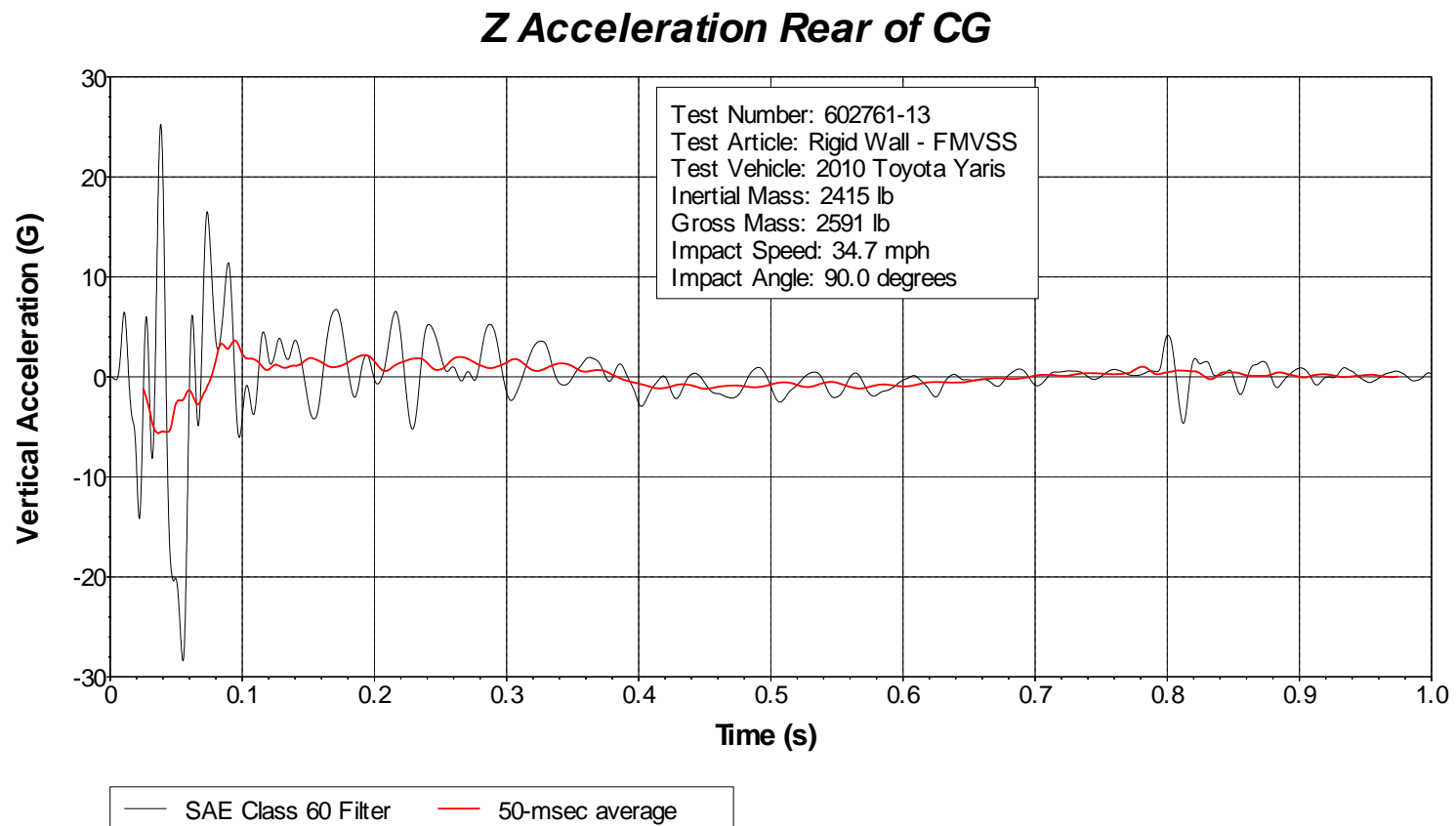
**Figure A-6. Vehicle Vertical Accelerometer Trace for Test No. 602761-13
(Accelerometer Located at Center of Gravity).**



**Figure A-7. Vehicle Longitudinal Accelerometer Trace for Test No. 602761-13
(Accelerometer Located Rear of Center of Gravity).**



**Figure A-8. Vehicle Lateral Accelerometer Trace for Test No. 602761-13
(Accelerometer Located Rear of Center of Gravity).**



**Figure A-9. Vehicle Vertical Accelerometer Trace for Test No. 602761-13
(Accelerometer Located Rear of Center of Gravity)**